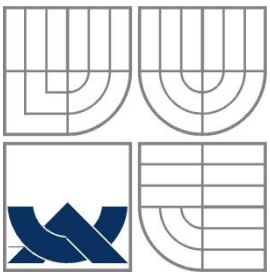

VYSOKÉ UČENÍ TECHNICKÉ V BRNĚ
BRNO UNIVERSITY OF TECHNOLOGY

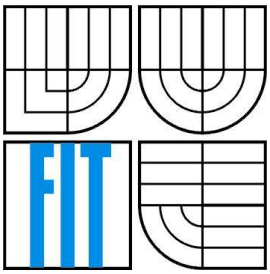

FAKULTA INFORMAČNÍCH TECHNOLOGIÍ
ÚSTAV INTELIGENTNÍCH SYSTÉMŮ
FACULTY OF INFORMATION TECHNOLOGY
DEPARTMENT OF INTELLIGENT SYSTEMS

BIOMETRICKÝ SYSTÉM PRO ROZPOZNÁVÁNÍ PODLE SÍTNICE A DUHOVKY OKA

BIOMETRIC SYSTEM FOR RETINA AND IRIS RECOGNITION

DISERTAČNÍ PRÁCE
PH.D. THESIS

AUTOR PRÁCE
AUTHOR
Ing. Josef Hájek

VEDOUCÍ PRÁCE
SUPERVISOR
doc. Ing. Martin Drahanský, Ph.D.

BRNO 2016

Abstrakt

Tato disertační práce se zabývá biometrickým a medicínským zařízením pro simultánní snímání duhovky a sítnice oka v jednom kroku. V případě biometrického zaměření je práce rozšířena o vzájemnou fúzi těchto dvou biometrik do jedné šablony, kdy multimodální systém vykazuje mnohem lepší parametry než systém unimodální, a to především ve větší unikátnosti, univerzálnosti a velmi obtížně proveditelnému útoku (až téměř nemožnému) na senzor. V případě medicínského využití práce dále rozvíjí detekci a klasifikaci nemocí pro základ expertního systému pro oftalmologické účely, který bude umožňovat pomoc lékaři při stanovení diagnózy nálezu v obrazu sítnice (či duhovky) oka.

Abstract

This thesis deals with a biometric and medical device for simultaneous scanning of the eye's iris and retina in one step. In the case of biometric use, the work is extended by mutual fusion of both biometrics into one template proving that multimodal system evinces better parameters than unimodal mainly in improved uniqueness, universality and difficulty feasible attack (almost impossible) on the sensor. In the case of medical use, the work is developing detection and classification of diseases as the basis of an expert system for ophthalmology purposes which can help medical doctors to make a reliable and quick eye disease diagnosis of pathological finding in the retinal (or iris) image.

Klíčová slova

biometrie, sítnice, duhovka, fúze, nemoci oka

Keywords

biometrics, retina, iris, fusion, eye diseases

Citace

Josef Hájek: Biometric system for retina and iris recognition, Brno, FIT BUT, 2016

Biometric system for retina and iris recognition

Prohlášení

Prohlašuji, že jsem tuto diplomovou práci vypracoval samostatně pod vedením doc. Martina Drahanského. Uvedl jsem všechny literární prameny a publikace, ze kterých jsem čerpal.

.....
Josef Hájek
Srpen 2016

Acknowledgements

First of all, I would like to thank my supervisor Martin Drahanský for his guidance and support during my whole Ph.D. study. My big thanks also belong to my parents Marta and Josef fort their endless love and support during my whole life, for the rest of my family and of course for my girlfriend Jana. I have enjoyed the work and valuable discussions with my office mates and colleagues working with me who have always been giving me a thoughts and ideas moving me towards my goals. The research has been significantly supported by several projects I was working on, namely *Device for acquirement and recognition of eye iris and eye retina* (MŠMT ED3.1.00/13.0271), *IT4Innovations excellence in science* (MŠMT LQ1602) and *Reliability and security in IT* (BUT FIT-S-14-2486).

Content

1 Introduction

Nowadays, a bigger emphasis is given to the need for securing personal data and about different ways of its realization, or about systems that should secure it more deeply and reliably. Individuals come across situations in which they have to prove their identity every day – when signing contracts, at work when entering and exiting, during card payments or when traveling abroad. This security mechanism and the number of tasks that it is associated with can seem too difficult and burdensome on a first sight. However, it practically prevents any misuse of the personal data and rights of a specific person and simultaneously proves to the subject (bank, seller, operator…), that they are really dealing with the right person that is before them.

Today, for securing the safety of personal data, one can use three basic safety mechanisms: (1) *Something that he or she knows* – password, PIN, secret button, set procedure, etc. The idea of this approach is a random and an easily remembered information, which however, has its downside in relatively simply obtaining of the information by an unauthorized person. Also, the more difficult the password or the procedure is, the higher the chances of being forgotten; (2) Medium comfort and security provide *something that is owned* (e.g. key, chip card, token, RFID tag). The idea of this approach is to own something that no other person possesses. There, however, again exists the risk that it can be obtained by an unauthorized person, and also the possibility of forgetting it (e.g. on a table at home). Obviously, also, a possibility of illegal copying is present. (3) *Something that is in the person themselves* (e.g. look, movements, behavior, expressions in different situations). The idea is that we ourselves possess the identification key. The truth is that we will not forget a biometric attribute at home but it can still be illegally copied and then used as a fake biometric attribute to access the system. We leave our fingerprints nearly everywhere and faking them is not that big issue. It is also possible that anywhere we are, someone will take a photo of us and then use our photography to access the system that allows the entry by a facial recognition.

The discipline that covers the third variant of an identity check, i.e. what we are and will remain – is called "*biometry*". The word biometry comes from Greek and consists of two words "bios" and "metron", where "bios" means life and "metron" means to measure. It is, therefore, a sort of "life measure". In IT, we use this word to describe a system or a procedure for recognition of human attributes. In biomedical field, however, the word biometry has quite different meaning – it refers to statistic calculations in biology or medicine (e.g. probability of forming of a new generation after mutation, the basis for genetic subjects). *Biometry* (IT definition) is automated recognition of human beings based on their characteristic anatomical features (e.g. face, fingerprint, retina, iris) and their typical behavior (i.e. behavior, e.g. dynamic attributes of signature, walking).

In today's security world, biometrics is an interesting and important approach. Ideally, the user interacts with a simple interface and in a matter of seconds, the biometric system scans the biometric characteristic, whether it is fingerprint or eye iris, and decides whether the user is allowed to pass or not.

This work is focused on the way of scanning and processing the features of a human eye for biometric and biomedical purposes. The features are iris and retina, as they include enough unique information that by its range, covers a set bigger than the current human population on Earth.

However, such systems are not perfect, and there is always room for improvement. Recently, it has been discovered that a viable course of the future of biometrics may lie in multimodal biometric systems, which combine more than one source of biometric information for evaluation (such as fingerprint and palm veins), unlike unimodal biometric systems, which only use one.

Biometry applies to different parts of the human body. If the part is damaged or removed altogether, further identification using this biometric is not possible. From all possible affections of our senses, loss of vision has the biggest impact on a person's everyday life. This impact is higher than a

loss of memory, voice or hearing, because 80 % of all sensory information that human brain receives, comes through our vision. The interesting fact is that a vast majority of visual losses can be prevented by an early recognition and diagnosis of the illness and its treatment. Visiting ophthalmologist can be stressful for some people not only because of fear of the examination itself but also for example because of a lack of time. This could be at least partially solved by automated devices, which could evaluate the current patient's condition without any human intervention and possibly even determine anamnesis. The goals of this work also include automated iris scanning and detection and classification of illnesses in fundus images.

1.1 Problem statement

We've been operating for some time already in the field of eye characteristics recognition. We have experience in biometrics not only with commercial devices but also with medical devices that we commonly use in the laboratory. We also know its current state on the scientific and research field. We have found that each approach has its disadvantages, but obviously also many advantages.

First, we will focus on biometric systems that are based on eye characteristics because biometry is a crucial part of this work. Relatively, lots of iris scanning and recognition algorithms exist. Devices are working, usable in practice, with compact dimensions and quite a good price. Its disadvantage is its inability to detect life and thus its easy fraudulence by e.g. specially tailored contact lens etc. For an area of high-security level, the iris is not recommended. If we now focus on eye retina, there is currently no existing biometric system that would be based on this modality. Eye retina has its disadvantages in more difficult scanning form, which is, however, an advantage for liveness detection, in bigger degree user cooperation and higher cost of the device; on the other hand, the possibility of creating fake eye retina is very low (nearly impossible), also eye retina possesses relatively lot of stable features that can be used for recognition of a big number of people. If we think about the possibility of mixing these two biometric characteristics into one multimodal biometric system, we come to a clear view that the combination has its purpose because the current trends of biometric systems lead towards multimodal biometrics. That kind of device, which would combine eye retina and iris, currently does not exist on the market neither does it exist in any functional concept which would enable using this technology in practice.

We also cannot omit medical (or biomedical) applications, where ophthalmoscopes and fundus cameras are used. These are very expensive; they also do not enable automatic eye retina scanning. The iris is not very interesting for medical use – in eye retina, much more diseases are visible. We can also say that there is no useful expert system on the market which would enable an automatic detection and recognition of diseases that show up in eye retina. As we are in contact with ophthalmologists and have presented our article in an ophthalmologic magazine [123] – which received very positive response – we think that our designed system fulfills their needs and expectations.

When designing and constructing a solution that would fulfill the criteria mentioned, it is necessary to consider these:

- User acceptance (fear of users from its usage).
- Amount of cooperation of user and device necessary.
- Quality of captured images.
- Scanning and processing time.
- Overall price of device and associated software.

By creating a complex and sufficiently robust device, we cover the requirements of both biometric and medical segment. The same device with small modifications (e.g. change of cameras) can be used in both areas, while the only significant change would be software which in biometric systems would extract biometric features with a task of comparing these features with a saved pattern in a database; and

in medical systems, it would build an image of the eye retina, would also save the iris, however the expert system would focus mainly on detection of diseases and suggest possible diagnoses, which would make the ophthalmologist's job easier.

1.2 Thesis contribution

In the previous chapter, disadvantages of current eye retina and iris scanning were discussed, both in biometric and medical systems. We have tried to reflect these disadvantages in our research and development and have found a solution, which would keep the mentioned advantages, but would eliminate as many disadvantages as possible.

Three main contributions that can be considered as core of the dissertation, are presented in the work. First (1) is the *construction of a device for both eye retina and iris scanning in one,* which is a world unique solution. For the construction, we have received a Czech national utility model [P02] (Czech Industrial Property Office) with publication number 26535 named "Ophthalmologic diagnosis device", furthermore, Czech national patent [P03] (Czech Industrial Property Office) with publication number 305278 and also international patent PCT [P01] with publication number WO/2015/043553 and title "Ophthalmic diagnostic apparatus and the way of its use", of which I am co-author. We have further presented the construction in publications [H01][H02][H03][H04]. The hardware itself was also being created as a part of the project "Device for acquirement and recognition of eye iris and eye retina", marked MŠMT ED3.1.00/13.0271 that was financed by the Ministry of Education, Youth and Sports of the Czech Republic. Second (2) contribution is the *design of fusion of two biometric modalities – eye retina and iris.* In literature, there can be found some kinds of combination; however, our design tries to reflect the current state of biometric systems and their related standards. The biggest difference from the published systems is mostly short processing time, small size of biometric pattern and precision up to 0.01 % ERR. Our solution and related methods were published in these articles – [R01][H05][H06]. Third (3) contribution is the *analysis of eye retina image with pathological finding*, consisting of the detection the disease and its diagnosis, and suggesting its removal. Our proposed procedure is unique and is based on our own database and databases DIARETDB1, STARE, and UNM (more details in chapter 4.4). Consultations were led by ophthalmologists, i.e. there are included also, innovative procedures to find secondary symptoms of selected diseases' types. The last part of the solution – methods and algorithms for the analysis of an image with a disease on the eye retina – was published here – [R02].

1.3 Thesis organization

The text in this work is divided into five chapters. Chapter 2 sums up the theory and current state of knowledge in the area of recognition using eye retina and iris. It describes basic prerequisites as e.g. eye anatomy, principles of devices for its examination or selected eye diseases. It also describes the current market state with biometric devices for recognition or the history that preceded it. Chapter 3 deals with iterative design and research optical device for eye retina and iris scanning combined in one specific apparatus. The described development was realized on FIT VUT in Brno and currently, the 3rd version of the optical system is under development. Chapter 4 talks about the design of eye retina and iris features fusion on the score level and thus give a base for very secure multimodal biometric system. Chapter 5 describes proposed methods for automated detection and diagnosis of diseases in retinal images. The last chapter sums the results of the work and outlines possible further development possibilities.

2 State of the art

This chapter describes biometric identification based on inner eye organs - iris and retina. These methods are very precise and are used in areas with highest security requirements. Eye attributes that are being scanned and used for identification are unique for each individual and probability of the two same identifiers is many times lower than for example with fingerprints.

While systems for iris recognition are relatively well known and expanded thanks to their smoothness and good user-friendliness, it is not the case with retina recognition. Currently, no device using retinal recognition can be found on the market. All of the so far sold devices were unsuccessful because of their low user-friendliness. This method is used in areas with high risk of sensor counterfeiting. The relatively complex process of retina scanning ensures certain safety against imitating retina pattern.

2.1 Anatomy of the eye

The human eye is an unique organ which reacts to light and similar to other parts of the body can be used for biometric recognition purposes such as fingerprints, hand veins and geometry, face, etc. In the eye, there are two crucial parts which have relatively high biometric entropy and thus are very suitable for recognition. The first one is the iris, i.e. the colored front part of the eye. The second one is the retina which is responsible for light sensing and cannot be observed by the naked eye because it is located on the back side of the eyeball. Both of them are very well protected against physical damage because they are inner structures of the eye. Iris and retina biometric patterns are unique for each individual although, e.g., the color of the iris is genetically dependent (also applies for monozygotic twins). The base anatomy of the human eye is described in Fig. 2.1.

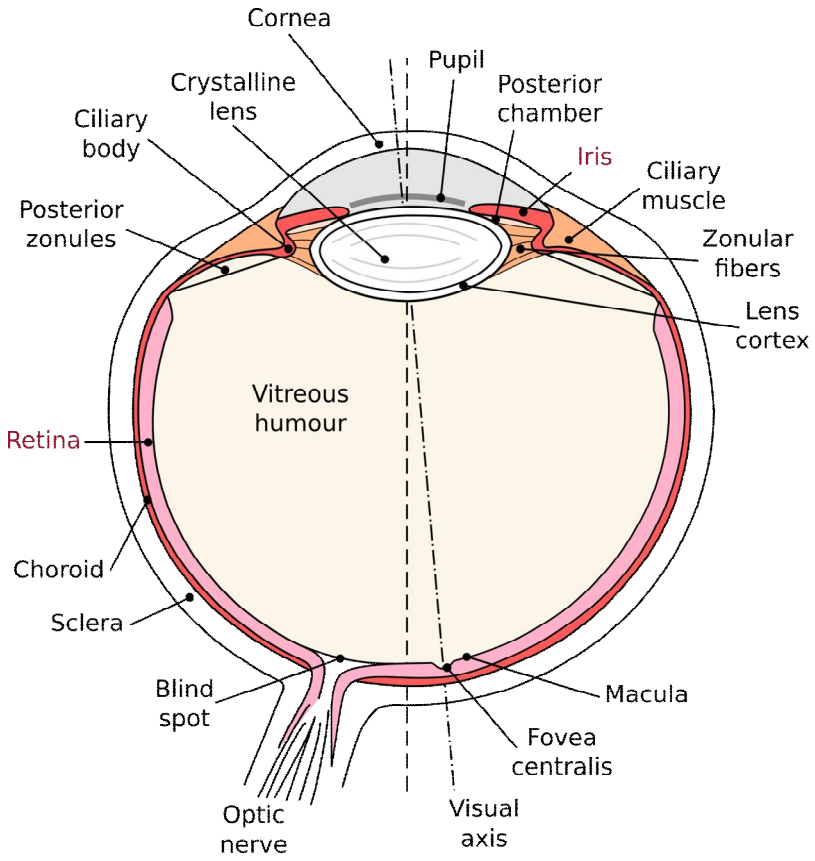

Fig. 2.1: Eye anatomy (modified from [135]).

The human eye consists from [2]:

- **Transparent crystalline lens** is located immediately behind the iris. It is composed of fibers that come from epithelial (hormone-producing) cells. It acts to fine-tune the focusing of the eye.
- **Ciliary body** extends from the iris and connects to the choroid. This annular structure produces aqueous humour, holds the intraocular lens in a place, and also has a supporting function during eye accommodation.
- **Iris** is colored annular structure regulating pupil diameter and thus amount of light coming into the eye. Eye color is defined by the iris.
- **Pupil** is a hole located in the center of the iris. For an external observer, it seems to be a small black spot because light coming through the pupil into the eye is absorbed by biological tissues inside the eye.
- **Cornea** acts as a window of the eye. It is a transparent front surface of the eye covering the iris and the pupil admitting light into the eye.
- **Posterior chamber** contains aqueous humour and is located behind the peripheral part of the iris and in front of the suspensory ligament of the lens.
- **Ciliary muscle** is a ring of tiny muscles enabling changes in lens shape and thus controlling eye accommodation at varying distances. The muscles affect zonular fibers in the eye. When the muscles contract, they pull themselves forward and move the front lens part towards the axis of the eye.
- **Zonular fibers** are connections of the ciliary body and the crystalline lens which suspend in position during eye accommodation.
- **Lens cortex** is a part of lens comprising secondary lens fibers (long, thin, transparent cells, form the bulk of the lens).
- **Posterior zonules** pull the ciliary body, anterior zonules and lens into the unaccommodated form.
- **Vitreous humour** is a transparent gelatinous mass filling the interior space of the eye. It contains no blood vessels and more than 98 % of its volume is water.
- **Choroid** is the vascular layer of the eye. Lies between sclera and retina and provides nourishment for the back of the eye.
- **Sclera** is the protective outer layer of the eye enclosing the eyeball except the part covered by the cornea.
- **Retina** is a nervous tissue layer covering the back of the eyeball. It consists large amount of light-sensitive cells in which stimulation of electrochemical reactions is initiated, and electrical impulses are transmitted to the brain.
- **Blind spot** is a small area where the optic nerve comes into the eye. On this area, there are no photoreceptors, i.e. there is no sensitivity to light.
- **Fovea centralis** is a small central spot or pit in the center of the macula containing only cones (no rods) which ensure the most sensitive color vision.

- **Macula** is a small circle shape yellowish area containing a maximum number of light sensitive cells thus ensuring maximum visual acuity. It is made up of almost wholly retinal cones.
- **Optic nerve** carries electrical impulses from visual stimuli in the retina out of the eye**.**
- **Optical axis** is the direct line through the center of the cornea, pupil, lens and the retina. Along this line, the sharpest focus is drawn when we look at an object.
- **Visual axis** is a visual line from the center of the pupil to the fovea. This axis gives the best color vision (because fovea consists of high-density cones and no rods).

The human eye is the most complicated and one of the most important sense organs from all. From the physical point of view, it is a transparent biconvex optical system, which focuses the light rays onto the surface of retina by help of cornea and eye lenses. The *cornea* is a front elastic part of the eye. It is transparent, without vessels, and with the fixed optical power of more than 43 diopters represents approximately two-thirds of the eye's total power.

Another optic element of the eye is a *lens* with the ability to change its shape and thus optical power and focal length. It allows to focus on an object at various distances from the observer (eye accommodation). The minimal and maximal distance which the eye is able to focus on is given by two points [26]:

- *Near point* – the shortest distance between an object and the observer which still gives a sharp image on the retina. In this case, the optical system of the eye has the largest optical power of more than 60 diopters. A healthy eye is able to focus on the object at a distance of 25 cm without any exertion.
- *Far point* – the longest distance between an object and the observer which still gives a sharp picture on the retina. The eye lens has the lowest optical power. For a healthy individual, this distance is in infinity.

The light entering the eye is controlled by the *iris*. The surface of iris has a shape of an annulus and is able to control the diameter of the pupil and thus the amount of light falling on the *retina*. It has a similar function as the aperture of a camera lens.

Fig. 2.2 shows the projection into the eye. The resulting image of the outside world is in the eye inverted (upside down), mirrored and reduced. The captured image is subsequently transformed to electric signals which are directed to the brain via the optic nerve. In the brain, the image is processed, i.e. it is flipped upside down and mirrored according to the reality.

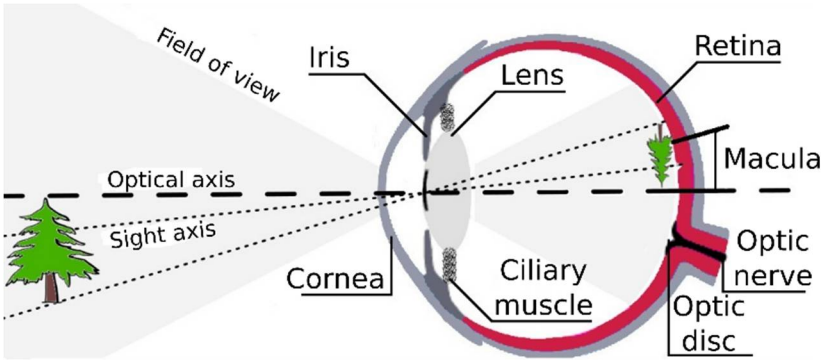

Fig. 2.2: Light projection into the eye.

A thorough understanding of eye anatomy is closely related to a proposal of optical system for acquirement of digital copy of the eye that can be used for medical as well as for biometric purposes.

2.1.1 Anatomy of the retina

As shown in Fig. 2.1, the *retina* is located on the back part of the inner surface of the eyeball. The retina is considered as part of the central nervous system and is the only one which can be observed noninvasively and directly. This light-sensitive tissue has a similar function like the film in a camera. Optical system within the eye focus an image onto the retina surface, initiating several electrical and chemical reactions. Nerve fibers in the retina transport these signals to the brain which interprets them as visual images.

Two types of photosensitive cells are contained in the retina – the rods and three different types of cones with sensitivity to various ranges of wavelengths; hence the cones enable us to distinguish miscellaneous colors. Only one type of rod is much more sensitive to light than cones, and that's the reason why we cannot recognize colors well in a dim light. A whole retina surface covers approx. 70 % of the inner surfaces of the eyeball and contains approximately 7 million cones and about 75 to 150 million rods.

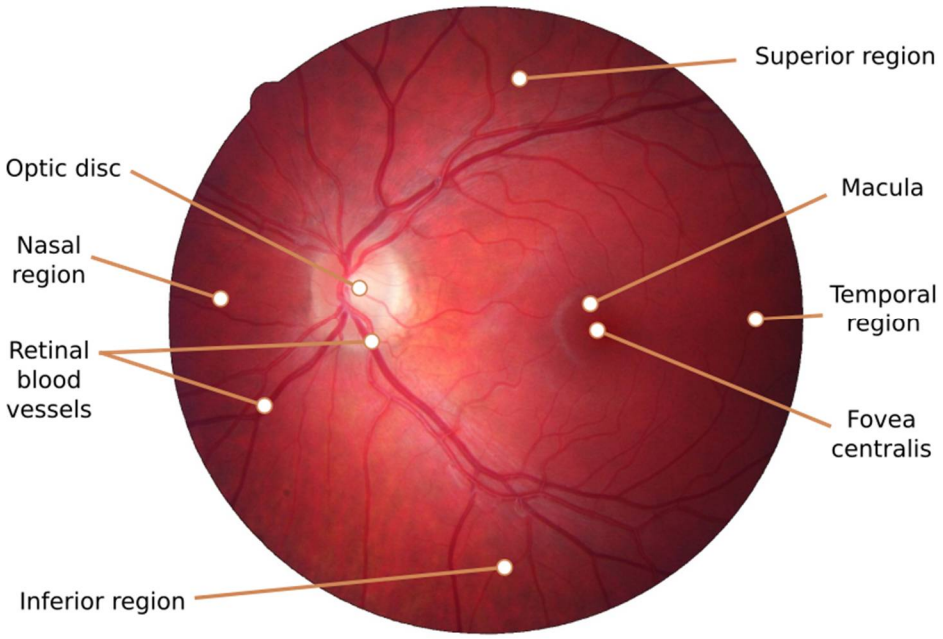

Fig. 2.3: Overview of the retina.

On the retina, there are two most conspicuous structures (see Fig. 2.3) – *optic disc* (blind spot) and a *macula* (yellow spot). The optic disc is actually the head of an optic nerve entering the eye and is also a point where the blood vessels, supplying the retina, come into the eye. On colored fundus images, it has bright yellow or even white color. It has more or less a circular shape, which is interrupted by protruding vessels. Sometimes the shape can be elliptical, which is caused by the non-negligible angle between the level of image and level of the optical disc. The diameter is approx. 1.8 mm and is placed from 3 to 4 mm to the nasal side of the fovea. Optic disc completely lacks any light sensitive cells, so if the light reaches this place, it cannot be visible for the person. In this case, the missing part of the object is completed by the brain (that is why it is also called *blind spot*). We can easily convince ourselves about the existence of blind spot. A test is shown in Fig. 2.4.

Fig. 2.4: Blind spot test.

When observing the cross with the right eye while the left eye is closed, at a certain distance from the image, the black circle disappears. This is exactly the moment when the image is depicted on the optic disc.

On the other hand, the macula is an area of the sharpest vision. It has a circular shape with a diameter of approx. 5 mm, and contains a high density of photosensitive cells, and cones predominate. In the fovea, there are cones only (no rods). Cells density decreases with distance from the macula to the rest surface of the retina. Interestingly, the name "yellow spot" is not derived from the color of the macula (which is rather dark red), but is according to its color observed in the eyes of dead people. The retina itself is a tissue with a thickness of 0.2 – 0.5 mm. It is described with several layers as shown in Fig. 2.5.

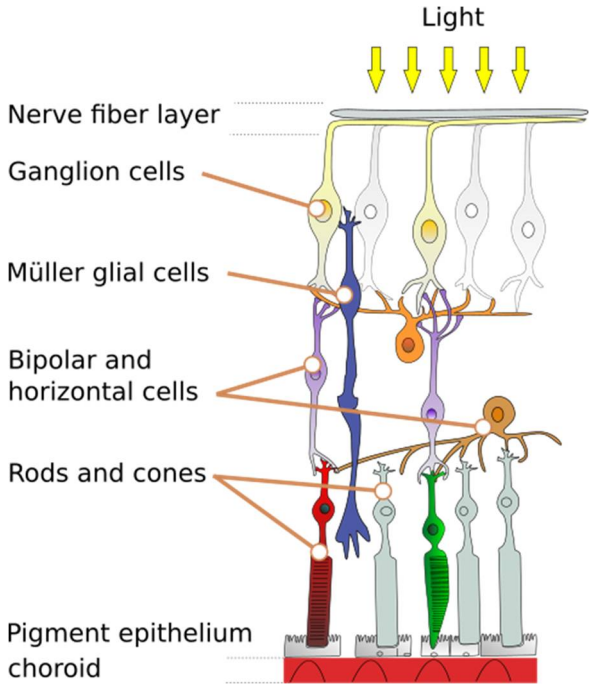

Fig. 2.5: Retinal layered structure (modified from [11]).

Light first passes through the optic fiber layer and the ganglion cell layer where the most amount of nourishing blood vessels is located. The light is transferred through the layer by Müller glial cells that act as optic fibers, and then is received by the photoreceptor cells, cones, and rods which convert the light into the nerve impulses sent through the nerve fibers and optic nerve to the brain. The absorption of photons by the visual pigment of the photoreceptors is firstly translated into a biochemical message and then an electrical message stimulating all the appropriate neurons of the retina. Nourishment of the photoreceptor cells is ensured by the layer of retinal pigment epithelium cells which are fed by blood vessels in the choroid.

2.1.2 Anatomy of the iris

The *iris* is a front colored part of the eye which is not hidden inside and can be observed by the naked eye. The annular shape with a central hole called pupil has the same functionality as an aperture of the photo camera – regulating the amount of light coming into the eye. The outer border of the iris is fixed, connected to the ciliary body while the size of the pupil can vary depending on ambient light. The pupil is not located exactly in the middle but is a little bit moved down, and separates the anterior chamber from the posterior chamber. The pupil appears to be black because no light is coming from the eye.

On the back side of the iris lies heavily pigmented layer – epithelium – preventing excessive light from entering the eye. The pigment that gives the iris its color is called melanin. The amount of melanin

gives the unique color of the iris. If less, long wavelengths of light are absorbed and short wavelengths are reflected thus, the eye seems to be blue. On the other hand, more amount of melanin causes brown color [1].

The iris can be divided into pupillary zone and outer ciliary zone. The size of the pupillary zone is given by the maximal size of the extended pupil. These areas are separated by a meandering circular ridgeline called *collarete*. Pupillary margin is encircled by fibers of sphincter papillae muscle lying deeply inside the stroma layer. Contraction of the sphincter causes pupil constriction which subsequently results in so-called contraction furrows in the iris. The depth of these furrows depends on the dilation of the pupil caused by the action of the dilator muscle which belongs to the anterior epithelial layer. The dilator muscle fibers are arranged in a radial pattern ending at the root of the iris. Another artefact giving the iris its typical structure are *crypts* occurring adjacent to the collaret, and smaller crypts are located on the iris periphery. The surface of the iris comprises a relatively high amount of structural and circular furrows, pits and contraction folds. All the described features contribute to a highly detailed iris pattern that is very diverse across human population. While some biometric traits change with age, the iris stops developing around the age of two years [124]. In the case of twins, iris recognition has an advantage over face recognition. Monozygotic twins may be nearly identical in terms of facial features, but their irises are highly likely to display several differences in texture.

It is also interesting to note that it was claimed that each area of the body is represented by a corresponding area and patters, colors and other characteristics in the iris of the eye. This technique is called *iridology* [122]and can be used to determine information about general health of the person. However, this practice has never been proven as a reliable medical examination method because it makes no anatomic or physiological sense, and well controlled scientific evaluation of iridology has shown entirely negative results.

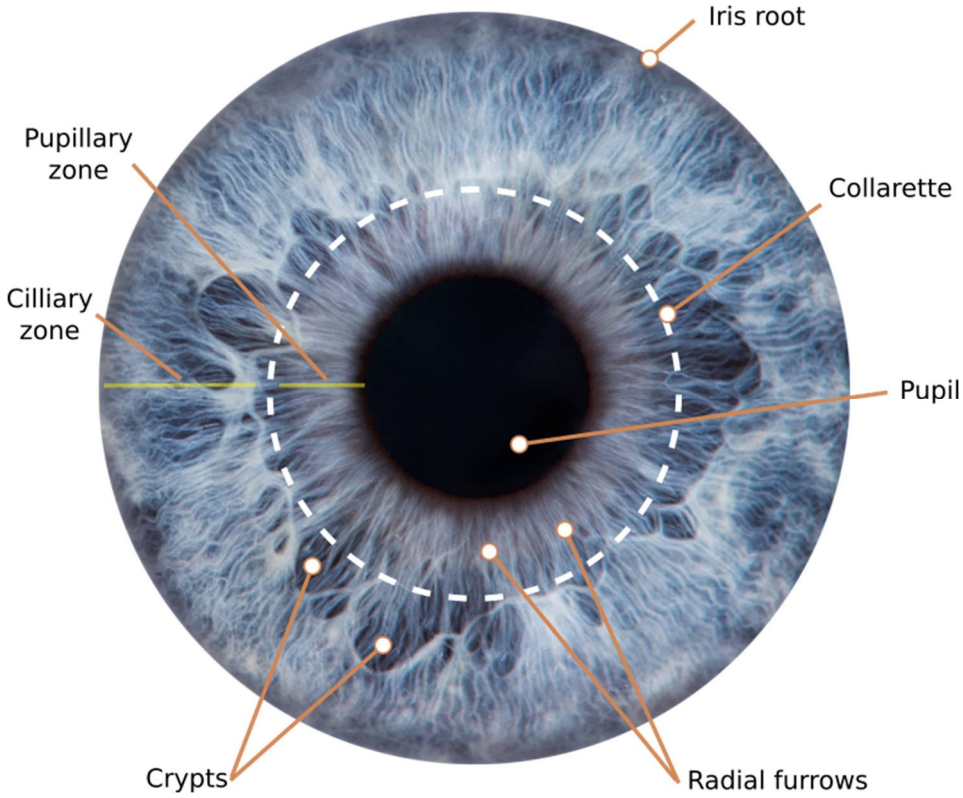

Fig. 2.6: Detailed iris anatomy.

2.2 Iris recognition

Iris recognition is currently one of the most secure technologies for access control systems. Due to the fine and unique texture of the iris, the probability of having the same iris texture is around 1 in 10^{78} [101], thus ensuring sufficient coverage of the population. However, the fact that the iris is located visibly, and it is possible to take a photo from a distance of some meters, the risk of the iris pattern copy and subsequent counterfeit is relatively high. Hence, there should always be some additional security mechanisms (e.g. liveness detection) for high-secured access control.

2.2.1 History of iris recognition

Although the patented and currently used algorithms have been introduced relatively recently, the concept behind iris recognition has a much longer history. The first idea about using pattern or coloration of the iris for recognition was published in 1886 by Alphonse Bertillon who mentioned in his work that "the features drawing of the areola and denticulation of the human iris" can be used for human recognition [5]. In 1936 the ophthalmologist Frank Burch proposed the concept of the method for individual recognition using iris patterns. However, since that time, it took more than six decades until two American ophthalmologists Dr. Leonard Flom and Dr. Aran Safir proposed and managed a patent for the iris identification concept in 1987. The concept was introduced, but they had no algorithms or implementation, and so their patent remained unrealized. Thus after two years, they approached Dr. John Daugman from Harvard University to develop algorithms for automatic and fast identification based on human iris. He formulated three characteristics which determine the iris as an ideal organ for recognition [41].

- It is an inner organ of the body very resistant to external influences.
- It is practically impossible to change its structure without causing eye damage.
- It is physiologically responsive to light, which allows to perform the natural liveness tests.

Dr. Daugman was awarded a patent for automated iris recognition in 1994. One year earlier, Defense Nuclear Agency of United States started to work on a prototype of iris recognition system which has been successfully completed and tested in 1995 thanks to the effort of doctors Flom, Safir, and Daugman. In the same year, the first commercial product became available [6]. The patented algorithms became widely licensed by several companies, and research on many aspects of this technology and alternative methods has exploded to rapidly growing academic literature on related topics – optics, sensors, computer vision, security, etc.

2.2.2 Daugman's algorithm

The algorithm invented by Dr. John Daugman was the first patented and subsequently deployed approach for automatic iris recognition system. It was the most significant milestone in iris recognition technology. Although patented more than 10 years ago, its principles are still used by some current iris recognition technologies.

The algorithm uses 2D Gabor wavelet transform. Each particular pattern on the iris is demodulated to obtain phase information for features extraction. Information is encoded into *Iris Code* bit stream, stored in databases allowing search at speeds of millions of iris patterns per second on a single CPU.

The first step of Gabor demodulation is locating the iris in the scanned picture. The iris must be scanned with high quality so that it can be mapped into phase diagrams containing the information about the iris position, orientation, and the number of specific identification attributes. It is then possible to

compare it with the database using a pattern once the extraction is done. The principle of Daugman's algorithm is depicted in Fig. 2.7.

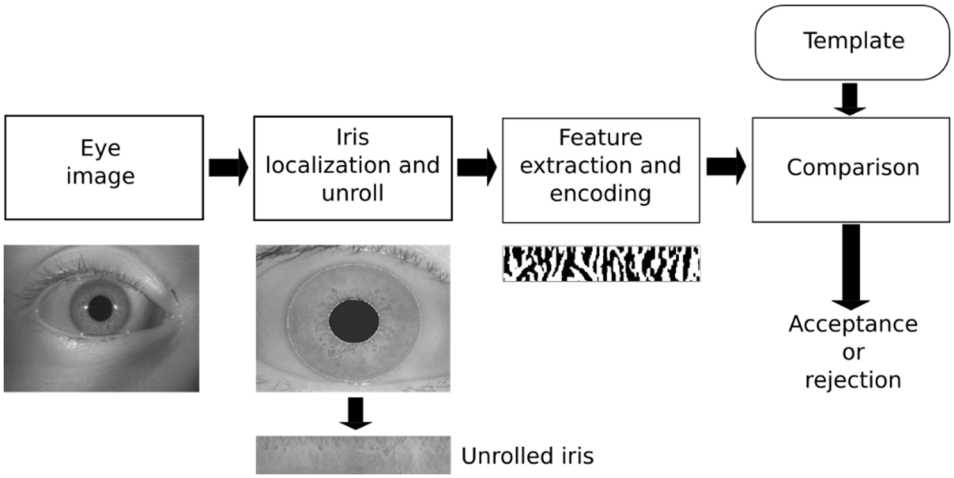

Fig. 2.7: Identification process according to Daugman's algorithm.

Firstly, the iris and its radius are located in the picture. It is done using the following operator [125]:

$$max_{(r,x_0,y_0)} \left| G_\sigma(r) \frac{\partial}{\partial r} \oint_{r,x_0,y_0} \frac{I(x,y)}{2\pi r} ds \right| \tag{2.1}$$

where $G_\sigma(r)$ is Gaussian function of smoothing according to σ, $I(x,y)$ is the rough input picture and the operator searches for the maximum in blurred partial derivation with attention to radius r and middle coordinates (x_o, y_0). The operator is basically a circular edge detector and returns the maximum if the potential circle shares the middle of the pupil and the radius. Examples of located irises are shown in Fig. 2.8.

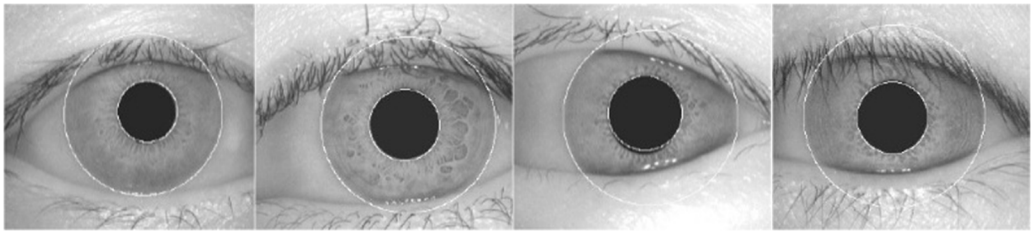

Fig. 2.8: Examples of located irises [14].

Another step is an eyelid localization. Using similar procedure as the one used when locating the iris – the exact position of the upper and the lower eyelid is found. Part of the previous formula used to detect the outline is changed from circular to arched, while parameters are set according to standard statistical methods of estimation so that they ideally correspond to each of the eyelid edges. Examples of located eyelids are shown in Fig. 2.9.

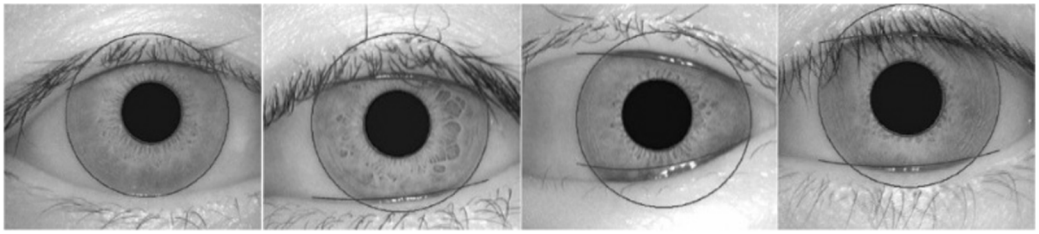

Fig. 2.9: Examples of located eyelids [126].

2.2.2.1 Daugman's rubber sheet model

Daugman's rubber sheet model maps each point inside the iris into polar coordinates (r, θ), where r is in interval $\langle 0,1 \rangle$ and θ is the angle in interval $\langle 0,2n \rangle$.

This model compensates pupil dilatation and size inconsistency thanks to the use of polar coordinates system which is invariant towards a size and translation. The model, however, does not compensate for rotational inconsistency, which is handled by the moving of the iris template in direction θ during comparison phase until both templates match together. Polar coordinate system usage is shown in Fig. 2.10 and Fig. 2.11.

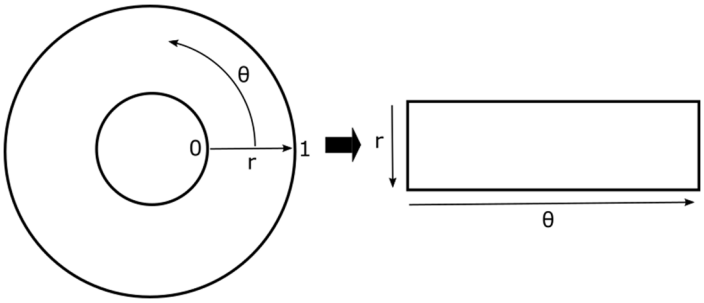

Fig. 2.10: Iris and pupil centers are coincident (modified from [128]).

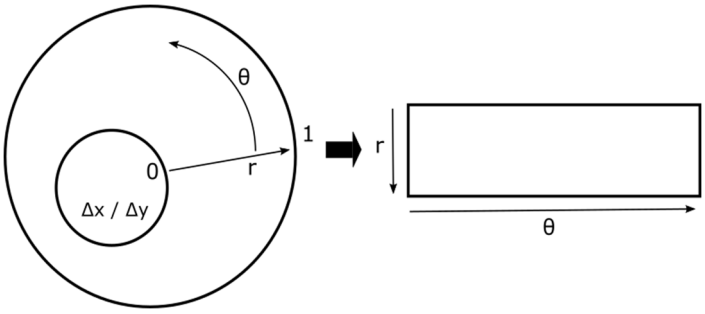

Fig. 2.11: Iris and pupil centers are not coincident (modified from [128]).

2.2.2.2 Iris features encoding

Gabor filter in polar coordinate system is defined as [129]:

$$G(r,\theta) = e^{j\omega(\theta-\theta_0)} e^{-\frac{(r-r_0)^2}{\alpha^2}} e^{-\frac{(\theta-\theta_0)^2}{\beta^2}} \tag{2.2}$$

where (r, θ) indicates the position in the picture, (α, β) defines effective height and length and ω is filter's frequency. Demodulation and phase quantization is defined as [125]:

$$g_{\{Re,Im\}} = sgn_{\{Re,Im\}} \iint_{\rho\emptyset} I(\rho,\emptyset) e^{j\omega(\theta_0-\emptyset)} e^{-\frac{(r_0-\rho)^2}{\alpha^2}} e^{-\frac{(\theta_0-\emptyset)^2}{\beta^2}} \rho d\rho d\emptyset \tag{2.3}$$

where $I(r, \phi)$ is the rough iris picture in polar coordinate system and $g_{\{\mathrm{Re,Im}\}}$ is a bit in the complex plane that corresponds to the signs of real and imaginary parts of the filter's responses. Illustration of the whole encoding process is shown in Fig. 2.12.

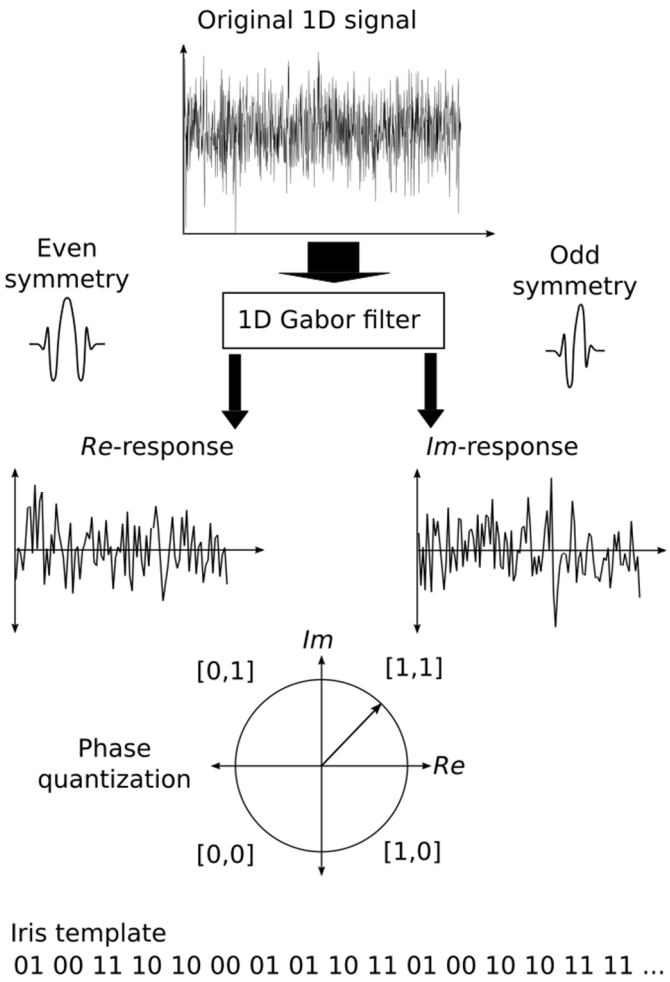

Fig. 2.12: Encoding process illustration (modified from [130]).

Iris' code contains 2,048 bits – that is 256 bytes. The size of input picture is 64 × 256 bytes, the size of iris' code is 8 × 32 bytes and the size of Gabor filter is 8 × 8. An example of the encoded iris information contains Fig. 2.13.

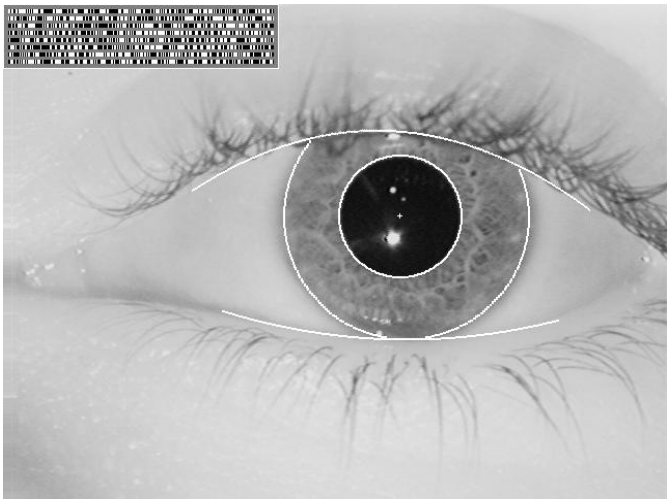

Fig. 2.13: Iris code example [125].

2.2.2.3 Iris codes comparison

The comparison is done by calculating the Hamming distance between both 256-byte iris codes. Hamming distance between iris code A and B is defined as the amount of exclusive sums (XOR) between individual bits [41]:

$$HD = \frac{1}{N}\sum_{j=1}^{N} A_j \otimes B_j \tag{2.4}$$

where $N = 2{,}048\ (8 \times 256)$, if the iris is not overshadowed by an eyelid. In that case, only valid areas are taken into consideration when calculating Hamming distance.

If both samples are obtained from the same iris, Hamming distance is equal or nearly equal to zero, thanks to high correlation of both samples. To ensure rotational consistency, one of the samples is shifted left or right and each time the Hamming distance is calculated, the lowest Hamming distance is then considered as a final result of the comparison. An example of iris code comparison is shown in Fig. 2.14.

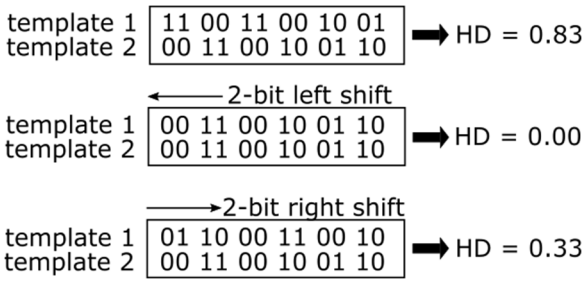

Fig. 2.14: Iris codes comparison.

2.2.3 Characteristic of the iris recognition technology

A selection of characteristics related to the suitability of iris recognition is listed below.

2.2.3.1 Acceptability

Acceptability of identification using the iris is on a middle level as no immediate interaction with the user is needed. The user only needs to stand in front of the device and look in the direction of the sensor from a given distance without moving his head. On the current devices, it takes approximately 2 seconds to scan and evaluate the picture of the user's iris. Systems for acquirement of irises on the fly (during walking) are in development and first versions are available on the market. However these solutions have higher false to acquire rates, because the probability to get a high quality iris sample during walking is lower in comparison with calmly staying cooperative user in front of the acquisition station.

2.2.3.2 Reliability

During iris scan, insufficient information may be gotten because of ambient lighting, eyes not being open enough and so on. However, it is relatively a reliable identification method.

The accuracy of the comparison of two iris samples is defined by the Hamming distance that is, the number of bits that are different in both iris samples. For example, if the Hamming distance is 0.2, two irises differ by 20 %. It is noted that a probability of incorrect comparison is 1:26,000,000, Hamming distance of 0.32 (i.e. about 1/3 same bits from both samples) is sufficient.

Fig. 2.15 shows a distribution of Hamming distances when comparing big amount of irises [18]. The graph creates a binomial distribution with 50 % probability (0.5). It also shows that it is highly improbable that two various irises could differ in less than 1/3 of information.

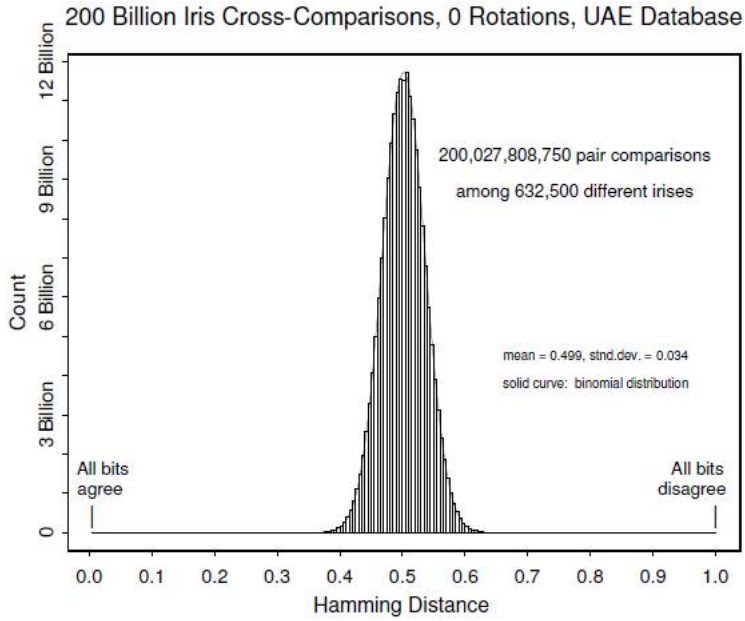

Fig. 2.15: Distribution of Hamming distance [18].

Tab. 2.1 shows the probabilities of false accept and false reject depending on the Hamming distance of two iris patterns. The Hamming distance value 0.342 is a point of equal error rate (ERR) where false accept and false reject rates are the same. This means that if the difference between currently scanned Iris Code record and one in the database is 34.2 % or greater, they are considered to be from two different individuals.

Hamming distance	False accept probability	False reject probability
0.280	1 in 10^{12}	1 in 11,400
0.290	1 in 10^{11}	1 in 22,700
0.300	1 in 6.2 billion	1 in 46,000
0.310	1 in 665 million	1 in 95,000
0.320	1 in 81 million	1 in 201,000
0.330	1 in 11 million	1 in 433,000
0.340	1 in 1.7 million	1 in 950,000
0.342	1 in 1.2 million	1 in 1.2 million
0.350	1 in 295,000	1 in 2.12 million
0.360	1 in 57,000	1 in 4.84 million
0.370	1 in 12,300	1 in 11.3 million

Tab. 2.1: Hamming distances and error rates probabilities [33].

2.2.3.3 Permanence

The iris is an internal organ, and thus well protected, but externally visible. Furthermore, the iris does not change with ageing – one enrollment should be sufficient for a lifetime with the exception of damage due to accident or disease.

2.2.4 Advantages and disadvantages of iris technology

Iris recognition is relatively new among other usual biometric methods, however, it has attracted attention from industry, government and also from the army due to its highly desirable properties for personal identification.

External visibility of the human retina ensures a relatively easy scan of its structure. On the other hand, some civil liberties campaigners have voiced concerns about privacy because the iris pattern can be captured from relatively long distance (up to tens of meters) without any cooperation and knowledge of the person.

2.2.4.1 Advantages

- **Pattern permanence** – iris pattern is well protected and stable through the whole life of an individual. It is not prone to external influences, unlike the face, hand or fingers. However, the iris can still be affected by eye diseases like diabetes or some other serious disease causing alternations in the iris.
- **Uniqueness** – remarkable uniqueness of the iris is given by richness of texture details – crypts, coronas, stripes, furrows etc. Even genetically similar people have totally different iris texture.
- **User friendliness** – iris is an externally visible organ and enables scanning from distance without any close interaction with a sensor. It requires minimal cooperation with the user. It also makes the recognition more hygienic in comparison to touch based biometrics such as fingerprint recognition.
- **Speed and scalability –** iris region images can be normalized into rectangular regions of fixed size thus, fixed length feature codes can be extracted extremely fast, and matching can be performed easily by the XOR operation. For this reason, the iris recognition is very suitable for large deployments with databases of thousands of users.
- **Relative simple liveness detection (anti-spoofing)** – is given by natural physiology of changing pupil size depending on ambient light or by eye movement called hippus [21].
- **Robustness** – iris recognition system is well resistant to changes in the external environment. For example, voice recognition cannot be processed properly with excessive background noise.

2.2.4.2 Disadvantages

- **Fear of eye damage** – one of the main disadvantages of using iris recognition system is that the user has to trust the system because sometimes it is said to be a harmful system when using it for a longer period time because the iris is constantly being scanned by infrared light.
- **Price –** e.g. widely used fingerprint recognition is much cheaper in general. However, iris recognition is still one of the most accurate biometrics and the prices for devices are dropping down each year, because of increasing amount of installations worldwide.
- **Reliability** – iris recognition can be easily affected by the use of contact lenses or glasses, eyelashes or reflection from the cornea and this often results in false rejection of the user.
- **Security** – it can be quite easy to counterfeit an iris sensor. An attacker needs to have iris pattern obtained from a user (is possible to take iris picture from a distance without any user cooperation and awareness) and print the pattern or make a fake contact lenses. For better security, the system has to be equipped with liveness detection (anti-spoofing).

2.2.5 Related standards

- *ANSI INCITS 379-2004: Information Technology - Iris Image Interchange Format*. This standard describes the format for transmitting visual information about the iris. This includes attribute definition, data record and samples, and matching criteria.
- *ISO/IEC 19794-6:2011: Information technology – Biometric data interchange formats – Part 6: Iris image data*. This standard defines two alternative formats for data representation. The first is based on direct saving into uncompressed format, the second one requires some pre-processing. However, data is compact and contains only information regarding the iris.

2.2.6 Commercial applications and devices

Many examples of practical usage do exist. These systems are most widespread in the United Arab Emirates, where they are used in airports and ports (c. 3.8 million comparisons daily). Another example can be the system at Schiphol Airport in Netherlands used by people with high flight frequency. In Czech Republic, this system has not been deployed yet for a practical larger scale application. Another non-critical example of use is at El Salvador Sugar Mill [136] where the clatter of time clocks has been replaced by a quiet time-and-attendance system based on iris recognition. The lines have been reduced and time fraud eliminated. In Afghanistan, UNHC (United Nations High Commission) uses iris recognition to control immigrants from surrounding countries.

Relatively large numbers of devices that are capable of iris recognition are currently available on the market. Some of them (just small selection) are mentioned below.

BM-ET200/BM-ET330 (Panasonic)

Panasonic BM-ET200/BM-ET330 [34] offers small wall mounted recognition device able to enroll up to 5,025 users depending on the mode the device is operating in. Templates are stored locally in ciphered internal memory. The number of users can be higher in the case of using Ethernet network deployment with database stored and maintained on the central server. Recognition time is 0.3 second with scanning distance of 30 – 40 cm. Supported operation modes are (a) 1:N – identification mode (one to many), (b) 1:1 – verification mode based on PROX Card or PIN input or iris data from local cache or server database (c) 1:1 verification with smart card (d) standalone-built-in web server for enrollment.

Fig. 2.16: Panasonic BM-ET200 [34].

IrisAccess 4000 (LG Electronics)

LG IrisAccess 4000 [35] offers iris recognition technology which can be easily integrated into current security systems through common Ethernet, USB or serial connection but local template database is not possible. The devices scan both irises and a variety of authentication modes can be configured

for the right, left or both eyes at the same time. Its optical system is also prepared for multi-biometric use allowing facial recognition. However, this has to be handled by external third party application. Scanning distance is 25 – 37 cm and offers a standard "one-to–many" identification mode with identification time from 1 to 2 seconds.

Fig. 2.17: IrisAccess 4000 [35].

iCAM D1000 (Iris ID)

Iris ID Systems Inc. is the key developer and driver of the commercialization of iris recognition technology since 1997. The recognition system iCAM D1000 is the sixth generation, and thousands of them are deployed in different countries worldwide. It is a 1,082 mm height wall mount device with autonomous positioning system for variously tall people. Straight interaction with the device is not required – scanning distance is 75 cm (±20 cm). It is able to capture the face and iris images in 2 – 3 seconds (dual capture) and transfer them to PC equipped with recognition software [119].

Fig. 2.18: iCAM D1000 [119].

BO 2120 EVM (Iritech, Inc.)

Another well-known player in the field of iris recognition technology is a company Iritech, Inc. offering Monocular or Binocular iris recognition devices and OEM modules ready to be integrated into existing product lines. An example of hardware module is an evaluation kit BO 2120 EVM [131]. It is

a small monocular system working in near infrared light spectrum with scanning distance of 5 cm and encrypted internal memory for up to 1,000 iris templates. Matching query against full memory of templates is within less than 0.5 second. Available application programming interface for several programming languages allows fast integration into a new or into the current devices where is a requirement for iris recognition technology.

Fig. 2.19: Iritech BO 2120 [131].

2.3 Retinal recognition

According to available information, the retina recognition is not currently used in practice at all. This is caused by several factors, e.g. complicated optical system, price, and low user-friendliness. Retinal recognition has clear advantages in uniqueness, a number of features compared to other biometrics (up to 400), and also, it is the only place in the human body with the possibility to observe the blood vessels non-invasively and directly. Also, no standards for retinal recognition currently exist; however, it is basically the image of the blood vessels similar to the one used in the recognition using hand or finger blood vessels. Tests of the first constructed device for retinal recognition reported no false accepts and three attempt false reject error rate (the user is rejected if a match is not found in three trials) of less than 1 % [3]. Any counterfeit of the retinal recognition system is very difficult, because, in the first step, the attacker should get a retinal image, which is not possible without user cooperation and awareness. In the second step, the attacker would have to imitate an optical system of the eye so that the biometric system could perform a scan of the retinal fake.

Human recognition which uses the pattern of blood vessels on the back of the eyeball is a very specific branch of biometrics. Although retina based technique of identification is often perceived as a very secure biometric approach, this method is not widely used due to a few major disadvantages. One of them is related to security. The retina is located inside on the back of the eye, and it is technically difficult and inconvenient to acquire the retinal image. The retina is not a visible part of the human body in comparison to iris or face, which allows being captured even from longer distances. In this case, it is necessary to have an appropriate optical system which is able to focus the whole eye through the pupil and take a picture of the retinal part. This process leads to complicated and expensive optic device.

On the other hand, it is very hard to counterfeit such recognition because the attacker would have to obtain a retinal image from the relevant individual and simulate an optical system of the eye.

2.3.1 History of retinal recognition

In 1935, ophthalmologists Carleton Simon and Isidore Goldstein who have been exploring eye diseases have found out that the pattern of blood vessels of the retina is different and unique for each individual. They have subsequently published a paper about using retinal blood vessels pattern as a unique pattern for identification [4]. Their research was also supported by Dr. Paul Tower who published a paper dealing with the study of twins in 1955 [5]. He found out that retinal vessels pattern gives the lowest similarity among other biometric patterns also for monozygotic twins. At that time, the idea of recognition based on retinal vascular pattern was relatively timeless.

With the concept of simple fully automated device that is able to acquire a retinal image and verify a user's identity came Robert Hill in 1975 – founder of EyeDentify, Inc. company, and gave immense effort for its development. However, a fully working device was introduced into the market after several years.

In that time, several other companies have been trying to use available medical fundus cameras and modify them for identification purposes. However, these cameras had several essential disadvantages, e.g. relatively complicated system for eye and device optical axes alignment, illumination in visible spectrum which was uncomfortable for a user and last but not least high price of medical fundus cameras.

Another attempt led to using illumination in a non-visible spectrum (infrared). For these rays is an eye almost transparent except choroid that reflects it back creating blood vessels pattern. Infrared illumination is not visible to human (thus is more user-friendly), and when the eye is illuminated in infrared range, the pupil is not contracted, and thus, it is possible to acquire larger surface of the retina thanks to a wider field of view.

The first working prototype was created in 1981. Camera optical system using infrared illumination was connected to a personal computer for pattern analysis. After intensive testing, an algorithm of simple correlation was chosen as the most suitable. After another four years EyeDentify, Inc. introduced the standalone product EyeDentification System 7.5 into the market which has been able to identify a person based on the retinal image and the PIN code stored in the internal database. The device was performing a circular scan of the retina using low-intensity infrared light resulting in a contrast feature vector. The image was composed from 256 12-bit logarithmic samples reduced into the record of 40 bytes for each eye.

2.3.2 EyeDentification System 7.5

The development of retinal recognition device was led mainly by EyeDentify Inc. company. This corresponds also with numerous obtained patents in this field. The first usable retinal recognition device was introduced in 1981. The product was called EyeDentification System 7.5 and continual improvement of the technology for another 5 years was finished by a system with three registration modes, verification, and identification. Functional principle of the device can be divided into three non-trivial subsystems [26]:

- *Picture, obtaining and processing signals* – optical system and camera must be able to capture an image of the retina in digital form that is suitable for the following processing.
- *Comparison* – the program in the device or in the computer extracts key features from the scanned image and compares these with the samples in database.
- *Representation* – every retinal pattern has to be represented in a way that can be quickly compared or saved into the database.

2.3.2.1 Optical scanning system

The mechanical construction of an optical device is a complex issue. It is the most important part of the recognition device because the quality of an input image cannot be increased by the following processing in any way, or it is minimally very difficult to enhance the quality. It is evident that the scanning device works on a principle of medical optical devices for eye examination. These so-called retinoscopes or fundus cameras are relatively complex devices, and that is reflected in their price.

Its principle is still similar to retinoscope where a light beam is focused on the retina, and a reflected light is captured by a CCD camera. Retinoscope's light beam is set so that the eye lens focuses it as a point on the retinal area. The focused part reflects a part of the sent-back light beam to the eye lens, which modifies it again, the light beam leaves the eye under the same angle as when entering eye (reversible image). By this way, it is possible to get an image of the eye surface about 10° around the visual axis.

First products of the company EyeDentify, Inc. were using a relatively complex optical system with rotary mirrors for covering the scanned area on the retina. This system is described in a patent US 4620318 "Fovea-centered eye fundus scanner" from 1983. The device was performing a circular retinal scan, mostly because of the light reflection from the cornea, where points in the middle would be unusable if raster scanning was used. To balance scanning and visual axis, so-called UV-IR cut filters (Hot Mirrors – reflect infrared illumination, but transmit the visible light) and focus point, which the user focuses on, were used. A schematic drawing of the patent can be found in Fig. 2.20. The distance between the eye and optics was about 2 to 3 cm from the scanner. The system of balancing on an optical axis is a pivotal issue and is described more in detail in patent US 4923297 "Optical alignment system" from 1986.

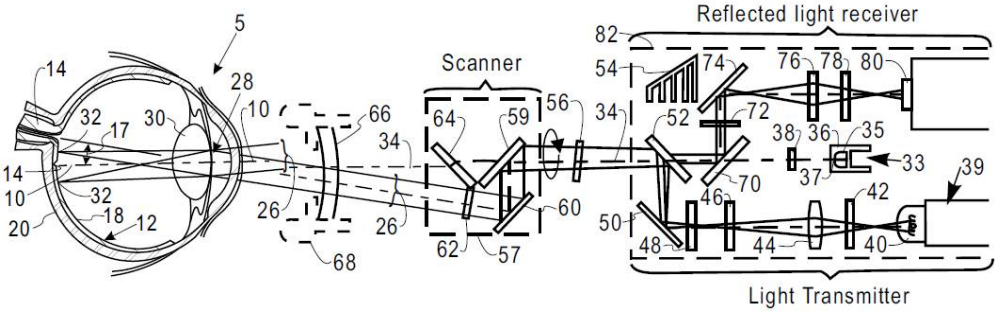

Fig. 2.20: The first version of the optical system used by EyeDentification system 7.5 (from patent US 4620318).

The newer optical system from EyeDentify Inc. is much simpler and also has the advantages of optical axis fixation with lower effort of the user needed, compared to the previous system. Its crucial part is the rotary scanning disc, which carries multifocal Fresnel lenses. This construction is described in patent US 5532771 "Eye fundus optical scanner system and method" from 1993.

To ensure that the scanned area is focused on the retina and that the user's eye lies on the scanning beam axis, fixation point/target, on which the user focuses his eye and which must stay in approximately same position for whole scanning, is used. That can be a series of optical networks with focal lengths of -7, -3, 0 and +3 diopters. It is assumed that the most users will be able to focus regardless of their optical defect. When the eye focuses on the target, the device is automatically balanced into the axis of the centered rotary disc on the eye fundus. If the user aligns two or more fixation patterns in one axis, infrared beam is centered on his pupil and the information can be read.

2.3.2.2 Comparison

Whenever the user is looking into the optical system's scanning camera, his head can be rotated slightly from the original scanned position during enrollment. Rotation algorithm (phase corrector) is capable of rotating the data by few degrees. This process is done multiple times until the best possible match is reached (highest correlation).

Comparison of obtained samples is done in a few following steps:

- Using sampling the reference, eye record is transformed into the area with the same number of elements as the obtained area, which ensures the alignment (samples overlay).
- Both areas are normalized so that both have RMS (Root Mean Square) value equal to 1 – intensities are normalized.
- Areas are correlated using a correlation equivalent to the time domain of the Fourier transformation.

The comparison quality is given by the correlation value where the time shift is equal to zero. It is in a range of +1 (absolute concordance) to -1 (absolute discordance). For a real application, experience has shown that the values around 0.7 can be considered as a concordance.

2.3.2.3 Representation

Representation of the retina is derived from an image composed out of annular areas (EyeDentificationSystem 7.5 works on the principle of circular scanning). The size of the scanned area is chosen considering the worst possible scanning conditions (highly reduced pupil), but that is still enough for biometric identification. This means that for these purposes, it is not needed to obtain an image of a too large area and resolution.

In relation to the EyeDentify, Inc. device, two main representations of retinal pattern have appeared [20]:

- Original representation has 40 bytes. Those contain information about contrast, coded using real and imaginary coordinates of frequency spectrum generated by Fourier transformation.
- New representation has 48 bytes. It does not contain information about contrast in the time domain. The main advantage of time representation is its faster and more effective processing with lower demands on computing performance.

The template of the retinal pattern contains an area of 96 four-bit contrast numbers from 96 scans of concentric circles in the time domain, i.e. $96 \times 4 = 48$ bytes. Intensities of the time domain can carry a value in interval <-8,7>, while normalization on this resolution is used – adjustment to 4 bits of intensive distribution.

2.3.3 Characteristics of the retina recognition technology

A selection of characteristics related to the suitability of retinal recognition is listed below.

2.3.3.1 Acceptability

Compared to the iris recognition in the case of the retina, acceptability is low. Many people are afraid of using this technology. They are convinced that a laser that could cause them an optical defect will be used. These concerns are however absolutely unnecessary because the laser is never used in this case. Another problem is the procedure of getting the retina image itself. It can take longer time depending on the user's cooperation and experience, which could bother some users.

With the retina, direct interaction of the user is also needed (to approach at a distance of few centimeters and focus on fixation points). At least with current methods, relatively big cooperation with the user is necessary. Therefore, the acceptability is really low.

2.3.3.2 Reliability

Concerning the retina recognition, its reliability is high. However, certain conditions during which it is not possible to obtain the retina picture of appropriate quality do exist. That is mainly and particularly, unsuitable ambient lighting during which the user's pupil is too contracted. Other problems come with optical defects and eye dysfunctions.

Retina recognition is not very extensive, which may be the reason why not many objective tests of this method exist. In 1991, a multinational company Sandia National Laboratory [19] tested products of EyeDentify, Inc. on hundreds of volunteers. The result was zero FAR and FRR lower than 1 %. However, at that time, the testing of biometric systems was in its infancy, therefore, we cannot be sure about the test's objectivity.

According to EyeDentify, Inc., the distribution frequency of each eye's pattern that was compared with any other was getting very close to the ideal Gaussian curve with expected mean value of 0.144 and standard deviation of 0.117 [20]. The corresponding probability in this distribution, expected value and standard deviation of threshold rating 0.7 is about 1 to million [20].

The method of retina recognition is very prone to certain conditions, which must be kept during every scanning. Conditions which could increase false reject rate are, for example, incorrect distance between the scanner and the eye, unclean optics, edges of contact lenses, and glasses. Ambient lighting can also result in subconscious pupil contraction, for that reason, it is sometimes not possible to use the scanner outdoor during daylight.

2.3.3.3 Permanence

The biological structure of the retina hardly changes during the lifetime of an individual. However, the recognition can also be influenced by injury of various parts of the eye, e.g., iris, lens or other parts limiting outer access to the retinal surface. Retinal blood vessels pattern can also be affected by several diseases like diabetes, glaucoma, high blood pressure or even heart disease.

2.3.4 Advantages and disadvantages of retinal technology

From all popular biometrics, the recognition by the retina has the most restrictions. They are not insuperable; however, currently, there is no system that can remove these imperfections on a larger scale. Retinal recognition is also affected by high false reject rate because retinal scanning still requires a relatively high user-cooperation which has a tangible impact on the quality of the retinal scan, causing a legitimate user to be rejected.

In comparison with other biometrics, retinal recognition offers relatively high universality, uniqueness, performance and well resistance against frauds. However, retinal recognition systems are still extremely expensive and less user-friendly.

2.3.4.1 Advantages

- **Pattern permanence** – retinal blood vessels pattern hardly changes within the lifetime of an individual.
- **Number of unique features** – the rich blood vessels structure can contain up to 400 unique features. Identical twins can also have significantly different patterns.

- **Protection** – the retina is located inside the eye and thus, is not exposed to threats from external environment. It is well protected and cannot be easily damaged such as fingerprints, hand geometry, etc.
- **Contactless scanning** – sanitary problems are eliminated.
- **Small size of template** – only 96 bytes has a current implementation which is very small in comparison to other biometrics. Thanks to this, it is very suitable for deployment in largely used databases and with a very short processing time.
- **Safety** – the retina is hidden inside the eyeball and is very difficult to acquire a retinal image without user cooperation and awareness. Even though the attacker would know retinal patterns, it is very difficult to imitate the optical system of the eye in order to counterfeit the sensor. After death, the retina degrades very quickly and thus cannot be used in the most cases for accurate post-mortem identification.

2.3.4.2 Disadvantages

- **Fear of eye damage** – low level of infrared illumination used in this type of device is totally harmless for the eye; however, there exists a myth in the general public that these devices can damage the retina. It is required that users are familiarized with the system so that, they can trust to it.
- **Outdoor and indoor usage** – a small pupil can increase false reject rate because the light has to come through the pupil twice (once towards the eye, then out of the eye), and the returning light beam can be significantly weakened if the user's pupil is too small.
- **User friendliness** – the need to approach the eye very close to the sensor and focus the alignment point in the device may reduce the comfort of the device usage more than any other biometric methods. It is also related to sufficiently scanned image quality and using eyeglasses and contact lenses.
- **Strong astigmatism** – people with an optical defect (astigmatism) are not always capable of focusing their eye on a fixation target properly, and thus correct template cannot be generated.
- **High price** – it is expected that the price of the device, especially an optical apparatus for recognition by the retina, will always be higher than for example the price of a device for recognition of fingerprint or voice.

2.3.5 Commercial applications and devices

Retinal recognition has primarily been used in combination with access control to high secured areas. This includes facilities such as nuclear development and plants, weapon development and production, government, military, secret organizations etc. One of the best documented application deployment of retinal recognition was in state of Illinois which used this technology to prevent welfare fraud by identification of welfare recipients [27]. Considering disadvantages only a few companies from all over the world have introduced or been developing retinal recognition systems.

EyeDentification System 7.5 (EyeDentify, Inc.)

The pioneer in retinal recognition development is EyeDentify, Inc. company, which designed and produced the EyeDentification System 7.5 (Fig. 2.21) and its latest model ICAM 2001, which was introduced in 2001.

According to extant leaflet [27], EyeDentification System 7.5 has been equipped by three modes. Recognition operation mode is the retinal pattern of the user compared with all the eye signature templates stored in a local memory, and a person is allowed or denied depending on existing appropriate template in the database. Second, PIN verification mode: compares the user with only one template identified by a PIN number. The device also allows both eyes verification which reduces the chances of false accepts in PIN mode to one in a trillion. The third mode is enrollment and ensures a proper scan of the retina in order to generate a template and store into database. The user has to keep the eye approximately 15 millimeters above the lens focusing on a green visual alignment target. This process normally takes less than one minute.

Fig. 2.21 EyeDentification System 7.5 [28].

In the PIN verification mode, the recognition process takes approx. 1.5 seconds. In the recognition mode with 250 retinal templates stored in a local database, the recognition is accomplished in approx. 3 seconds. The device also provides the following features [27]:

- Stand-alone system or value added component is to increase the security of the currently deployed systems.
- Non-volatile data storage with capacity of up to 1,200 enrollees. The database can be backed up to an external memory.
- System management program control prevents unauthorized users from altering system configuration.
- Average throughput (since first interaction with the device to final acceptance/rejection decision) is from 4 to 7 seconds.
- RS-232 interface for communication with an external system at a speed of 9,600 bits/s or auxiliary port with a speed of 300 – 19,200 bits/s.
- Dimensions 30.5 × 38 × 20.3 cm.
- The price at product release time was 2,500 USD.

ICAM 2001 (EyeDentify, Inc.)

The last known scanning device produced by EyeDentify, the ICAM 2001 [29], was pulled out from the market due to its high price. Users found also the ICAM to be somewhat intrusive. The main difference between the older model was mainly in the size of template database (could handle up to 3,000 retinal patterns) and also the device was much more compact with a dimension of 23.5 × 15.2 × 10 cm. False reject rate was specified by 12.4 % (one try) and 0.4 % (three trials).

The company TPI (Trans Pacific Int.) offered also a scanner similar to ICAM 2001. The product was called EyeKey, however, nowadays no information about it is known anymore. According to [30], the design was exactly the same – from this, it can be concluded that the TPI was presenting the ICAM 2001 as its own product with added value in increased user database to 300,000 users and with 15 second comparison time within all stored templates [29].

Fig. 2.22: ICAM 2001 [29].

Handheld retinal scanner (Retina Technologies, LLC.)

Another manufacturer is, for example, Retinal Technologies, since 2004 known as Retina Systems coming from Boston (US), however, any exact specifications of their system are not publicly available.

Fig. 2.23: Handheld retinal recognition device [121].

One million USD of initial funding received Retinal Technologies for the development of an inexpensive way to deploy retinal scanning using a small hand-held retinal camera that fits into the palm of the hand [121]. The price was set at just 50 USD only, which is much less compared to the solution of EyeDentify, Inc. company. It was claimed that the scanner uses a patented aspheric lens array capable of capturing a retinal image at distances up to three feet from the user's eye based on ophthalmoscope laser scanning. Templates are stored as codes with length up to 60 bytes. It was also claimed that glasses, contact lenses, and existing medical conditions do not interfere with the scanning of the retina. This technology was primarily intended for medical use in hospitals, but its appearance on the security market was also expected. With the recent information found, Retinal Technologies was looking for another two million USD to market the technology [32]. No further information about this product can be found,

and it is very possible that it was a marketing issue only with regard to low price and small dimension of the device totally different from the devices from EyeDentify.

2.4 Multimodal biometric system

In today's world full of security issues, biometrics is an interesting approach. Ideally, the user interacts with a simple interface and in a matter of seconds, the biometric system scans selected biometric characteristic(s) and decides whether the user is allowed to pass or not.

However, such systems are not perfect, and there is always room for improvement. Recently, it has been discovered that a viable course of biometrics may be based on broader use of multi-biometric (multimodal biometric) systems in the future [58] which combine more than one biometric characteristics for evaluation (e.g. such as fingerprint and palm veins), unlike unimodal biometric systems, which use only a single source. The generalized model of a biometric system can be considered as a unimodal biometric system, i.e. such one which uses a single source of evidence for the identification of persons or verification of their identity. In contrast to this model stands a multi-biometric system. As the name suggests, a multi-biometric system uses more than one source of evidence (biometric characteristic) [58].

If designed correctly, such systems can be expected to be more accurate than their unimodal biometric counterparts [59]. Better security counts also amongst the most prominent benefits of multi-biometric systems. By using more sources of evidence, the security of such systems can be substantially improved.

In the case of a unimodal biometric system, specifically, the one which recognizes fingerprints, it might be easy to spoof the sensor with a spoof produced from latent fingerprint and cheat even very intricate liveness detection algorithms [60]. The deployment of a multi-biometric system can effectively prevent this risk by requiring another biometric modality. Multi-biometric systems can also help with situations in which unimodal biometric systems are considered to be discriminative. If an individual lacks a particular trait, or if a trait is severely deformed so that the sensor cannot acquire it, then such individuals might be able to provide another biometric trait, and thus the system may allow them to enroll.

Another advantage lies in the fact that some biometric characteristics, e.g. voice, can be damaged by a noisy data signal. Multi-biometric systems can remedy this inconvenience by using a supplementary algorithm or a different modality.

Multi-biometric systems can operate faster in environments that necessitate a large database. Using more than one biometric trait as search criteria, a database that contains thousands of entries might be scanned more efficiently. For example, one trait would refine the list of potential candidates for an identity match, while another one could be then used to determine the identity from the reduced list [61].

On the other hand, multi-biometric systems are not without disadvantages. Usually, there are several methods of implementing such a system and some perform poorer than others with certain biometrics, while others perform better. It is, therefore, important to contemplate the aims of the system and to design it accordingly.

A multi-biometric system usually brings forth the question of additional cost. Not only does the system have to accommodate additional resources such as a sensor or a chip for a surplus algorithm, but the cost of fusion of the acquired data has to be taken into account as well. Any new biometric trait required from users might also cause significant inconveniences. The question that arises from these facts is whether the costs incurred by the aforementioned are outweighed by the overall benefits of the system [58].

2.4.1 Biometric fusion

An important aspect of a multi-biometric system is the fusion of gathered information. At a certain point during the recognition routine, it is necessary to merge the data into a single entity before proceeding further.

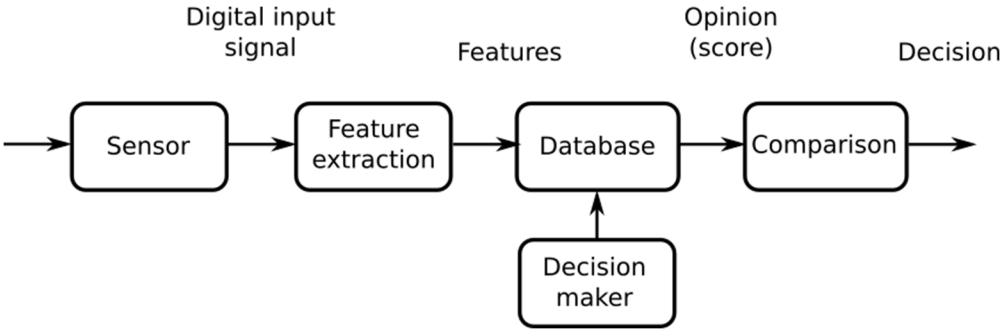

Fig. 2.24: Model of a common biometric system.

This in itself poses a significant challenge in the designing phase of a multi-biometric system development. As shown in Fig. 2.24, there are four separate operations that the system performs. At each of them, fusion can generally be introduced into the system.

It is worth noting that as the data advances through the system, their amount is compressed along the way. However, this does not necessarily imply that the sooner the fusion occurs, the better the results are [62].

While the data at the sensor level are arguably of a larger quantity than those at the feature level, the latter has usually been stripped of superfluous details and noise. On the other hand, it is possible that the feature extraction module may have produced specious results which could have been otherwise remedied at the sensor level.

The classification of biometric fusion is shown in Fig. 2.25.

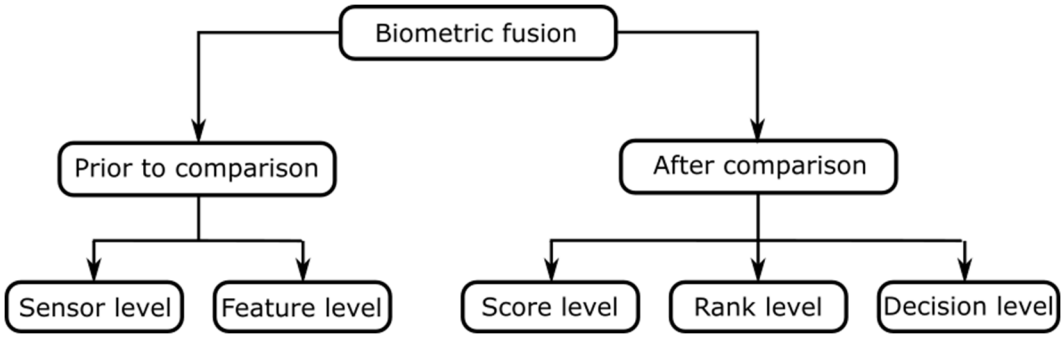

Fig. 2.25: Levels of biometric fusion [66].

Biometric fusion can be broadly divided into two sections – *fusion before comparison* and *after comparison*. The reason for this classification results from the fact that after comparison, the amount of information available to the system decreases by a significant margin which is commonly far greater than, in the other cases [58].

2.4.1.1 Sensor-level fusion

The sensor-level fusion [63] involves joining multiple sources of raw evidence prior to extracting features. This can encompass text, images, videos etc. At this level, the obtained data contain the most information available. In image processing, a particular method of fusion is employed, often referred to as mosaicking. In this process, a composite image is constructed from overlapping component images [58].

2.4.1.2 Feature-level fusion

In the feature-level fusion, sources of evidence are consolidated after features have been extracted from respective samples. Following this, fused feature data is then passed to a feature comparator module and the system proceeds as if dealing with a single source of biometric evidence. Feature sets of distinct modalities or feature sets of identical modalities that have been extracted by different algorithms pose a challenge for numerous reasons [58]. It may be a problem to fuse two chosen modalities, if the basis on which they should be fused is not known. In these cases, it may be difficult to produce a fused set of features that would satisfy the demands on improvement over a unimodal biometric system. This might be exacerbated by the situation in which feature sets of different modalities are not compatible. One of them may vary in length, while the other one may be represented by a fixed-length set of features [64].

2.4.1.3 Rank-level fusion

It should be noted that the rank-level fusion is only applicable in those biometric systems that are set to identify a person, not to verify his/her identity [65]. It is still one of the more frequently applied methods of fusion. After processing the feature vector and acquiring the comparison score, the set of probable matching identities can be sorted in descending order and thus, a ranked list of candidate identities can be created. The aim of this level of fusion is to merge the ranks produced by individual biometric modules in order to get a consolidated list of ranks for each identity.

2.4.1.4 Decision-level fusion

The decision-level fusion is particularly useful in situations where two or more finished biometric systems are available, and they need to be combined [63]. More often than not, the decision-level fusion is the only option in this case.

2.4.1.5 Score-level fusion

Score-level fusion is commonly used and preferred in multimodal biometric systems in general because matching scores contain sufficient information making genuine and impostor case distinguishable and are relatively easy to be obtained. Given a number of biometric systems, matching scores for a pre-specified number of users can be generated even with no knowledge of the underlying feature extraction and matching algorithms of each system.

2.4.2 Bimodal eye biometric system

Biometric systems in real-world applications are usually unimodal and thus can handle only one single biometric source of information (biometric characteristic). Unimodal systems are susceptible to a variety of issues such as intra-class variations, inter-class similarities, noisy data, non-universality, and spoofing. By combining the *iris* and *retina* into one solution, it is possible to get very robust biometric recognition. The most important issue of a biometric system is the uniqueness of its biometric information included in the specific biometric characteristic, which influences the strength of such biometric system. The variability in biometric characteristics of the population can be described by biometric entropy. It is also related to a biometric fusion where they could be needed to quantify the biometric information for each biometric characteristic separately and the possible gain from their fusion.

In addition, the anatomic position allows capturing both images at once. An advantage of a bimodal system is also the variability of modes it can operate in. In the case of any requirement for the high secure system, both biometric characteristics can be processed on the same level of protection. In another case, the quality of scanning can be weighted, e.g., if one of these biometric characteristics is evaluated as less reliable (e.g. because of low-quality image acquisition), the second one is preferred if

scanned properly. It also leads to a significant improvement of FMR (False Match Rate) and FNMR (False Non-Match Rate) and higher reliability for the user – if there is no possibility to acquire one of the biometric characteristics for any reason, the system is still able to recognize him / her on the base of the second biometric characteristic.

The bimodal eye biometric system enables to fuse information at the feature level, matching score level and decision level. We identified several current papers addressing the problem of iris and retina fusion. In [102], the score level fusion of the left and right irises and retinal features is presented. The weighted average of the scores was applied to all possible combinations of the two irises, and equal weights were assigned to each iris. The fused score is then obtained by a linear combination of these two scores. Since two different scores are obtained for the iris and retina, score normalization needs to be performed. Then, the final score is obtained from the scores of fused irises and retinas. Another approach in patent [103] simply attaches both iris and retina codes together. With the mentioned codes, it is possible to perform fusion by logical operations or join them into a bigger one. Several approaches can be used on the image level. For example, we can merge the images and evaluate them (e.g. by Daugman's algorithm). In this case, one of them can be used as a mask for another one and their mutual relation such as angle or color is then computed.

Nevertheless, the first concept of the simultaneous iris and retina recognition in a single device was published by David B. Usher et al. [42] in 2008. However, the algorithms were not described in detail, and the preliminary results were focused mainly on image acquisition. The first device combining the iris and retina in one single device was introduced as a flagship of eye biometrics by Retica Systems Inc. [104] in 2006. The device is described as a combined hardware and software solution which allows capturing and fusing data from both the retina and the iris, creating the most secure and accurate biometrics in industry. Recognition device called Cyclops was dedicated for high level secured utilization such as border security, facilities, military and defense, nuclear plants, etc. Retica Systems Inc. had a plan of selling hardware or software solution or the software licenses for incorporation into existing biometric systems. The hand-held version has been also supposedly under development. However, the whole project was probably a marketing issue only, because the device codenamed Cyclops had never been introduced and brought to the market [8].

In general, a proposal of ocular biometric device can be divided into four parts:

- **Combined optical system** constructed in order to acquire retina and iris images. In the case of the retina, it is very important to get a sharply focused image and suitable field of view with appropriate surface of the retina. This is related to pupil size and ambient light intensity which must be as low as possible preventing contractions of the pupil. On the other hand, when acquiring an iris image, it is very suitable to have small pupil in order to get the larger surface of the iris. The illuminating light forming bright Purkinje reflections [132] within the iris reflects from the exterior and interior surfaces of the lens and the cornea. These have to be suppressed or restricted out of the region of interest (e.g. restricted to pupil region). Unwanted reflections can be a big problem for any optical system in general and has to be kept at minimum including ambient light sources. Optical system also involves appropriate retina and iris illumination which must be with respect to the pupil size and allowed intensity, preventing the eye from damage.

- **Aligning system** to get the eye optical axis in one line with the optical axis of the device. This is very important when acquiring the retina because the beam of light entering the eyeball is limited by contraction of the pupil and thus the required field of view is significantly decreasing with the mutual distance of both axes. This applies mainly for retina imaging. The eye and device axes positions must be such that the imaging axis is targeting the surrounding of the blind spot where the most amount of biometric features such as

vessels bifurcations or crossings are located. Alignment can be done by two approaches or their combination – the user moves the head towards the device focusing a fixation light point built-in in the device, or the device is moved towards the user's eye depending on the feedback from a camera. Illumination during the process of alignment has also to be comfortable for the user with respect to pupil size as mentioned above. Near infrared light is usually suitable. Alignment for the iris image acquisition is not so strict, given that the iris can be captured much more easily even from various distances and angles.

- **Image acquisition** – the first step preceding acquisition is an eye localization and identification of boundaries between the iris and the sclera, and the iris and the pupil which are not usually concentric. Borders estimation is also related to an identification of areas of the iris that are covered by eyelashes, eyelids, and areas of bright reflections. Several methods have been described initially, based on Daugman's rubber sheet model (see chapter 2.2.2.1) [9] or Wildes et al. [10] who also introduced a paper proposal using circular boundary model. Lately, Wildes also presented an algorithm using edge detectors and Hough transforms to segment the eye image, where also, two parabolas were used to find the eyelids. Paper [14] deals with enhanced Daugman's integro-differential method, optimizing its computation time and problem of locating the pupil center outside the image. The same method is improved in [16] optimized for eye tracking. In a paper [17], it presents an approach for fast iris localization using contrast stretching and leading edge detection. Once the iris is localized, and the exact position of the pupil is known, optical axes of the eye and the device must be aligned into one axis. Then is possible to get an iris image and refocus the optical system to be able to take the retinal image. Focusing on the back of the eye has to be in near infrared light spectrum to prevent the iris contractions. However, the focus in infrared range can vary against visible spectrum depending on the used wavelength. In other words, the object focused in infrared range is not focused in the visible spectrum and vice versa. It is a property of optical system, but both focuses (infrared and visible) are in mutual correlation shifted by a given constant. At the end of this localization and focusing process, it is finally possible to obtain proper iris and retinal image suitable for recognition itself. Retina and iris image acquisition requires various optical setup and cannot be performed at one time. After the iris image is obtained, it is important to align optical axes of the optics and eye to acquire the retinal image.
- **Image feature extraction and matching** – this is the last step of identification and in the case of multimodal biometric systems, the extraction is usually followed by some kind of biometric fusion. Features can be joined at different levels of fusion prior to comparison (sensor and feature level) or after the comparison (score, rank and decision level). Feature extraction and matching methods are described in more detail in previous chapters dealing with appropriate iris and retina biometric.

2.5 Eye liveness detection

2.5.1 Iris

During liveness testing of the iris, a few possibilities are feasible. The most common is the reaction of the iris to lighting changes when the pupil is stretching at lower and contracting at a more intensive light. This reflex is subconscious and the reaction time is usually between 250 to 400 milliseconds.

The pupil contracts and stretches a bit also, under permanent light conditions – this periodical effect is called hippus [21].

Another form of liveness detection can be performed by eye movement or winking according to scanner's voice commands.

Measurement of spectrographic attributes of tissues, fats and blood, are used by more modern devices. Blood reflects very well in the infrared illumination as well as pigment melanin in the iris. This effect is called coaxial back retinal reflection, called the 'red eye effect' during photography, where the light is reflected back to a camera if strong light is used.

Purkinje reflexes from the retina, and the lens surface can be also used for eye liveness detection. When the outer eye surface is illuminated by an appropriate light source, under certain conditions, an image reflected from the front, and back retina surface can appear on the inner surfaces of the eye.

2.5.2 Retina

Retinal imaging is a relatively difficult process that cannot be easily imitated. To counterfeit that kind of scanner, it would be necessary to use very accurate model of eye optics with the same attributes as real eye, which is very difficult and almost impossible. Not many information about retina liveness detection exist; however, it is possible to use again medical information, e.g. inanimate retina has a different color. The light reflectivity of the retina or blood flow in blood vessels can be also detected.

Since the eye is a very sensitive organ, we cannot use any invasive method. Reciprocal liveness detection similarly to iris can be used. However, such detection system could be counterfeit, if after successful liveness detection a real eye is changed for the fake one. For that reason, it is better to test the liveness using various methods. The first method is detection the color of the macula. By this test, one can find out if the detected eye is living or dissected. Only after death that the macula becomes yellow; until that, it has a reddish color.

Another possibility is liveness detection based on eye movement. A similar principle is used in medicine during eye fundus examination. A medical doctor needs to see the whole retina and not only a part which can be seen from a direct view. Therefore, the device is equipped with a focus point which a patient looks at and towards which he moves the eye so that nearly the whole retina can be seen. This can also be utilized in liveness detection. The device is equipped with a similar focus point and in a few times is randomly moved. During each move, the retina is scanned, and the blind spot or macula position is compared. If the position is varying on each picture, the eye is evaluated as living.

2.6 Eye diseases

Every part of our body can be affected by a disease during our lives, whether it is curable or incurable. By incurable disease, we will understand the kind of disability that cannot be eliminated surgically or anyhow else without consequence in the form of loss of biometrical information (e.g. amputation). Curable disease, on the other hand, is removable with minimal consequences (e.g. inflammation, laceration). The retina can be affected by both types of diseases, of course.

For a long time, the eye was an organ that was on the first look dark and untouchable. This started to change in the mid-19th century thanks to the discovery of ophthalmoscope. Using an ophthalmoscope, it was possible to see the big part of the inner eye. By examination of the eye's background, eye specialists can check the rear part of a patient's eye and determine its health condition. For this eye fundus examination, ophthalmoscope is used. Equipped with rotary lenses, it allows the zooming of individual parts of the retina up to 15 times.

This chapter also describes the most spread diseases of the retina which is much more likely to get sick than the iris.

2.6.1 Equipment for retinal examination

2.6.1.1 Direct ophthalmoscope

While using the ophthalmoscope, the patient's eye is examined from a distance of few centimeters through the pupil. Currently, several types of ophthalmoscope are known, however the principle is essentially the same: the eyes of both the examinee and the doctor are on one axis, and the retina is lighted by a light source that incidents on a semi-transparent mirror or a mirror with a hole located in the observation axis at an angle of 45° [12]. The disadvantage of a direct ophthalmoscope is the relatively small examination area and the need of skill to operate, and also the cooperation of the patient. The field of view (FOV) for this device is approximately 10 degrees. To increase the angle when observing the eye with a direct ophthalmoscope, different approaches can be used. These include placing the device as close to a patient's eye as possible or dilating the pupil. The principle of direct ophthalmoscope is shown in Fig. 2.26:. The light beam falls on a small part of the pupil and does not overlap the observing ray, which minimizes the probability of disruptive reflections. The light beam is shown by yellow line, the observing ray is purple.

Complete techniques of ophthalmoscopy were published by a Czech scientist Jan Evangelista Purkynje in 1823. For the following 25 years, many people with miscellaneous specializations were working on creating an ophthalmoscope, but the first usable ophthalmoscope was introduced by Hermann von Helmholtz in 1851. He managed to do it based on the work of Brucke, who however had not been able to explain, what the picture of the final rays that enter the observed eye and then come out of it was.

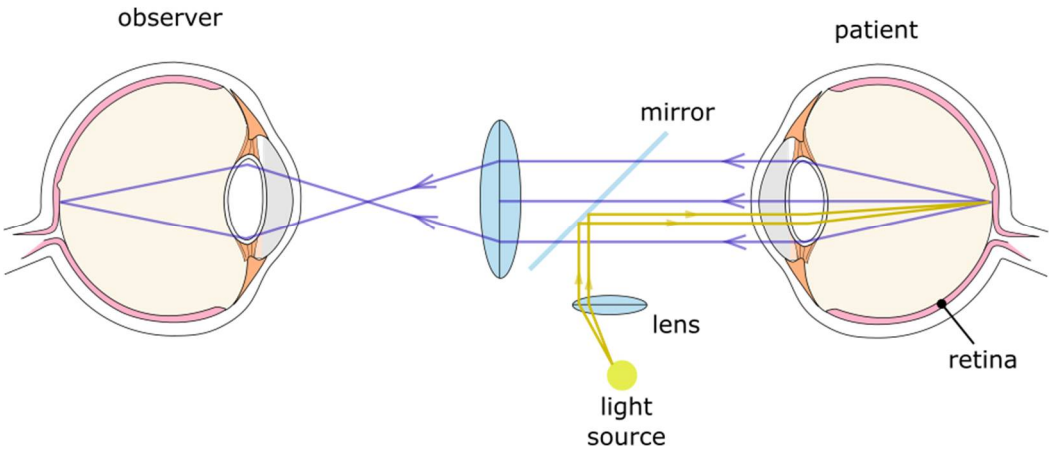

Fig. 2.26: The principle of direct ophthalmoscope [84].

2.6.1.2 Binocular indirect ophthalmoscope

Most of the important red and yellow details in the retina such as vessels, hemorrhages, or exudates are visible against light red background of blood-filled eye choroid. Subtle and with the naked eye nearly invisible changes can be important symptoms of an ongoing disease. Even better results with direct ophthalmoscope can be achieved with binocular indirect ophthalmoscope [84] that provides a wide field of view, stereoscopic feeling, and also high contrast resulting image. Logically, this results in other disadvantages – patient's pupil must be dilated, the device is bigger, heavier and more expensive. For patients, the most inconvenient is brighter radiation, sometimes even painfully penetrating.

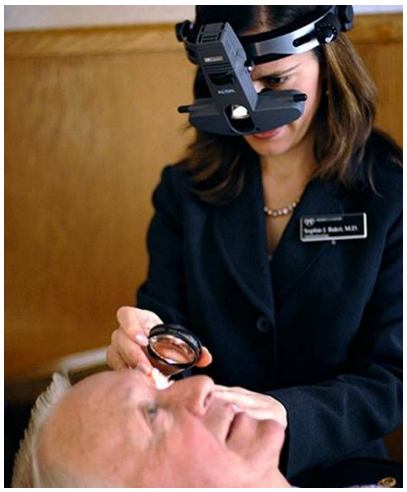

Fig. 2.27: Indirect opthalmoscopy examination [134].

2.6.1.3 Fundus camera

For more in-depth examination of the back part of the eye, fundus camera, which has currently and probably the greatest significance in retinal examination, is used. It allows creating a colored photography of nearly whole retinal surface. The optical principle of this tool is based on the so-called indirect ophthalmoscopy [25]. Fundus cameras are usually equipped with a source of white light, which they use to illuminate the retina and then scan it using CCD sensor. Some types can also find the middle of the retina and focus on it automatically using frequency analysis of the scanned image.

This device is usually described by maximal degree, under which it is possible to detect the light reflected from scanned ocular apparatus angle of view. The angle of 30°, which is considered as a standard angle of view, captures the image of an object 2-5 times bigger than it really is. Wide angle fundus camera captures an image under the angle of 45° to 140°. Depending on the enlargement or reduction of the angle of view, the size of the object that is captured in an image is proportionately changed. Narrow angle fundus camera uses an angle of view of 20° or less.

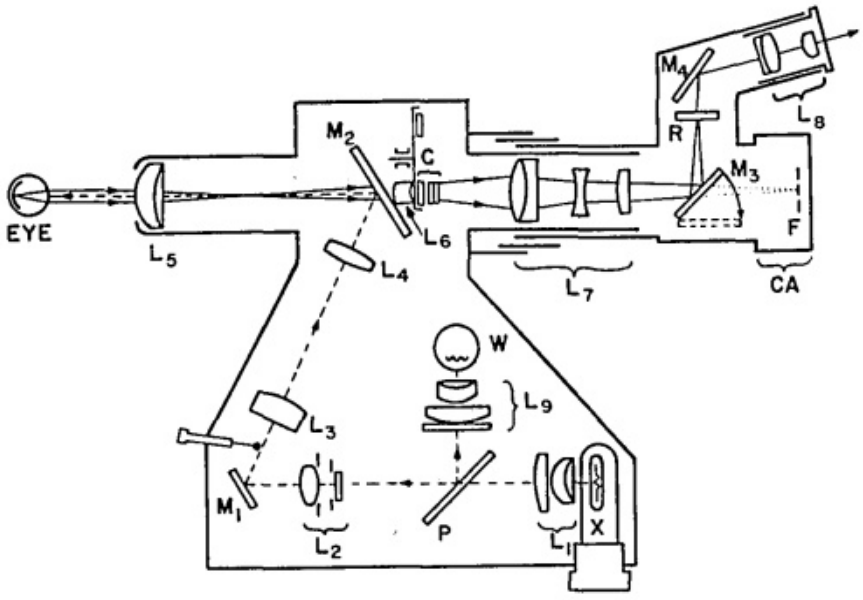

Fig. 2.28: The optical principle of the fundus camera [85].

The light is generated either by a built-in lamp or using electronic lighting and then projection through a set of filters to a rounded mirror. This mirror reflects light to a group of lenses which focus

the light. The mask on the uppermost lens shapes the light into a circle with gross edges. The light is then again reflected from the next round mirror with a central hole, stands out from the camera using lens objective and continues on to a patient's eye through the cornea. Provided that both lighting systems and image are correctly aligned and focused, the resulting image of the retina stands out from the cornea again back to the device through an unilluminated part of the lens. The light continues through the mirror's central hole to a part of the device for astigmatic correction, to the lenses for dioptric compensation and a final image is shown on the output lenses of the camera. The optical structure of fundus camera's optics is outlined in Fig. 2.28.

During scanning by the fundus camera, a patient sits in front of the camera's optics with his chin placed on a chin rest and his forehead in a device's forehead rest. The person that is taking the pictures will focus and align the optics to achieve the best possible result. The created photography is then used to determine the patient's diagnosis.

In Fig. 2.29, there is shown an example of the current state of the art of fundus cameras. Canon CR-1is a non-mydriatic fundus camera with dramatically reduced brightness, improved overall comfort, and significantly shorter exams. One of the advantage of non-mydriatic fundus cameras is that the pupil of the eye does not have to be dilated or enlarged by use of mydriatic eye drops thus the examination is more comfortable. For digital imaging, standard DSLR camera is used to obtain a high-quality retinal image with resolution depending on the camera which is used. Canon CR-1 allows wide angle view of 45° and 2× digital magnification. Focusing is performed in two simple steps by aligning two halves of a split pupil image followed in, and by the adjustment of split lines and working distance dots in the retinal display. This ensures that the correct focus and working distance are achieved for the sharp image.

Fig. 2.29: Canon CR-1 non-mydriatic fundus camera.

2.6.2 Macular degeneration

Macular degeneration is a disease that is in 90 % of cases formed with increasing age – then we also talk about age-related macular degeneration (ARMD), and it is the most common cause of blindness for patients over 65 years. It is estimated that more than 8 million people in the USA have ARMD in some stadium. With increasing percentage of older people, its presence is still increasing, and it also increases with rising ability to handle other eye diseases. In the rest of the cases, the macular degeneration appears among children or young people in the form of Best disease or Stargardt disease [22]. These diseases are formed based on inheritance.

With macular degeneration, the retinal area that creates the middle of a field of view is damaged. As a consequence, a serious disorder of central field of view emerges. In its middle, a patient sees just gray shadow or even a black spot. The peripheral vision, however, stays unaffected. Macular degeneration can appear in two forms – dry (atrophic) and wet (exudative). Among the most common symptoms belongs blurry gray or black smudge in the center of the field of view (known as central scotoma). An

affected person sees deformed straight lines, blurry font or inappropriate shape of different objects. Color vision is also affected, the colors seem faded. Side vision stays sharp on one or both eyes [22]. An example of a retina affected by macular degeneration is depicted in Fig. 2.30.

Fig. 2.30: Example of macular degeneration with druses.

Many epidemiologic studies use definition that describes ARMD as degenerative disease of individuals aged over 50, characterized by the presence of one of the following lesions [86]:

- **Soft (big, ≥ 63 µm) druses**. The presence of individual, soft, indistinct druses is considered as a bigger indicator of ARMD than the presence of soft clear druses. The presence of druses with size over 125 µm is also much more important than the presence of smaller druses.
- **Areas of hyperpigmentation** that are associated with druses, with the exception of hard druses surrounded by pigment.
- **Areas of depigmentation** associated with druses. These areas often appear as a shadow of druses and are most often sharply bounded.
- **Visual acuity** is not used for defining ARMD because advanced changes caused by ARMD can be present without changing central fixation.

2.6.2.1 Druses

This is easily visible as yellowish bearings lying deep in the retina. Druses are distinguished by size and shape and sometimes they have crystalline look resulting from calcification [86].

As an eye where ARMD is not developed, it is considered that the eye on which no druses are observed or only a few small (smaller than 63 µm), druses with the absence of other ARMD symptoms. An eye in the initial stage of ARMD is one which contains a few (less than approx. 20) middle-sized druses (63 µm to 124 µm) or pigment abnormalities (increased pigmentation or depigmentation), without any other symptoms of ARMD. Advanced stage of ARMD is geographic atrophy that interferes into the center of the macula or choroidal neovascularization (CNV). Druses are described by the following characteristics [86]:

- **Types –** druses are generally separated into hard and soft with several subtypes. Soft druses are generally bigger and have a soft look. They have distinct thickness and predisposition to connecting; therefore, they show bigger variation in sizes and types. A cluster of soft druses has a squiggly appearance.
- **Degree of eye fundus affection –** this can be evaluated by a number of druses, area of affection or druses' density which means whether they are separated, touching themselves or if they cluster together.
- **Distribution –** the greatest importance is attributed to druses that are present in the inner macula, which is defined as an area of inner circle with a diameter of 3,000 μm. In Fig. 2.31 can be seen an eye with many clearly visible, soft, yellow druses that are present mainly in the inner macula area.
- **Color** of druses is referred to as yellow, light or white.

Fig. 2.31: Soft, yellow druses in the inner macula area.

2.6.3 Diabetic retinopathy

Diabetic retinopathy (DR) is a non-inflammatory disease of eye retina. It is formed as a result of the overall damage of blood vessels during diabetes mellitus [23]. Classification of diabetic retinopathy is generally based on the seriousness of intraretinal microvascular changes and the presence or absence of retinal neovascularization. Retinopathy is classified as non-proliferative diabetic retinopathy (NPDR), if only intraretinal microvascular changes are present. This initial stadium then moves into the proliferative phase, in which new vessels are formed.

Wrongly compensated diabetes affects tiny vessels in the eyes, which are getting blocked and as a result, the blood supply of the retina is reduced. Another form of retinal damage occurs when blood vessels are leaking, fluid is coming out and causing retinal edema. Both insufficient blood supply and retinal edema destroy the ability to see. The eye tries to correct the situation by growing new blood vessels (neovascularization); however, that substandard and harmful break up can cause eye extravasation (hemophthalmia) and tractional retinal detachment. Diabetic retinopathy has two forms: non-proliferative and proliferative [120].

Abnormalities of fundus during non-proliferative stage are microaneurysms and intraretinal abnormalities, which are the result of changes in retinal vessels transmittance and eventual blockage of retinal vessels. Vessels' blockage leads to bad blood supplying which appears as an increasing number

of hemorrhages, vessel abnormalities, and intraretinal microvascular abnormalities. Retinal hyperperfusion is put in connection with the development of proliferative diabetic retinopathy.

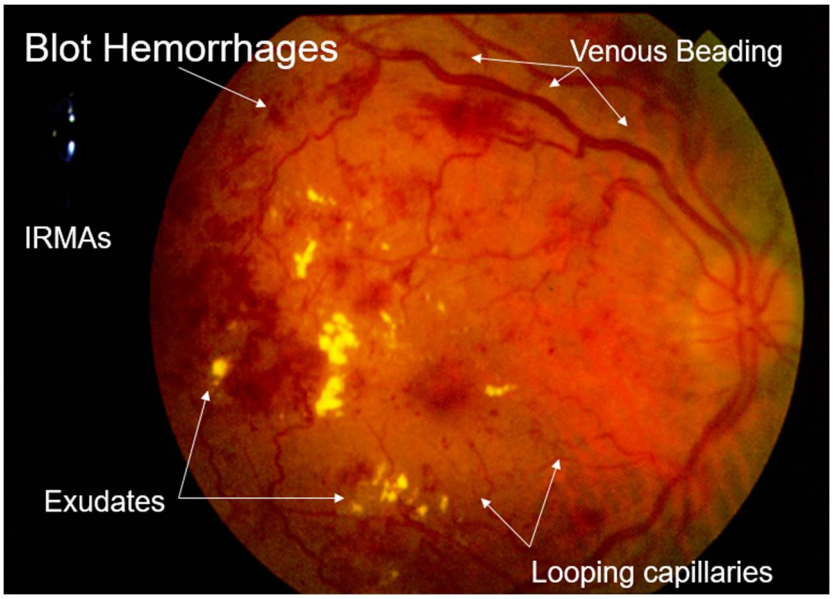

Fig. 2.32: Advanced stage of diabetic retinopathy [87].

Diabetic retinopathy is characterized by the presence of the following lesions [86]:

- **Microaneurysms of retinal capillaries** – usually the first visible symptom of diabetic retinopathy. Microaneurysms are ophthalmologically defined as dark red dots with a diameter ranging between 15 µm and 60 µm. Most often, they are present in posterior areas. Despite that microaneurysms can appear even during other vessel diseases, they are considered to be a typical sign of NDPR. For individual microaneurysms, it is typical that they appear and then disappear with time. Microaneurysms alone without the presence of other symptoms of diabetic retinopathy don't have high clinical importance. In spite of that, the increase of their presence in the retina is connected with the development of retinopathy and increased probability that with their increase, other microvascular changes connected to diabetic retinopathy will appear, exists. In Fig. 2.32, there is shown a very severe diabetic retinopathy. It is characterized by excessive retinal bleeding and also by intraretinal microvascular abnormalities.

- **Hemorrhages** are also red dots that develop as a result of the weakening of microaneurysms' walls or tiny vessels and following the rupture of these walls. Hemorrhages exist in two forms. In the first one, hemorrhages have a character of dots. These pathologies look like little light red dots. The second type of hemorrhages looks blurry and is bigger.

- **Exudates** – with increased creation of microaneurysms, it is possible that excessive transmittance of retinal capillaries occurs. This leads to the formation of retinal edema, usually in the macular area. Macular edema is defined as the thickening of the retina caused by the gathering of liquid in the macula. Macular edema is often accompanied by hard exudates in the retina. These hard exudates are lipid sediments that are probably piled up under an influence of lipoprotein leak. Clinically, hard exudates are well boarded, white-yellow intraretinal sediments, normally visible on the edges between edematous and non-edematous retina. The liquid that is creating the edema can come and leave with no visible consequences. Lipid sediments are on the contrary with the liquid connected with the retinal damage and permanent loss of vision, especially if they are located under the center of the macula.

2.6.4 Toxoplasmosis

Toxoplasmosis is a parasitic disease that ranks among zoonoses, which are diseases transmissible from animals to humans. They appear all over the world. In European countries, about 10 to 60 % of inhabitants have created antibody toward toxoplasmosis, depending on their eating habits. In the Czech Republic, the seropositivity (presence of antibodies in the blood) is about 20-40 %. The disease usually appears only by increased temperature, flu conditions, headaches, fatigue or swollen lymph nodes. Acute disease can sometimes transform into a chronical stage, often, the infection, however, occurs without any notice and is recognized only by finding specific anti-toxoplasma antibodies in the blood, which can in lower levels last for a whole life (latent phase of infection). A lot of toxoplasmosis' types exist – ganglionic, eye (Fig. 2.33), brain, gynecological, etc. Other forms of toxoplasmosis are not that common [24].

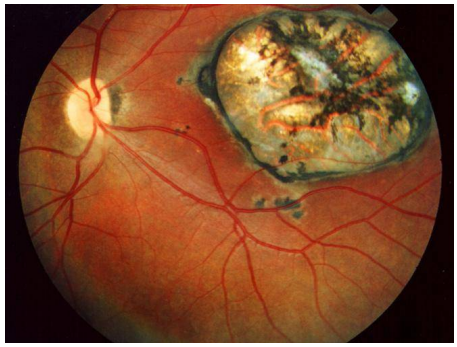

Fig. 2.33: An eye affected by toxoplasmosis [133].

3 Design of an eye multimodal system

This chapter deals especially with a proposal of lower levels of the multimodal device which means optical setup, positioning, illumination and device control. Although the work is focused mainly on the biometric field, the parts of the proposed system are expected to be used also in the area of ophthalmology. This has also been described already in the approved Czech patent [P02] and in utility model [P03], which deals with the methodology of device use and subsequent evaluation. The international patent [P01] describes an ophthalmic diagnostic device for the acquirement of eye retina and eye iris, connected to an expert system for determination of eye disease. The system has already undergone a series of changes over the last years, and at the time of finishing this Ph.D. thesis, the third version is being finished. Previous versions have been published in [H01] [H02] [H03] and [H04]. The system is supposed to be used in the following fields:

- **Medical use.** In medicine, a photographic documentation and subsequent images archiving of the retina and iris is necessary for the chronological monitoring process of a patient's health condition. It may not be just a disease of these two inner organs of the eye. The iris is a unique tool for tracking the status of a human organism by iridology [122] – on this topic, there were posted countless scientific publications, but it is still not clear whether it is a serious science or only a medical fraud [96][36]. The eye retina is the only place on the human body where it is possible to observe vessels by a non-invasive way and directly. The retinal image analysis can be helpful for a diagnostics of eye diseases as well as for making diagnose of diseases related to the cardiovascular system. An automatic and autonomous analysis can be very helpful for making the diagnosis of many diseases, e.g. macular degeneration [3], hypertension [37] and glaucoma [38]. The cardiovascular problems can be detected automatically by the measurement of veins diameters and curvatures [39][40].

- **Biometric use.** From the biometric point of view, the eye retina and iris, respectively, are completely unique and have a large entropy of biometric information. Moreover, the iris and retina are well protected against injuries and external influences. The iris contains a large number of features such as arching ligaments, ridges, crypts, rings, etc. The iris is widely used for biometric purposes [41]. On the other hand, the retinal recognition is not so much attractive. There must be a complex optical system for image acquisition enabling fully automated user interaction. Currently, there is no biometric device on the market which is able to perform the retinal biometric identification.

The current devices, whether biometric or medical ones, generally do not have any possibility of getting the iris and retina simultaneously in one particular apparatus using one optical system.

In the field of biometrics, the concept of multimodal recognition systems combining iris and retina were presented in [42]. Although the multimodal system is theoretically very safe and difficult to counterfeit, at the moment, there is no developed and constructed device which would be able to perform retina and iris recognition in practice. It is primarily the retinal scanner part that significantly complicates the construction and use of such device [20].

In medicine, there are used ophthalmology devices for patient examination. While the iris can be examined relatively easily using a magnification glass, the retinal examination requires a more sophisticated optical setup based on commonly used optical approaches: direct ophthalmoscopy, indirect ophthalmoscopy and ophthalmoscopy with the slit lamp [14] as already mentioned in chapter 2.6.1.2.

3.1 Design of iris and retina imaging system

A practical design of the eye bimodal biometric system is briefly described in this chapter. The device was completely developed at the Brno University of Technology (CZ). It is still under constant improvement and currently we are working on the third version of the optical system. A brief description of our system in the following text is provided.

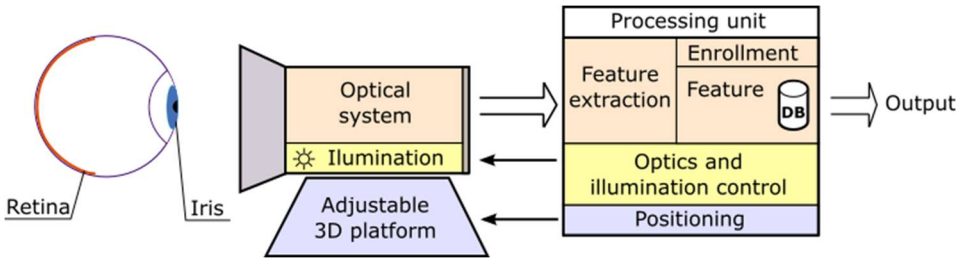

Fig. 3.1: Block diagram of the proposed system.

The optical system is responsible for image acquisition and allows the focusing on iris and retina. An integrated illumination source operates at both visible and near-infrared light. The whole optical system is mounted on an adjustable 3D platform which is controlled by a feedback from the camera image. The positioning algorithm adjusts the optical axis of the device according to the optical axis of the eye. Thanks to the very precise 3D movable platform, we assume that the proposed biometric system will be more user-friendly and in addition, the time of scanning will be much less than in the case of the system described by Usher [42].

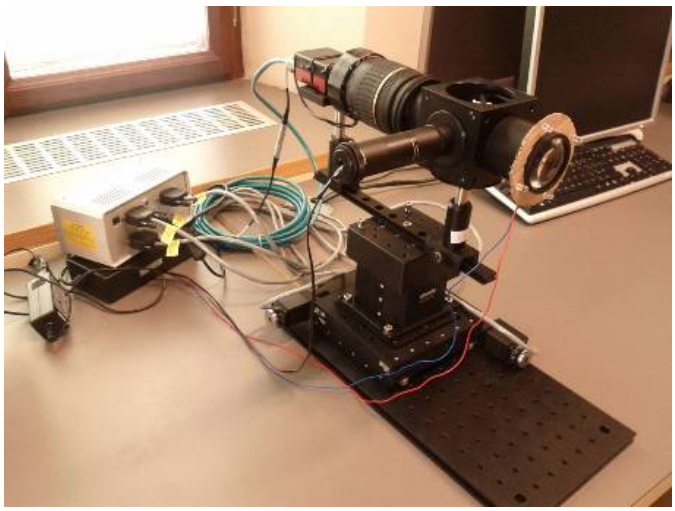

Fig. 3.2: Real design of the proposed system – version 1.

The central component of the system is the *signal processing unit*. It receives and processes output images from the optical system. After evaluation, the unit sends the result to the output (e.g. computer, access system). Fundamental modules of the unit consist of *feature extraction module* which extracts features from retinal and iris images provided by the optical system. Subsequently, a biometric template is generated. The *enrolment module* allows enrolling a new user into the system. A template is stored in a *database* located locally on the device or remotely (e.g. via an Ethernet connection). *Feature matching module* matches just extracted templates with the templates stored in a database. *Optics and illumination control module* controls optical system (retina and iris focus, aperture) depending on the feedback from the camera. This module also controls source and intensity of illumination. *Positioning module* allows moving the optical system in three axes in order to align the optical axis of the eye and optical axis of the device. The positioning is controlled by the feedback from the camera image.

3.2 Optical system design

This chapter deals with the iterative process of development and design of an optical system. In the following chapters is described the principle of proposed optical system and its design which has been realized.

The emphasis primarily put on retinal imaging has been included in the proposal because this is the most complicated part of the whole system. The image of the iris (as an organ visible by naked eye) can be obtained much easily.

3.2.1 Requirements

The optical setup itself is designed to fulfill the requirements resulting from both physiological properties of a human eye and needs for medical eye examination or biometric pattern recognition. These requirements place emphasis particularly to imaging of relatively large areas of human eye iris and retina combined with computer processing and thus to optically design integrating digital imaging cameras and pertaining optics allowing the creation of an image in the plane where the camera active element is placed. Similar setups were already reported many times [43][44] but the design of one multimodal device represents a quite new approach of integration, miniaturization and cost reduction.

The requirements for the optical design were derived from human physiology and – especially in the case of the human eye – from the most conventional deviation – refractive disorder (myopia & hyperopia [127]). Following the interval of these deviations allows us to design the device, which is usable for the vast majority of human population.

- **Illumination** is one of the most important parts of the optical system at all. One of the main aims in designing any optical system is to avoid unwanted image artefacts, especially reflections from the cornea and lens. These are known as the Purkinje reflections and must be kept as minimum as possible including ambient light. For their suppression there can also be used in optical elements such as anti-reflective coating applied to the surface of lenses or crossed polarizers reducing reflections. Illumination must also comply with the requirements for maximal radiated power to avoid potential eye damage. These limits provide standards such as IEC/EN 60825-1, IEC 62471 or Directive 2006/25/EC of the European Parliament and of the council [106].

- **Output quality**. The resulting image acquired by the optical system must always be stable and independent of external influences (ambient light, user's eye position, etc.) with well recognizable features in high details. In the case of the retina, it is a large field of view of the inner surface of the eyeball uniformly illuminated with high contrast of blood vessels and other important artefacts (optic disc, macula, etc.). High contrast is important primarily for subsequent digital image processing. Iris texture should be emphasized. The exterior and interior surfaces of the cornea and lens reflect the illuminating light forming bright reflections within the iris images. The iris optical system must minimize their size and restrict them to different dedicated regions, where they are not interfering the resulting image.

- **Autonomy and speed of scanning**. The platform should be designed with high friendliness for the user and also for the person whose eye is being scanned. The speed of scanning is also important. If, for some reasons, a person cannot be scanned automatically (due to high eye defect, non-cooperation, etc.) the system should ensure at least semi-automatic assisted scanning. Optical system positioning of medical devices takes the most

time of patient's examination. The optical system should be placed on the adjustable platform which ensures positioning to the most suitable position for scanning. The adjustable fixation target on which the patient focuses the sight ensures also imaging of the chosen part of the retina's surface.

- **Cost**. Output quality, requirements for automation and other capabilities affecting complexity and the total cost of the device have to be corresponding with the purpose of the device use, e.g. in the case of biometric use, it is not necessary to have a large field of view of the retina and image resolution. On the other hand, a high-quality output is supposed to be essential for proper medical examination. This should be reflected in the construction and thus the total price of the device.

3.2.2 Ophthalmoscope & web camera

For the first experiments, a direct ophthalmoscope from Welch Allyn company was used [46]. The model PanOptic 11820 provides panoramic view of the fundus with magnification 26 % and field of view (FOV) up to 25° which is five times larger than standard ophthalmoscopes.

Proprietary unique design patented by Welch Allyn allows a greater working distance between patient and examiner, comfortable for both. Illumination is converged to a point on the cornea by Axial Point Source Optics enabling an easy entry even in the case of highly contracted pupil. The illumination pathway creates a wide illuminated area of the surface of the fundus. HPX halogen illumination is also optimized for prevention interference from unwanted glare and reflections.

Fig. 3.3: Setup with Welch Allyn Panoptic Ophthalmoscope.

Fig. 3.3 shows a device assembled for the first experiments capturing the eye's retina. The mentioned PanOptic 11820 ophthalmoscope was used with standard Logitech webcam C270. This model offers Carl Zeiss optic; Full HD 1080p or 1280 × 720 resolution and USB connection with a computer.

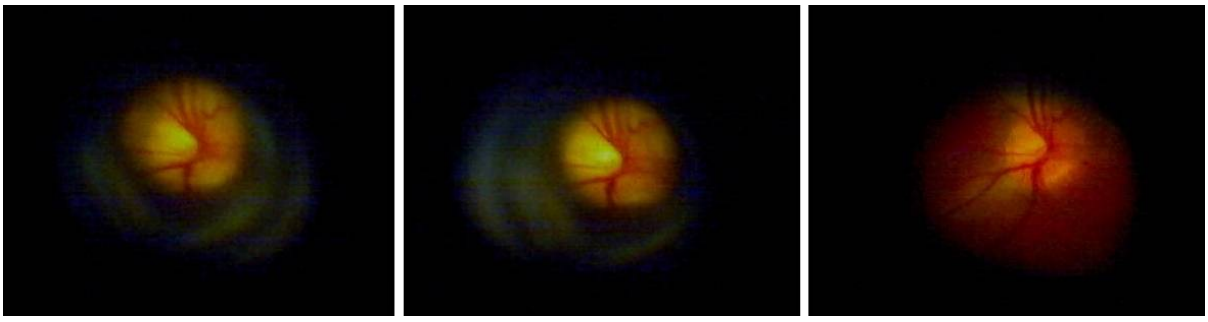

Fig. 3.4: Examples of retinal images obtained with PanOptic ophthalmoscope and web camera.

Fig. 3.4 shows examples of obtained retinal images. In the obtained pictures there can be clearly seen branching blood vessels coming from the optic disc (blind spot), observed FOV is approximately 20-25°. Scanning distance has an impact on the visible retinal area, and the FOV is cut off by the iris borders on the first two pictures from the left side. The obtained pictures are sufficient to reach biometric requirements. From the medical point of view, it depends on how much retinal surface, area and detail is needed to be observed. However, it can be compared to the observation by the standard direct ophthalmoscope with a larger FOV. The following figures show possible processing procedure which can be easily automated to extract the feature vector for biometric purposes.

Due to various lighting conditions and different eye properties of each individual, in the first step, the picture must be normalized resulting in the changes of pixel intensity values. This is achieved by histogram stretching method, improving the contrast by stretching the range of intensity values. The picture is also converted to grayscale because color information in this case is not needed any more and could affect the following processing. The normalized picture can be seen in Fig. 3.5.

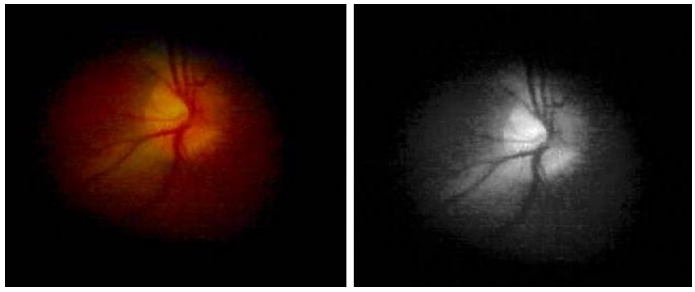

Fig. 3.5: Original (left), and normalized picture (right).

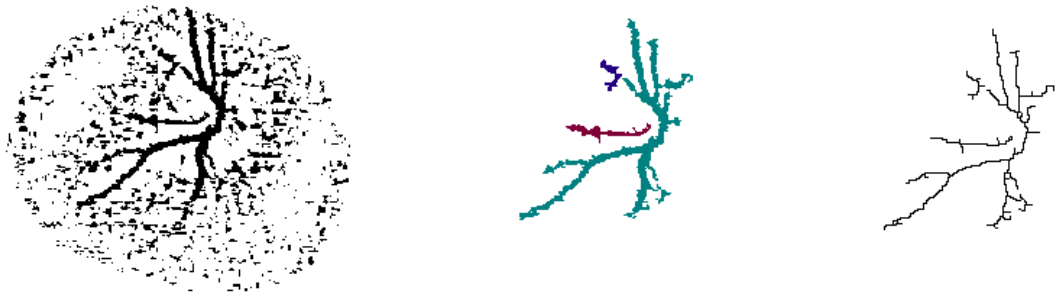

Fig. 3.6: Applied operations of thresholding, blob filter, thinning (from left to right).

The following operations are used in order to get a picture ready to be converted into the feature vector where bifurcations (crossings) and their positions are used as a biometric template. This includes four basic steps:

- Thresholding of the grayscale image to highlight the main blood vessels.
- Filtering of blobs in image of defined size in order to remove small not relevant artefacts (noise removal).
- Thinning as a preliminary operation for feature detection.
- Bifurcation and crossing detection. The resulting feature vector contains their positions.

As was shown in the previous text, by the relatively simple setup and processing, it is possible to get retinal images with still sufficient number of features for the retina recognition.

The described system with a camera has a relatively small field of view and does not enable automatic retinal scanning, due to the used ophthalmoscope and the principle of its scanning. The cooperation of both patient and trained doctor who has to position the ophthalmoscope, focus it and obtain

an image is necessary. It can, however, work as a very cheap tool for documentation and allows to save the data of the patient's eye fundus.

3.2.3 Experimental ophthalmic multimodal imaging system – first version

The proposed optical system is based on the principle of indirect ophthalmoscope and on illumination by an intensive light placed near or on the same axis as the observing axis. The same optical system is used for the acquisition of retinal and iris images. It differs only in illumination and in focusing distance.

3.2.3.1 Illumination

In the optical system, two kinds of illumination unit are used – retinal and iris illumination systems.

For the retinal scanning, there are used LEDs with embedded lens and beam angle of 60°. We tried to use the white visible LED as well as LED in near-infrared (NIR) spectrum. A visible light may not be comfortable for a subject (user) due to its relatively high intensity which is required for the acquisition of high quality retinal images. It also causes pupil contraction making image acquisition more difficult. However, white light is necessary for the inspection of the retinal coloration. In order not to bother a user by illumination, a NIR light was used for a proper focus on the retina.

For the iris recognition, illumination at the same NIR wavelength is also used. As described in [8], image acquisition under the NIR light allows to observe the iris structure more precisely than in visible light. Based on our previous experiments, we have used the illumination with the wavelength of 780 nm. Four infrared LEDs are used for iris illumination located at the ring around the eyepiece.

3.2.3.2 Optical system

The optical system is shown in Fig. 3.7. It is actually an indirect ophthalmoscopy system similar to that used in standalone fundus cameras.

The illumination must be carefully designed so that the axis of this system is not directly on the viewing axis, but slightly deflected to avoid unwanted reflections. The light source is then displayed in a different part of the pupil to the viewing axis. Moreover, the crossed polarizers are used in the illumination and viewing path to suppress additional reflections in the optics.

A camera Imaging Source DFK72BUC02 with the resolution up to 2,292 × 1,944 pixels (depending on the frame rate) is used for the image capture. The embedded infrared filter (IR) was removed from the CCD sensor to have a capability of scanning in IR spectrum. The quantum efficiency of CCD sensor at 780 nm is almost 25 %, which is sufficient with respect to the price of this camera. The objective type mounted to the camera is Computar H3Z4512CS with variable focal length 4.5 – 12.5 mm. The lens is focused on the intermediate image created behind the ophthalmic lens with an optical power of 18 D (Volk 18D). This lens was chosen as a tradeoff between sufficient field of view (44°), image magnification (3.4) and reasonable large working distance (55 mm). It is also possible to mount an optional IR filter (wavelength 780 nm) in the front of the camera in case of scanning in IR spectrum.

The LED ring located in the eyepiece is used for a uniform illumination of the iris. The eye must be located in a focus distance of the optic system to get a proper image of the iris.

During the retinal scanning, the eye must be positioned farther from the optics so that the pupil is located in a focal point of the ophthalmic lens. The retinal light source with a diffuser is used. The light beam is firstly directed to the eye by a 50:50 beam splitter, passes the front objective lens and enters the eye. The light reflected on the retina goes back via ophthalmic lens and beam splitter to the camera.

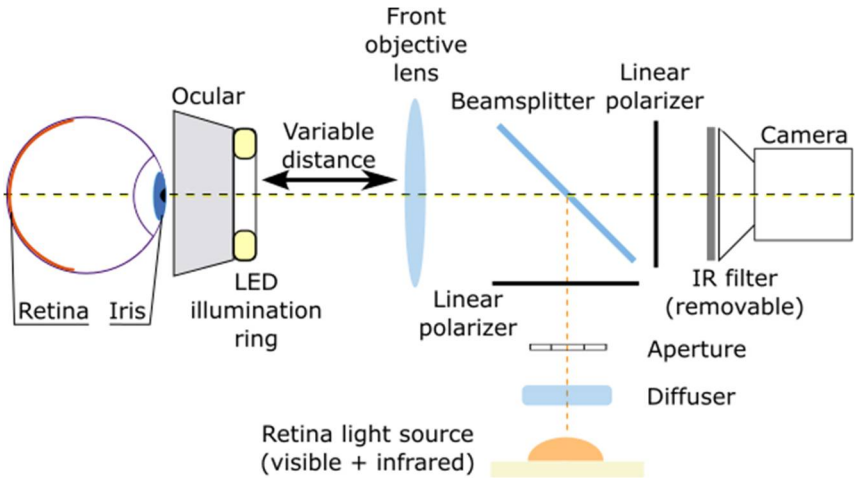

Fig. 3.7: Optical system design – version 1.

3.2.3.3 External fixation point

The fixation point is used to get a proper turn of the eyeball. It allows getting an image of the retina focused on a specific area, e.g. on the optic disc where it is possible to find the largest amount of biometric information.

The fixation is performed using the method when the user is looking with one eye into the device and by the second eye at an external fixation point, at a target located out of the device. Looking at the external target and turning the eyeball of one eye causes the simultaneous movement of the second eyeball looking to the device in the same direction. Thus, it is possible to turn the examined eye to a required position. It is supposed that the optical axes of both eyes are parallel, of course.

This fixation system can be affected by eye pathologies, which influence vergence of the vision. Therefore, for subjects with vergence dysfunction (strabismus, exophoria, esophoria), it can be difficult to make a scan using this proposed device.

3.2.3.4 Experimental results and discussion

The following figures show real results from our proposed device – in Fig. 3.8, there are retinal pictures. Although the images are rather dark, the optic disc and the blood vessels can be clearly seen. The field of view is comparable with the standard fundus cameras. The images were taken in a visible spectrum of light respectively by a short-term light pulse to avoid pupil contraction and thus a reduction of the FOV.

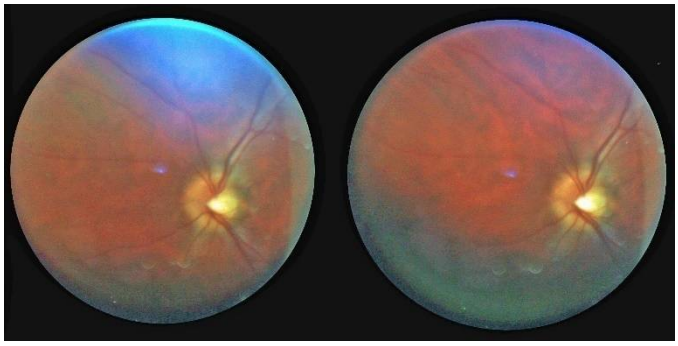

Fig. 3.8: Acquired retinal images.

The iris images taken in an infrared light spectrum of 780 nm are shown in Fig. 3.9. There are obvious retinal red reflex and corneal reflexes in the pupil. The iris artefacts can be seen, however, in some parts, the image is blurred due to the small depth of field of the optical system.

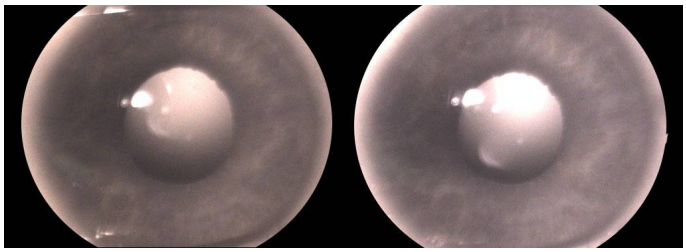

Fig. 3.9: Acquired iris images.

We showed that a relatively simple optical setup could be used for iris and retina imaging. Nevertheless, some additional components and modifications have to be included to make this system more autonomous and reliable.

There is one external fixation point. However, this technique is not so precise and still requires relatively high effort from a subject (user). One possible solution is a floating point instead of a static one. A possible approach is a display located outside the device; there will be a plot fixation target observed by the second eye of the user. By moving this point, the viewing axis will be continuously changing in correspondence with the area of the retina which will be required to be captured. An autonomous system will detect the area of interest and automatically move the fixation point on the display.

The whole optical system is mounted on an adjustable 3D platform which can be controlled by a feedback from the camera image. The positioning algorithm adjusts the optical axis of the device according to the optical axis of the eye. The increase of the depth of field is also necessary when scanning the iris. This needs additional experiments with camera aperture and intensity of iris illuminators. This is also connected to the quantum efficiency of the camera and properties of the ophthalmic lens, which might be removed.

The proposed system is placed on an adjustable platform which controls its position in three axes and allows automatic eye scanning. One disadvantage is a static fixation target, which does not allow scanning of various parts of the retina based on the eyeball rotation. Also, the quality of the output image, especially of the iris, is not very high. The usage of optics that allows a higher depth of field would help in this matter.

3.2.4 Experimental ophthalmic multimodal imaging system – second version

The second version of the optical system was designed by a computational model in the ZEMAX® environment. The Gullstrand-Le Grand [45] eye model was used to simulate the human eye optics during the designing process.

The optical setup, understandably, consists of two essential optical axes which are created by R50T50 plate beamsplitter (BS_1) (Fig. 3.10). The BS_1 is the most fundamental part of this novel approach. It allows us to deal with two practically independent optical systems behind the BS_1. The position of conjugated planes in the optical schemas of both the iris and retina are designed not to interfere with the imaging area of the other parts of the system.

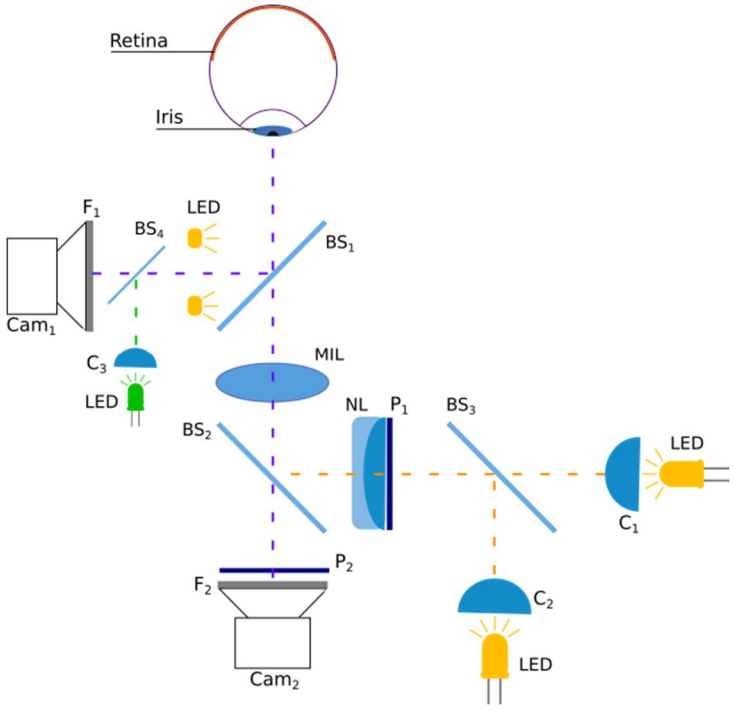

Fig. 3.10: Optical setup of bimodal iris & retina imaging device.

The optical setup description: optical axes of iris (red) and retina (green) imaging and illuminating branches (yellow); BS_1: main beamsplitter; BS_4: eye navigation beamsplitter; C_3: eye navigation condenser, diffuser and diaphragm; F_1: long-pass IR filter (edge 800 nm); CAM_1: iris camera objective; MIL: main imaging lens; BS_2: imaging/illumination beamsplitter; P_2: linear polarizer; F_2: short-pass VIS filter (edge 800 nm); CAM_2: retina camera objective; NL: negative lens; P_1: linear polarizer; BS_3: IR/VIS illumination beamsplitter; C_1: retina VIS illumination condenser, diffuser and doughnut-shaped diaphragm; C_2: retina IR illumination condenser, diffuser and doughnut-shaped diaphragm.

The position of BS_1 relatively close to the eye is the result of contradictory conditions in simulations of both optical branches. One could argue that the placement of the BS_1 further from the eye could lead to an increase of the displayed face area in the iris plane and thus to the possibility to use smaller BS_1, which could lead to lower costs. The second condition – to display sufficiently large area of the retina – however, requires placing the main imaging lens (MIL) as close as possible to avoid enormous dimensions (and thus unavailability) of MIL. Therefore, taking into account the costs and available dimensions of elements suitable for BS_1 and MIL, we used rather, a large BS_1 relatively close to the eye which allows us to use MIL commercially available with acceptable price. Final 3D model of the optical setup based on our proposal is shown in Fig. 3.11.

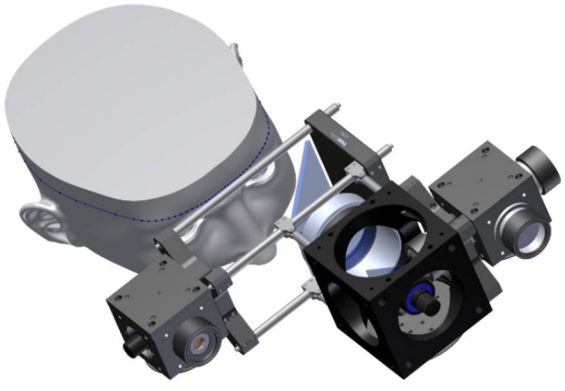

Fig. 3.11: Final 3D model of the proposed optical system.

3.2.4.1 Iris imaging

The iris imaging in this setup follows classic macrophotography principles, and the iris is shown in IR part of the electromagnetic spectrum [41]. Part of the light scattered from the iris (and the adjacent part of the face) is reflected on BS_1 and propagates almost unchanged through R20T80 beamsplitter BS_4. When light reaches long-pass filter F_1 (edge filter, 800 nm), the part of the spectrum up to 800 nm is cut-off and only the IR part of the spectrum passes to the objective. The objective OBJ_1 has focal length 12 mm and F1.6. The objective is mounted to a monochrome autofocus camera (not plotted in the figure) with 1/2.5'' CMOS imaging area and 1.25 mm autofocus range. CMOS technology has sufficient quantum efficiency even in near IR region, so this camera is an applicable variant (Imaging source DMKAFUK031).

The iris and the adjacent part of the face around the eye are illuminated by IR (intensity peak: 820 nm) light-emitting diodes (LEDs) placed on an illuminating ring around the iris-imaging branch's axis (plotted as two light bulbs close to BS_1). This ring also contains several white LEDs to control the iris aperture for the retina imaging purposes. 50 % of light from the illuminating ring is reflected by BS_1 on the iris, and scattered light can be collected by the iris-imaging system.

3.2.4.2 Retina imaging

The retina could be shown in both IR and visible part of the light spectrum. The 20D (f' = 50 mm) MIL is used as a cornerstone of the retina-imaging branch. The light scattered from the retina propagates via optical system of the eye. Part of the light beam passes through BS_1 and propagates along the optical axis via MIL, R30T70 beamsplitter BS_2, linear polarizer P_2 (to avoid the reflection from the eye surface nearly perpendicular to the optical axis [48]), short-pass IR filter F_2 and enters to objective OBJ_2. OBJ_2 has focal length 8 mm and F1.6. The objective is mounted to a color autofocus camera (not plotted in the figure) with 1/2.5'' CMOS imaging area and 1.25 mm autofocus range (Imaging source DFK72BUC02).

The retina is illuminated in IR part of the spectrum by IR (intensity peak at 780 nm) LED placed behind condenser C_1 and in VIS by white LED placed behind condenser C_2. The light from both diodes propagates equally via the diffuser, doughnut-shaped diaphragm (to remove unwanted light incidents perpendicular to the optical-axis surface of the eye) and condenser to create a parallel beam of light. Both beams meet on BS_3 and continue together via linear polarizer P_1. The P_1 changes the illuminating wave to a linear polarized one and with P_2 (could be understood as an analyzer) creates the second hurdle to eye surface reflections. The doughnut-shaped diaphragm is then displayed by negative lens NL and MIL to the iris plane with the diameter slightly smaller than the diameter of the eye pupil. The light beyond the iris plane creates a divergent cone, which with scattering in vitreous creates a retina illuminated uniformly enough for the imaging purposes.

3.2.4.3 Experimental results and discussion

The whole realized optical system can be seen in Fig. 3.12. All the optical components have been purchased from Thorlabs [49] (shop specialized on optical components and accessories). The difference between focusing of IR and the visible light spectrum is perceptible as the focus is a bit moved. While in the visible spectrum range, iris is focused correctly, during lighting by IR, it is a bit blurry, and artefacts are not so visible. It is, however, a significant improvement in comparison with the previous version of the optical system. Iris artefacts can be seen, and the result is therefore well functional for biometric usage. On the other hand, the image still has reflections from the sclera and lens which were not fully removed by linear polarizers. Also, the illumination is not homogeneous thanks to the use of LEDs without a diffuser.

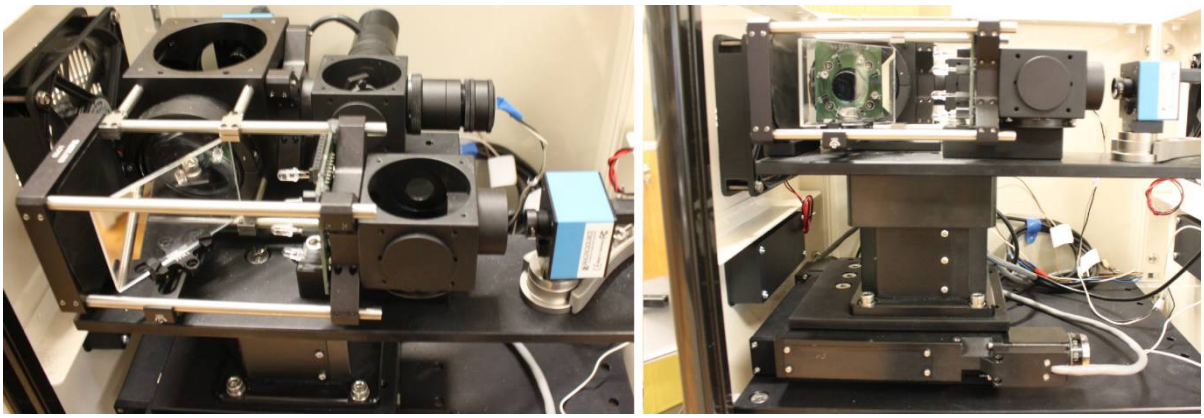

Fig. 3.12: Construction of the real optical system.

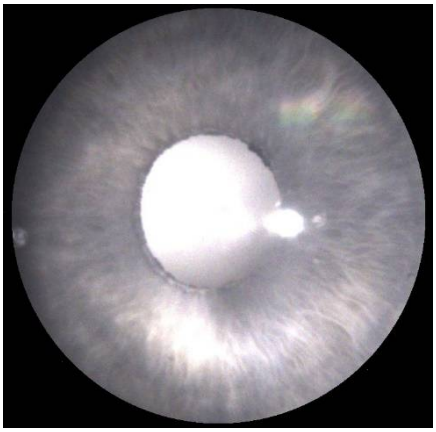

Fig. 3.13: Scanned iris.

We have accomplished similar results during the scanning of the eye retina as in the previous version of the optical system. It has turned out however, that the usage of the diffuser and condenser for retinal illumination does not fully deal with inhomogeneous lighting. Overshadowing of the retinal part is very often caused by the inaccurate placement of the eye to the device axis, where the edge of the pupil overshadows a part of the retina that is being scanned by a camera placed in the direct vision axis.

Another disadvantage is that in the whole optical system, too much light is lost on the beam splitters, which is compensated by a higher lightning intensity. This leads to reflections, and it is difficult to set up the system for the optimal balance between good illumination of retina / iris and number / intensity of reflections.

3.2.5 Experimental ophthalmic multimodal imaging system – third version

The third version of the optical system was designed in cooperation with Palacký University Olomouc, Department of Optics (CZ). At a time of writing this thesis, the development was still in progress, however, it is at least possible to describe the final proposal of the optics and the mechanical construction.

3.2.5.1 Design of the optical system

When displaying a retina through an eye lens, a bundle of parallel beams that shows individual retinal points comes from the eye. That means that for an optical system in its basic setup, the object lies at infinity. The field of view of the optical system is then determined by the angular value, and it was set at approximately 50°. This field of view should then be displayed on the camera chip area. The length

of the chip diagonal is 10 mm. However, there are also other requirements. Towards the eye, a LED used for the system's focus must be projected. When recording the image, the retina must be illuminated. It is assumed that this will be accomplished by a system of LEDs, as the scattered light will go through the eye pupil to the inner eye area.

From these requirements, it is obvious that an optical system cannot be realized by a simple system, e.g. by ocular. If a projection is using a simple ocular with set field of view and chip size, the focal length of ocular would be $f'_{ok} \approx 10{,}7$ mm. Since the achievable distance of the eye pupil from the last ocular's optical area in the direction of the eye is comparable to focal lengths of ocular at most, the eye would have to be located in a close proximity to the ocular. That is obviously not very convenient for measurement, and it would also be difficult to find a space to meet the mentioned additional functions. Therefore, an optical system with two lenses which consists of the ocular and objective (in a direction from the eye to the chip) was chosen. It is basically a reversed usage of the telescope's magnifying glass. In that case, ocular with longer focal length can be chosen, and the image created by this ocular is displayed by the objective to the correct camera chip size. A space between the ocular and objective can then be used for displaying of the focusing diode and illuminating eye retina.

For a 50° field of view (±25° from the optical axis), a five-lens ocular of Erfle type was chosen. The focal length of this ocular is $f'_{ok} = 27.7$ mm, which – as the overall calculation reveals – enables placing the eye pupil to a distance of 25 to 31 mm from the nearest optical area of the ocular. The diameter of the image that was created by the ocular is $d_{ok} = 23.2$ mm. This value must be then reduced to the mentioned 10 mm by the next lens, lateral magnification of the lens is thus, $\beta_{ob} = 0.43$. The whole calculation is based on an assumption that the pupil's diameter, when measured, will be about 5 mm. Then, however, the objective will be relatively light, and for that reason, a pretty difficult six-lens structure is used. If an easier structure is used, it is not possible to reach the required state of residual aberrations of the optical system, i.e. a state which is based on the pixels' size of the chip. In the narrowest place of the cumulative beam between the ocular and the objective, an iris is used with LEDs placed on its perimeter. The fixation target is projected through a beamsplitter with reflectivity $R = 0.2$ which is located in an angle of 45° in the area between the ocular and the iris. This allows reaching the necessary correction state and fulfilling essentially the only requirement – angular width of the bundles displaying points of the LED must correspond with the angular width of the beam bundles when displaying retinal points in the area between the ocular and objective. However, usage of beam splitter produces a lateral offset of the system's optical axis. This has to be taken into account in the mechanical construction.

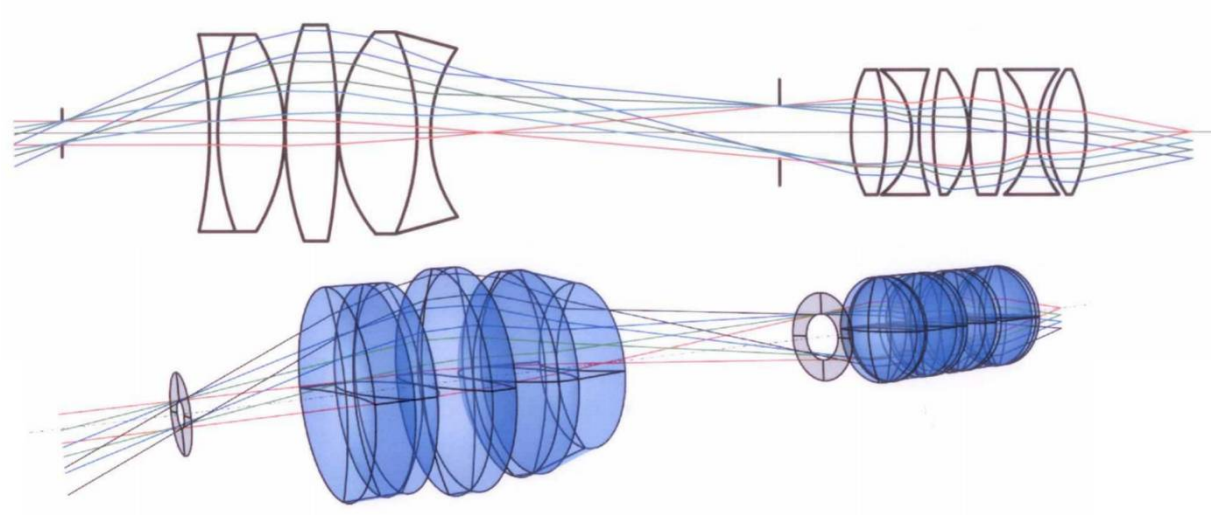

Fig. 3.14: 2D and 3D models of the optical setup.

The focal length of the whole optical system has a value of $f' = 13.47$ mm. Since the diameter of parallel beams' bundles on the system's entry is given by a minimal value of 5 mm, the shortened label of this system 2.5/13.5 is used.

The optical system works mostly in the range of visible light. The system is therefore adapted for the wavelengths of the Fraunhofer spectral lines *e, C'*a *F'* for wavelengths 546.1, 643.8 and 480.0 nm.

In Fig. 3.14, the 2D and 3D models of the described optical system are shown. In these schemes, by the first iris from the left, the location of eye pupil is shown; the second iris is located at the narrowest place of the cumulative beams' bundle, which is also the position of the board with illumination. The positions of the beamsplitter and coated lens of the fixation target LED are not shown. These basic elements with an optional location are part of the mechanical construction's documentation.

3.2.5.2 Mechanical design

The whole optical system is divided into two lens tubes – objective lens tube and ocular lens tube. To suppress unwanted reflections, the whole device has to be built inside a housing which prevents the access of ambient light. The objective lens tube is static whereas the ocular lens tube is movably driven by a stepper motor NEMA 17 ensuring focus on the retinal surface in a given range.

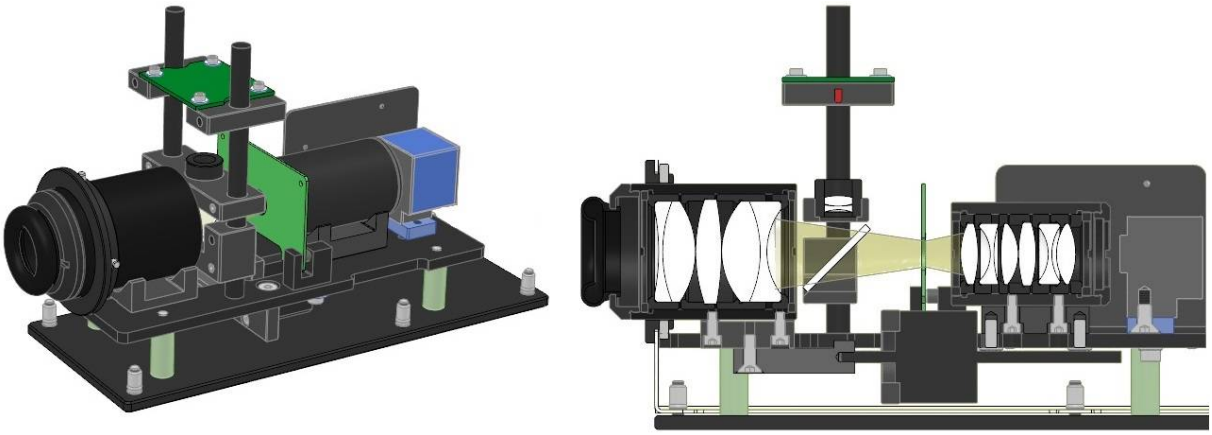

Fig. 3.15: A mechanical concept of the proposed system.

For retinal imaging, the same camera type has been used as in the previous version. Its parameters, especially gain in a given wavelength range and resolution have been proved sufficiently (Imaging source DFK72BUC02). The camera is connected via a USB interface to the computer. The illumination ensures two infrared (780 nm) and visible light spectrum LEDs placed circularly on the iris located between both tubes at a place where the rays' going through the system have the smallest diameter. The eye fixation target is realized by a movable LED (white color) located out of the main optics axis and projected through the beamsplitter. The brightness of the illumination, fixating point, and motor control is controlled by an electronic circuit connected via UART interface to the main computer. The whole imaging process is driven by a computer which is able to adjust the system to the optimal configuration, thanks to the feedback from the camera.

3.2.5.3 Discussion

The previous optical systems were not suitable for scanning of larger datasets of users. This last version has been primarily focused on retinal imaging because iris imaging for medical and biometric purposes is not so challenging. Based on previous experiences, mechanical and optical constructions have been significantly improved, and it is supposed that after a few minor changes, it will be the final version of the part for retinal imaging. During the development, it was also thought to be a part of the

iris imaging whereby a simple change of a few optical components will be possible to acquire the iris image with a sufficient depth of field.

4 Iris and retina biometric fusion

This chapter describes algorithmic processing of human eye retina and iris. It is however not a feature extraction per se, but locating and segmenting typical artifacts such as optical disc or macula in the case of retina. In the next part, different approaches for features extraction are presented and then used for fusion into one biometric pattern.

Detection of artifacts and feature extraction have been published in articles [H03][H05] and [H06]. The fusion itself in [R01].

4.1 Retinal features extraction and matching

Since the retinal vascular pattern is considered as the main source of biometric features, the first step is usually a segmentation of the vascular tree. The segmentation is followed by the feature extraction, which is based on the detection of bifurcations and crossings of the blood vessels.

Generally, the positions and/or mutual positions of these points, together with some additional features, are used for building a feature vector to cope with translation, rotation and scale invariants. For example, the work [108] used orientations of blood vessels in specific bifurcation point together with four nearest bifurcations in their feature vector. The Mahalanobis distance gives recognition rate 98.87 % for different datasets. In [107], there was defined the so-called principle of bifurcation orientation for each bifurcation and together with their positions the point pattern matching method was applied. They achieved total FRR = 4.15 % and EER = 1.16 % for a database containing 2,063 images with small overlap (up to 25 %) from 380 subjects diagnosed with diabetes.

One of the main disadvantages of this approach is the detection of bifurcations and crossings using morphological thinning. This step can lead to various results based on the thinning methods. Therefore, the major part of the current approaches try to avoid this issue using the whole segmented vascular tree. Eigenvalue analysis of vascularity followed by multi-scale image registration to cope with the spatial transformation between the acquired and template image was introduced in [109]. They achieved 100% recognition rate for their own dataset of 284 retinal images. In [110] sampled binary vascular image along defined lines was used in order to extract binary signals for matching achieving over 95% success on about 400 retinal images. Barkhoda et al. [111] used a skeletonized image of vascularity for feature extraction in specific angular and radial partitions. Application of the fuzzy system with Manhattan distance measure leads to 99.75% accuracy using DRIVE dataset. On the other hand, in [112] there was used original intensity image for extraction intensity profiles along circles centered in the fovea, which must be detected. They achieved an averaged FAR per subject below 0.02 for 58 subjects.

4.1.1 Optic disc localization

Several papers deal with the optic disc localization. For example, [73] uses methods called Principal Component Analysis and Gradient Vector Flow Snakes for optic disc borders recognition. This model is very computationally intensive but gives a high accuracy of the blind spot detection. Another approach mentioned in [74] is based on the assumption, that an optic disc roughly takes up to 5 % of the area of the brightest pixels. This method is very fast. Based on thresholding, it is very important to choose an appropriate threshold value which is computed from the average pixel intensities of background and foreground pixels. However, based on experiments on chosen retinal databases, this algorithm is not very precise.

Another work deals with the detection of the optic disc on an image with high levels of gray [88]. This approach works well if there are no pathologies in the image, which would be bright and very contrasting against the background. The principle of area threshold was used in [89] where disc outlines are detected using Hough transformation. That means that image gradient is calculated and as a disc, an area that corresponds the most to its shape is chosen. The problem of this attitude is that the optical disc does not always possess a circular or elliptical shape in the image. It can be overlapped by vessels that protrude it. The principle of Hough transformation was used also in [89]. Despite some improvements, problems were present while detecting the optical disc when the contrast of the images was too low or when the disc's shape was unconventional. Backward vessel tracing that comes from the optical disc, was introduced in [91]. This method is one of the most successful for the localization of the optical disc. Its disadvantage is high resources consumption.

4.1.1.1 Searching pixels with highest average intensity of surroundings

This algorithm was inspired by the approach mentioned in [75]. This is based on low-pass filter application (a new pixel intensity value is decided by an average from the surroundings). The pixels of highest intensities are highlighted, and the brightest area is considered as the center of the region of interest (ROI). Subsequent operations are applied to this area only. The following procedures comprise the application of several filters on the ROI and circle detection using Hough circle transformation [76].

The morphological dilatation and Gaussian blur remove blood vessels from the ROI which may have a negative impact on edge detection. Then Sobel edge detector is used and subsequently an image is converted to a binary form, using thresholding. Noise reduction is performed by morphological erosion. In the last step, Hough transformation is used for the optic disc circle detection. The result is the optic disc center and also its diameter. An example of the whole procedure is shown in Fig. 4.1.

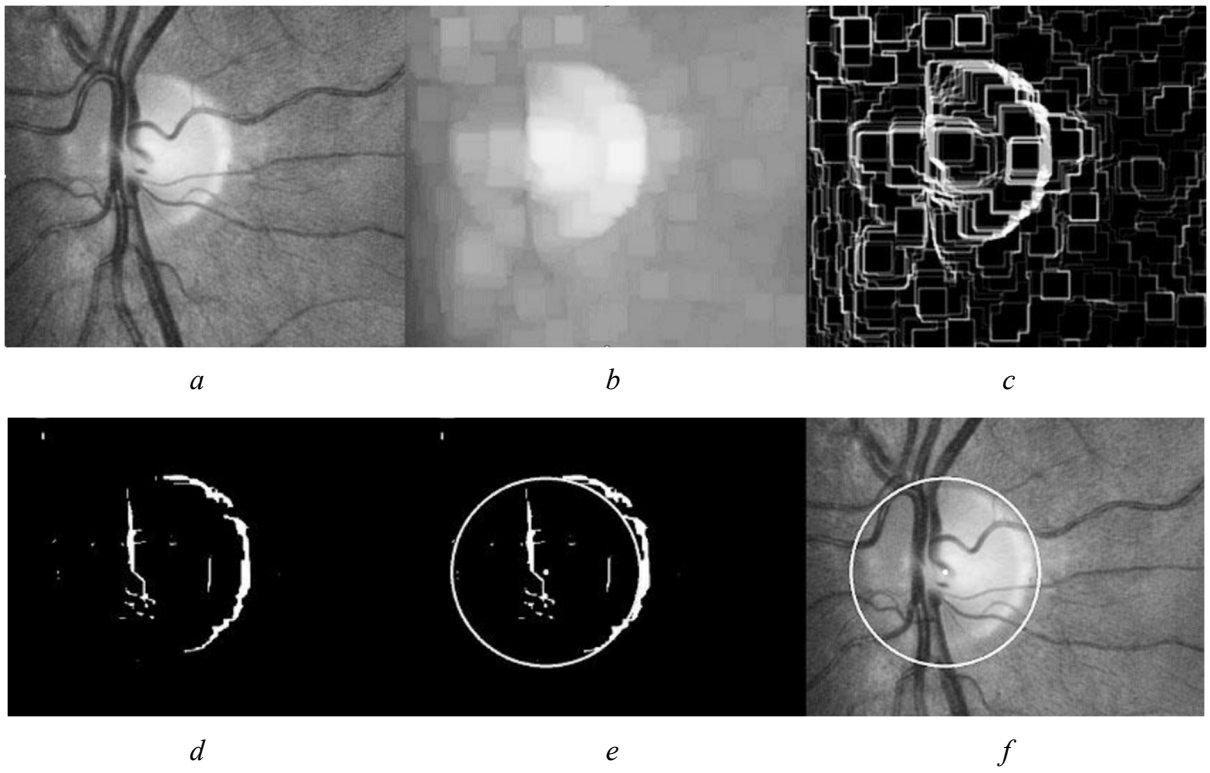

Fig. 4.1: Optic disc localization: a) region of interest; b) removed blood vessels; c) Sobel edge detector; d) eroded binary image; e) Hough circle; f) circle in the original image.

4.1.1.2 Localization based on watershed segmentation

This approach is based on watershed segmentation described in [92]. Various color specters were compared, red (RGB) channel comes out as the most effective for the detection of the optic disc outlines, where its outlines are the most continuous and also the most contrast to the background. Since that channel has a very small dynamic range; and also, since the optical disc belongs to the brightest objects in the image for the detection; it is better to use a brightness channel from the HSV model. For disc localization, the variation of gray level is used. As the optic disc is a bright visual object and vessels appear to be dark in the image, the gray level in papillary areas is higher than in other image areas. That is true only if no disease symptoms or other bright artefacts are present on the dark background. That can be addressed by using a shading corrector. In the image with the gray adjustment, the local variation for each pixel is calculated. The global maximum in this adjusted image is situated in the pupil or next to it, which makes it easier to work with a subset of pixels cut from the original picture which does not contain exudates which could disrupt the optical disc detection. Vessels which could distort the result are eliminated before the watershed segmentation [93] for finding the outlines of the optical disc is used. Then the watershed segmentation is used, and its result is the optic disc outline. The result can be seen in Fig. 4.2. The left image shows partial detection only; the highlighted region overlaps its border. The correctly localized optical disc and the borders of the optical disc corresponding to the borders of the highlighted region are shown in the right image.

Fig. 4.2: Highlighted optic disc in fundus images.

4.1.1.3 CLAHE and median filter

The red color channel of the original image is used, because the optic disc is the most conspicuous there. Such image is processed by CLAHE [128] and median filter, then the Canny edge detection is performed, and Hough circle transformation [76] is used to detect the optic disc. An example is depicted in Fig. 4.3.

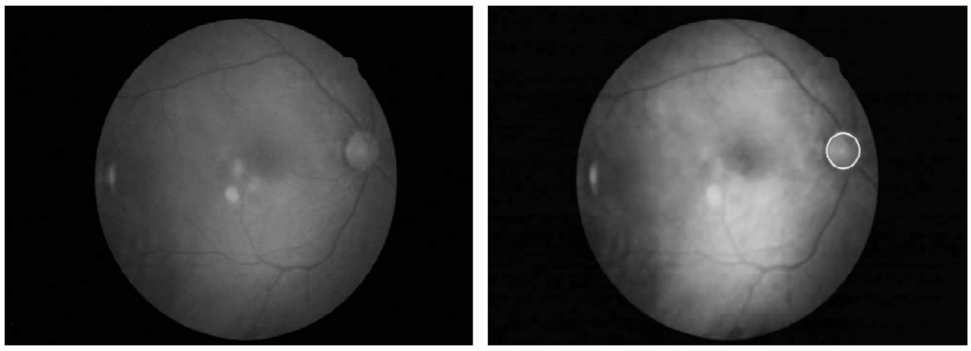

Fig. 4.3: Red channel of the retina image (left), filtered image with optic disc detected (right).

4.1.2 Fovea localization

In literature, various approaches for macula detection exist. In [94], principle based on macula outlines detection was introduced with subsequent optimization using ant colony algorithm. The principle from [95], in which it is first necessary to localize the middle of the optic disc and vascular bed, was also introduced. Then the position of the macula is detected based on the distance from the middle of the optical disc. Thanks to thresholding combined with the obtained mask of the vascular bed, the darkest pixels in the candidate area are searched. Another approach from [91] uses a multilevel thresholding without the need to detect the candidate areas on the retina to detect the macula.

4.1.2.1 Anatomical based approach

Described fovea detection is based on anatomical characteristics of the eyeball, mentioned in [71]. It is based on the assumption that the angle of the optic disc center and the fovea joint is between -6° and +3° from the horizontal line. Their distance roughly corresponds to double of the optic disc's diameter. This defined sector is used, and the rest of the image is marked by the white color. This approach requires the optic disc diameter and position.

The whole procedure comprises a few steps. The ROI is chosen by the sector-shaped area given by the angle, center and distance of the optic disc. The rest of the operations are similar to the optic disc detection described in chapter 4.1.1.1. The low pass filter is applied on the ROI, and the lowest intensity pixels are marked (the fovea is darker than the retinal background). Then the fovea is marked as a center of the largest detected area.

4.1.2.2 Multilevel thresholding-based approach

The algorithm is characterized by low time consumption, and that is one of the reasons why it was also used. The suggested algorithm for the macula detection uses the principle of multilevel thresholding and localizing of ovals through all the image levels. The described approach was inspired by [91].

In the first step, the red channel is extracted from the RGB image because it contains less information than the other channels about vessels and veins in the retina, which can negatively influence the results of ellipse detection. The macula normally does not have a circular or oval shape and its circumference is often irregular. For preprocessing, a blurring filter is used. Then the resulting image of the retina is segmented in a cycle, where each iteration means limit value increased by one during thresholding. The result of one iteration is shown in Fig. 4.4. This way, thresholding runs throughout all 256 levels, as the retina image in this stage is like a gray picture with 8-bit information for each pixel. By analysis of the resulting images, it has been discovered that threshold values from 100 to 230 have results that possess the most information about the macula position and thus are the most appropriate for the next step, during which ellipses are being searched in final particular images.

Fig. 4.4: Red channel of the retinal image after thresholding.

The outlines of ellipses are being searched throughout all thresholding levels. All found ellipses from all threshold levels are saved for further processing. Before that, ellipses that do not fulfill the condition that their eccentricity must be larger than 0.5 and simultaneously smaller than 1.5 are removed. Eccentricity is calculated from a rectangle (defined by Eq. (4.1)), which bounds the ellipse with the width (w) and height (h) of this rectangle. The elimination of these inconvenient ellipses is important for removing of misleading areas because the shape of the macula is either a circle or an ellipse with a small eccentricity. On thresholding levels, the blurring filter is used again.

$$exc = \frac{\sqrt{w^2 - h^2}}{w} \tag{4.1}$$

This is done in order to highlight the round shape of areas on the image. Clustering of found ellipses by their center of gravity is depicted in Fig. 4.5. The blue pixel is the group's center of gravity; the green pixels are the ellipses' centers of gravity that belong to the group, and the red pixels are the centers of gravity of ellipses that do not belong to the group [91].

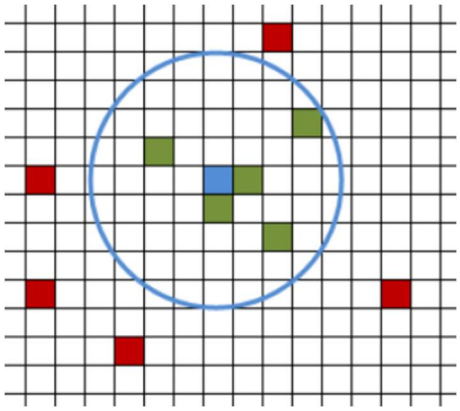

Fig. 4.5: Ellipses clustering.

The last part of the macula detection algorithm consists of all the found ellipses. In the beginning, one group for all ellipses is created, and its center of gravity is the same as the center of gravity of the first ellipse. All ellipses are added to this group. Subsequently, all ellipses are shuffled in cycles. If the distance of the shuffled ellipse's center of gravity to the group's center of gravity to which it belongs is bigger than the chosen threshold, a new group is created. To this newly created group, the ellipse is added, and its center of gravity is selected as the group's center of gravity. When all ellipses go through this process, for each group, the center of gravity is calculated as the average center of gravity of all ellipses that belong to the group.

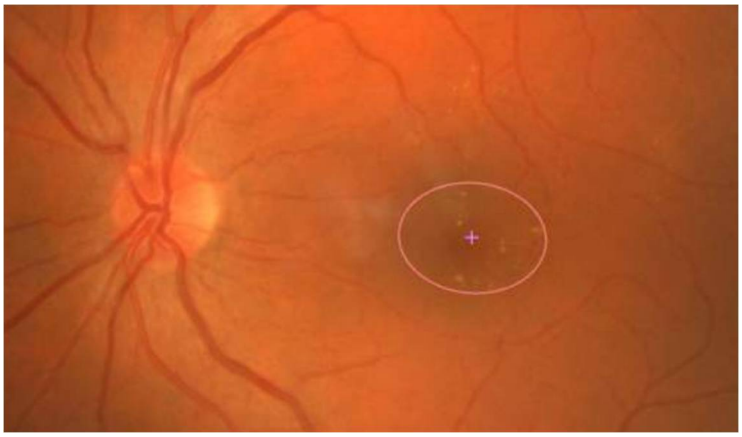

Fig. 4.6: Result of the macula detection in a fundus image.

After this recalculation, all ellipses are evaluated again and if their center of gravity is too far from the group's center of gravity and the found area of the macula circumscribes an ellipse, they are moved to another group or a new group is created for them. That is repeated until no ellipse has to be moved between groups during the evaluation cycle. As the macular area, the biggest ellipse from the group is chosen. The fundus image with marked macula is shown in Fig. 4.6.

4.1.3 Blood vessels segmentation

The basic approaches for blood vessels detection may be divided into two groups – based on morphological operations and based on 2D filter applications realized by different methods such as matched filters [79], Gabor waves [113], etc. Segmentation in the first group is based on morphological operations and is less computationally intensive. For example in [73] there is described a very fast segmentation using stop-hat operation.

4.1.3.1 Thresholding

It is desirable to convert an image into a binary form for subsequent processing. This is made by thresholding. The threshold is computed for every input image with the assumption that blood vessels take up approximately 3-10 % of the retina image (according to a specific type of imaging device). Another way is the use of adaptive thresholding. However, the main disadvantage of this method are the small white fragments, which are misclassified as vessels.

As shown in Fig. 4.7, not only the retinal veins are highlighted but also the noise which must be removed before bifurcations can be detected. This is achieved by filtering out blobs and by morphological dilatation of the image. This removes small holes and increases the vessels continuity.

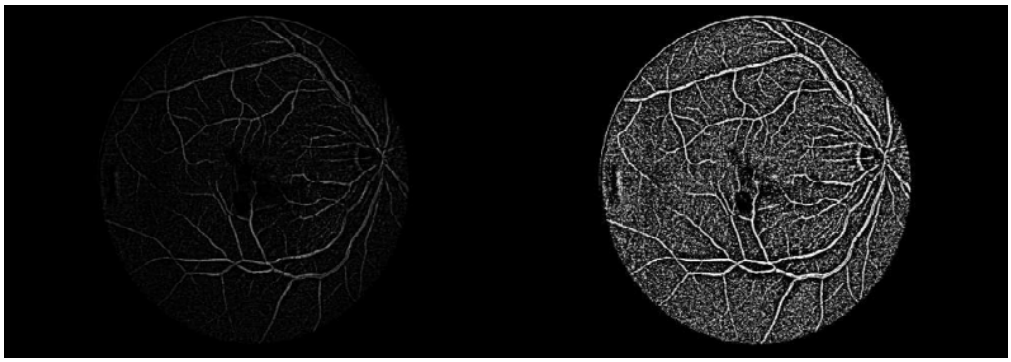

Fig. 4.7: Retinal image before (left) and after (right) thresholding operation.

4.1.3.2 Segmentation using matched filter

The described approach is based on the matched filter for blood vessels detection. All following operations are applied on the green channel of the given image because of higher contrast than in blue or red channel. The whole procedure is depicted in Fig. 4.8.

- **Automatic contrast adjustment –** despite the use of the green channel, blood vessels may have low contrast due to the poor quality of source images. In this case, it is necessary to adjust the contrast. Commonly used methods, such as histogram equalization, are not very suitable in the case of retinal images. The manual contrast adjustment has mostly the best results, but unfortunately, it cannot be applied in the case where the pictures have to be processed automatically. Inspired by [73], the method called *Fast Gray Level Grouping* gives satisfying results for a given set of retinal images. The principle and implementation details are described in [77]. The main advantage of this method is the fact that the new histogram will have nearly a uniform distribution.

- **Matched filter** – the most important part of the blood vessels detection process is the vessels segmentation from the image background. A 2D filter response, which is defined by Eq. (4.2) is used.

$$\mathbf{K}(x,y) = -e^{\left(\frac{x^2}{2\sigma^2}\right)} for\ y \leq \left|\frac{L}{2}\right| \tag{4.2}$$

L stands for the minimal length of the vessel, where it does not change its orientation and σ is the standard deviation in Gaussian (normal) distribution. The exact procedure of the filter generation is based on [47]. The obtained filter is 12 times rotated (each time for 15°), and all the 12 filters are applied on an image. Their responses are added together with their weight resulting in the final response.

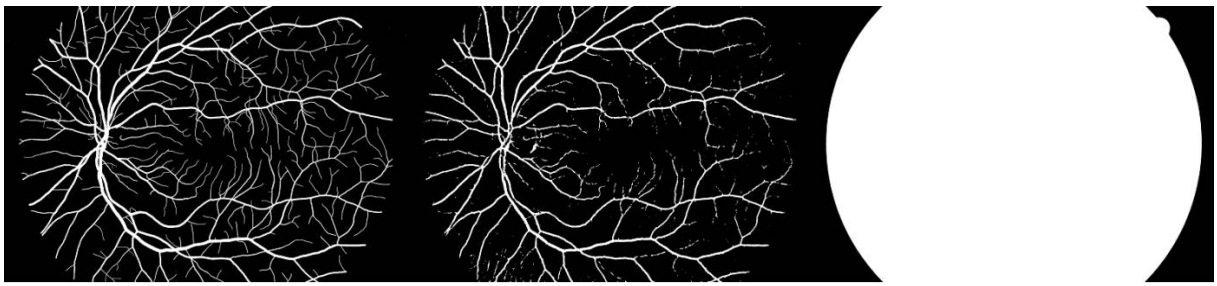

a *b* *c*

Fig. 4.8: Example of the described blood vessels segmentation: a) manually segmented vessels; b) matched filter algorithm used; c) mask of the retinal region in original images.

4.1.3.3 Segmentation using the difference between the filtered image and the original

This method of segmentation has been found as the most suitable for the following fusion thanks to its accuracy and computing speed.

- **Image enhancement** – the input image is enhanced by using the smoothing filters in order to reduce the noise and make the vasculature more visible. In order to obtain the most salient information from the image, the green channel is selected for further processing where the contrast is adjusted by using the Contrast limited adaptive histogram equalization algorithm [81]. This algorithm differs from the simple histogram equalization by calculating histograms for partitions of the image and is added in order to reduce the amplification of the noise inherent to adaptive histogram equalization.

- **Blood vessels detection** – the difference between the filtered image and the original, along with adaptive thresholding is used to segment the blood vessels. The preceding step for segmenting the veins is the application of the median and blurring filters. This produces a relatively smooth image which is then compared with the non-filtered one. The differential image that results from this comparison is calculated according to the Eq. (4.3):

$$diff(x,y) = \frac{255}{max}(original(x,y) - filtered(x,y)) \tag{4.3}$$

where max is the maximum value of intensity difference of the pixels. Although the vascular structure is visible at this point, there is a significant level of noise, and the veins need to be segmented perfectly. The result of this method can be seen in Fig. 4.9.

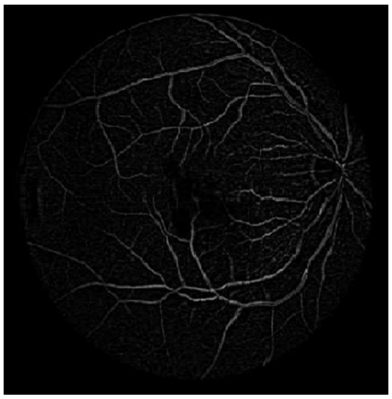

Fig. 4.9: Obtained differential image.

4.1.3.4 Thinning

It is essential that thinned vessel must lie strictly in the middle of the original vessel. The simple but fast and well-working algorithm comes from [9]. The thinning is executed from four directions to ensure the position of thinned vessels in the middle of the original one. The algorithm can be described in accordance with [80] as follows:

1. While points are deleted do
   a. For all pixels $p(i, j)$ do:
      i. If $2 \le B(P_1) \le 6$

         $A(P_1) = 1$

         $P_2 \times P_4 \times P_6 = 0$ in odd iterations, $P_2 \times P_4 \times P_8 = 0$ in even iterations

         $P_4 \times P_6 \times P_8 = 0$ in odd iterations, $P_2 \times P_6 \times P_8 = 0$ in even iterations

      ii. Then delete pixel $p(i, j)$

Where $A(P_1)$ is the number of 0 to 1 transitions in a clockwise direction from P_9 back to itself, and $B(P_1)$ is the number of non-zero neighbors of P_1. The result of thinning algorithm is depicted in Fig. 4.10.

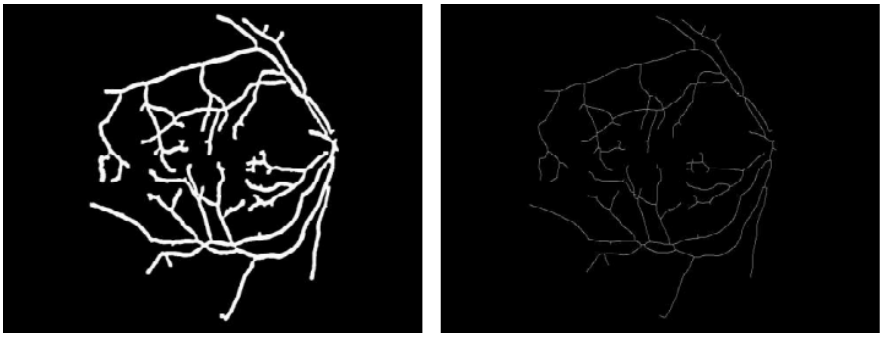

Fig. 4.10: Segmented blood vessels (left) after the thinning operation (right).

4.1.4 Bifurcation localization

Bifurcations are obtained by evaluating every white pixel and its immediate neighborhood. If a bifurcation is to be marked, there must be at least three separate paths that diverge from a given pixel. To calculate this, the neighborhood is analyzed for the number of white pixels and their continuity. If three or more separate white areas are detected, the algorithm regards that pixel as a bifurcation, and

marks it and stores it in a list of points. If thinning yields an imperfect image with clustered bifurcations, the algorithm has to filter out such bifurcations. The only problem may be caused by the short pieces at the ends of the vessels created as a side effect of thinning. This problem is solved by the definition of a minimal length of the whole 3 vessels coming out from the point.

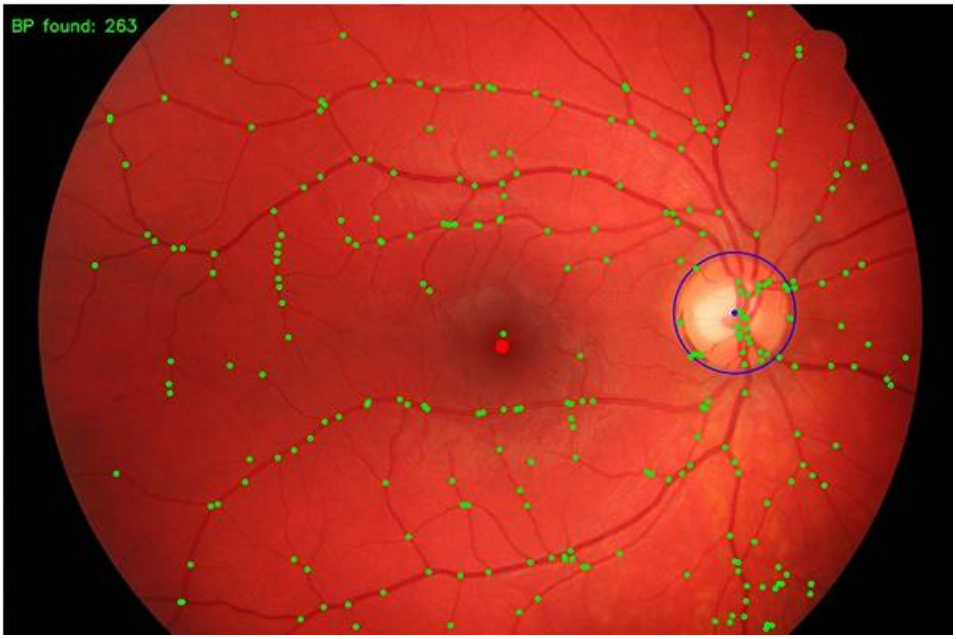

Fig. 4.11: Automatically detected bifurcations in an original image also with the optic disc and fovea.

4.1.5 Feature comparison

The comparison module takes two feature vectors. The position of the optic disc is utilized to align bifurcations before image comparison. The adjusted vectors are compared, and the respective score is calculated in accordance with the level of similarity. The score is normalized so that it falls within the interval <0, 1> where a higher value indicates a better match.

First, the two vectors have to be aligned before comparison. This is achieved by taking the optic disc centers and translating the bifurcation points of one image. Since the rotation or angular displacement of images is minimal, only the translation is taken into account.

Next, the similarity score needs to be calculated. The algorithm is as follows:

1. For every bifurcation point b_1 in the smaller array of bifurcations B_1
   a. For every bifurcation non-matched point b_2 in the larger array of bifurcations B_2
      i. If Euclidean distance between b_1 and b_2 is shorter than the *threshold* and is currently the shortest, mark b_2 as selected
   b. If there is a match, mark selected b_2 as matched and increase the number of matched bifurcations n
2. Calculate the similarity score

Then the score is obtained accordingly to Eq. (4.4):

$$score = \frac{2n}{|B_1|+|B_2|} \tag{4.4}$$

4.2 Iris features extraction and matching

There is a considerable range of articles focused on the iris recognition. One of the first automated iris recognition systems based on the utilization of Gabor wavelet filters was proposed by Daugman [114]. Several leading and most cited articles can be mentioned, just to outline the widely used approaches for the person's recognition based on the iris characteristic [41][115][116]. Usually wavelet-based [114][41] or texture-based [115] methods for iris recognition are utilized. Other well-known approaches adopted discrete cosine transform (DCT) [116] to the iris pattern encoding. Somewhat recently, new methods for iris characteristic have been published in [117][118][15]. These approaches utilized the key point descriptors like SIFT (*Scale-Invariant Feature Transform*) [117] and SURF (*Speed Up Robust Features*) [118] for the description of the local iris image areas. Also, inspired by earlier approaches, a new approach using wavelets and Gabor filters in combination with support vector machine and Hamming distance classifiers was proposed in [15].

The current iris recognition approaches usually achieve classification accuracy more than 99 %. In spite of the current methods, they are very precise and reliable (for ideal images); still, some drawbacks concerning image quality and image acquisition do exist.

4.2.1 Pupil and iris localization

The pupil can be localized by applying an appropriate thresholding technique. First, however, a median filter is applied to the image. This step smoothes out the image and eliminates pixels with outlying values, which further helps in the segmentation procedure.

In order to determine the threshold value, the histogram of the image is calculated. In the lower half (the darker part) of the histogram, a pronounced peak can be found. This, together with the surrounding values, mainly denotes the pixels of the pupil. Therefore, the desired threshold has to be found around this peak. The chosen threshold is higher than the value of the peak in the histogram to ensure that the majority of the pixels of the pupil is included.

After thresholding is applied, the largest black area in the acquired image is bound to denote the pupil. Since it is elliptical in shape, detecting its center and radius can be determined simply by seeking its widest areas. The pupil itself is not entirely circular, but it can be substituted by a circle for the sake of simplicity and avoiding computational complexity.

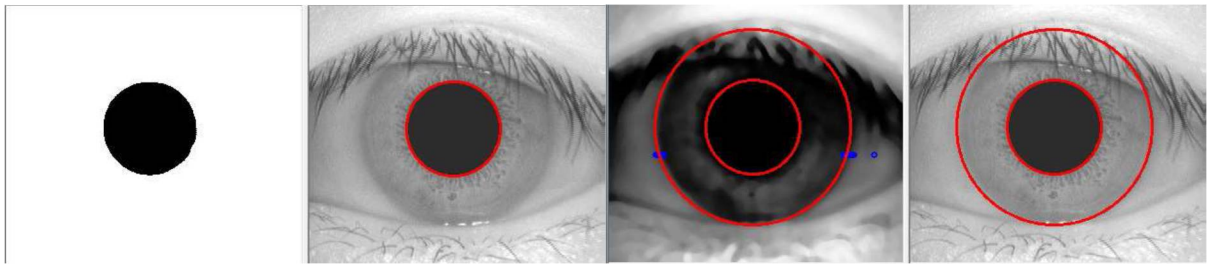

Fig. 4.12: Segmented pupil (left) and the iris. The blue points denote the detected shifts in pixel intensity.

While the pupil and its surroundings were distinguished from each other by a striking shift in the pixel intensity, the outline of the iris was not so distinct. Therefore, a different approach must be adopted. Although the shift in pixel intensity is not so pronounced, it is present nevertheless. To facilitate its detection, the contrast of the image needs to be adjusted. Together with the use of the median filter, this accentuates the current area of interest which is the outer edge of the iris.

While not being as sharply defined as in the case of the pupil, the outer edge of the iris can be detected by searching for places where the pixel intensity changes clearly over a certain distance. Within the input database, as mentioned above, this approximation gives satisfying results, however this method

is not always applicable because of poorer quality of some images. To mitigate this issue, a failsafe method using 1D Haar wavelets is employed. Although the iris is not entirely circular as well, it is still safe to substitute it by a circle. Additionally, the iris and the pupil are not concentric in general, but to make the algorithm faster and simpler, it has been assumed that they actually are.

Combined with the detected points where the edge of the iris is located, the radius of the iris can be calculated and thus the extraction of the iris from the image is completed. The whole localization procedure is depicted in Fig. 4.12.

4.2.2 Features extraction

The approach at this point varies, but in this algorithm, the unrolling of the iris precedes the segmentation of eyelids. For this unrolling, the Daugman's rubber sheet is used. At this point, the rubber sheet is reduced to a rectangular image with the width of 360 pixels.

Eyelids and eyelashes are filtered out by the detector of pixel intensity change along the border of such rectangular image (the stripe). Given the fact that the rough location of the eyelids is predictable, the algorithm defines set boundaries within which the detection is performed. Once the horizontal borders are determined, the algorithm similarly detects the height of the eyelid. When this is done, two masks in the form of tetragons are generated, which have to be taken into account during the final phase of the feature extraction. Of course, this is true only if there are eyelids in the image.

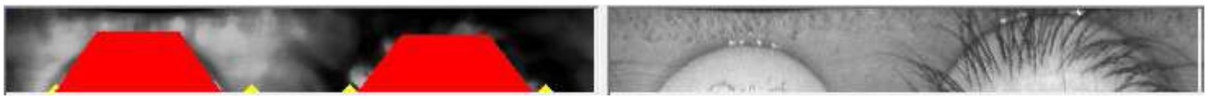

Fig. 4.13: Eyelid detection and mask generation. The yellow points denote the borders of examined regions.

4.2.2.1 Features extraction using Gabor filter

Gabor filter is represented by the following alternating function:

$$g_{\lambda,\theta,\varphi,\sigma,\gamma(x,y)} = e^{-\frac{(x\cos\theta+y\sin\theta)^2+\gamma^2(-x\sin\theta+y\cos\theta)}{2\sigma^2}}\cos\left(2\pi\frac{x\cos\theta+y\sin\theta}{\lambda}+\varphi\right) \tag{4.5}$$

with the values of wavelength $\lambda = 2$, orientation $\theta = 0°$, phase offset $\varphi = 0$ and aspect ratio $\gamma = 0$.

Before vector quantization, the issue of data reduction has to be addressed. As the height of the stripe can vary (depending on the radius of the iris), the answer to this problem also involves the solution of the issue of potentially varying dimensions of the stripe.

In order to resolve this, certain angular and radial slices of the rubber band are selected for quantization, so that the expected feature vector is of the desired size. During this part, it is necessary to take the eyelid mask into account and map it in accordance with the feature vector. The quantization itself is achieved by using cosine and sine filtering with the resulting vector size of 2,048 bits. This represents a 128×8 pixel encoding of the resulting iris stripe, with one real and one imaginary bit for every pixel. At this point, the feature vector is complemented by a corresponding mask.

4.2.2.2 Features extraction using LBP

The local binary pattern is a method used for classification in computer vision. It is a powerful tool for texture classification first described in [82]. The method describes pixel in the image by a feature vector which is defined with regard to the surroundings [83]. In this case, a basic LBP has been used considering 8-neighbourhood.

The LBP is computed by the following method. Each center pixel marked value g_c is compared with 8-neighbourhood $g_0 - g_7$, where 0-7 is the index determining the feature position in the resulting vector of size 8 bits (1 byte). The vector value is given by comparison with the pixel in the center. Depending on if the value is smaller or higher the value in resulting vector is 0 or 1. The base principle of the LBP is depicted in Fig. 4.14.

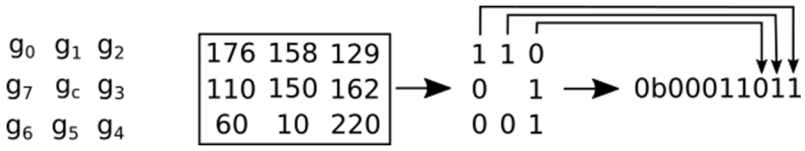

Fig. 4.14: LBP principle.

And from mathematical point of view, it can be expressed by Eq. (4.6).

$$LBP_{P,R} = \sum_{p=0}^{P-1} s(g_p - g_c)2^P, s(x) = \begin{cases} 0, x > 0 \\ 1, x \leq 0 \end{cases} \tag{4.6}$$

where g_p is a value of the surrounding pixel with index p, g_c is a value of the center pixel, P is the surroundings size (in our case 8) and 2^P is a position in the resulting vector. The computed value is then stored on the original position of g_c pixel. Example of the resulting image is shown in Fig. 4.15.

Fig. 4.15: Example of LBP applied on iris image.

4.2.3 Features comparison

Unlike the retinal part, the iris feature comparison is relatively simple. Given two feature vectors, exclusive OR (XOR) operator is applied to the corresponding bits. In this algorithm, if the values are equal, the similarity score is incremented. The masks of respective vectors are used to filter out those pixels which do not include the iris. This reduces the number of pixels to be compared. Thus, the resulting score is normalized so that it fits within the interval between 0 and 1 as depicted in Eq. (4.7).

$$score = \frac{score}{2{,}048 - maskedBits} \tag{4.7}$$

Because of potential differences in the angular position of the input image which were neglected in the feature extraction phase, the score is calculated for several slightly differing angles ranging approximately from -16° to 16°. The highest score is then selected as the final score and passed on into the decision-making process.

Another but actually very similar approach is to use Hamming distance of two feature vectors according to Eq. (4.8).

$$H = \frac{1}{L}\sum_{j=1}^{L} A_j \oplus B_j \tag{4.8}$$

Where L is the size of compared vectors.

4.3 Score-level fusion

The score-level fusion is described in detail, as it has been used as a main fusion method for experiments in this work. Some of the results presented in this chapter were achieved in a close cooperation with a MSc. student working on his diploma thesis [97].

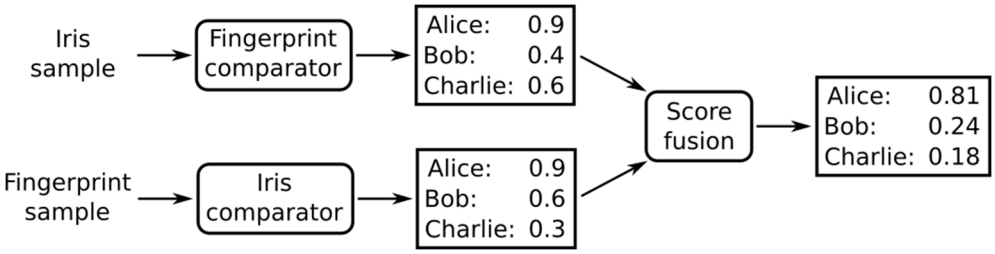

Fig. 4.16: Example of biometric fusion at the score level.

It is relatively undemanding to combine the scores generated at this level. Additionally, the score data contains an important information about the input pattern; thus the fusion at the score level is also the most frequently employed approach in multimodal biometric systems. An example of the score level fusion procedure is depicted in Fig. 4.16 – in this case the resulting score for each person is calculated as a multiplication of scores of each particular trait. Score-level fusion can be divided into three categories [58]:

- density-based,
- transformation-based,
- classifier-based.

Normalization

Individual comparative units might not produce a homogenous data. For example, the data may differ in their range, representation, or probability distribution. Therefore, it is necessary to address this issue and normalize the output data of comparators [67].

One of the methods of score normalization is called decimal scaling. This is usually applied when the scores are on a logarithmic scale – see Eq. (4.9):

$$ns_j^t = \frac{s_j^t}{10^{n_j}} \tag{4.9}$$

Where $n_j = \log_{10} max_{i=1}^{N} s_j^i$ and s_j^i is the i^{th} score produced by the j^{th} comparator. In case of problems with outlying values or uneven tail distribution, the median and median absolute deviation can be used.

Tanh-estimators [68] present a robust and highly efficient way of score normalization. The function is defined as Eq. (4.10):

$$ns_j^t = \frac{1}{2}\left(\tanh\left(0.01\left(\frac{s_t^j - \mu_{GH}}{\sigma_{GH}}\right)\right) + 1\right) \tag{4.10}$$

where μ_{GH} is the mean and σ_{GH} is the standard deviation estimate given by Hampel estimators and their parameters a, b, c. Tanh-estimators significantly reduce the influence of scores from the tail section of distribution and are not sensitive to outlying values. However, if there are many values in the tail, the method might prove as inefficient. In order to achieve the best results, the parameters have to be selected carefully.

4.3.1 Theoretical framework

The score-level fusion has been discussed more in detail in [69], in which the authors defined a theoretical framework for combining scores of distinct comparisons.

Given the problem of classifying an input pattern X into one of M possible classes $\{\omega_1, \omega_2, \ldots, \omega_M\}$, let's assume that there are R classifiers, each representing a given biometric pattern by a specific measurement vector. Let's denote x_i the vector used by the i^{th} classifier. Each class ω_k is represented by the probability density function $p(x_i|\ \omega_k)$, and its probability is $P(\omega_k)$.

According to the Bayesian theory, given measurements x_i, $i = 1,\ldots, R$, and the pattern X should be assigned to the class ω_i so that the a posteriori probability of that interpretation is at its maximum as defined by Eq. (4.11) [69]:

$$\begin{aligned} &assign\ X \rightarrow \omega_i\ if \\ &P(\omega_i\ |x_1, \ldots, x_R) \geq max_{k=1}^{M}\ P(\omega_i\ |x_1, \ldots, x_R) \end{aligned} \tag{4.11}$$

where $k = 1, \ldots, M$. The a posteriori probabilities $P(\omega_k \mid x_1, \ldots, x_R)$ can be expressed using Bayes theorem as follows – Eq. (4.12) [69]:

$$P(\omega_k|x_1, \ldots, x_R) = \frac{P(x_1, \ldots, x_R|\omega_K)}{P(x_1, \ldots, x_R)} \tag{4.12}$$

where $p(x_1,\ldots,x_R)$ is the joint probability density of unconditional measurements. It is defined in terms of conditional measurement distributions as Eq. (4.13) [69]:

$$p(x_1, \ldots, x_R) = \sum_{i=1}^{m} p(x_1, \ldots, x_R|\omega_i)\, P(\omega_i) \tag{4.13}$$

4.3.1.1 Transformation-based fusion

The previous definitions can be used to deduce rules for the score-level fusion [69], where the number of classes M can be reduced to two because there are only two types of classes – genuine users and impostors. Namely, these rules are [69]:

- product rule,
- sum rule,
- max rule,
- min rule,
- median rule.

The *product rule* is based on the assumption that the feature representations $x_1,\ldots,x_R$ are statistically independent. It can be denoted in accordance with Eq. (4.14):

$$\begin{aligned} &assign\ X \rightarrow \omega_i\ if \\ &\prod_{i=1}^{R} P(\omega_r|x_i) \geq \prod_{i=1}^{R} P(\omega_k|x_i)\,, k = 1, \ldots, M \end{aligned} \tag{4.14}$$

The problem with the product rule is that it is sensitive to errors. If merely one classifier yields a probability close to zero, the resulting product is then also lowered to a near-zero value and this may lead to an incorrect classification decision.

The *sum rule* is based on the assumption that the a posteriori probabilities do not deviate notably from a priori probabilities, although it is worth noting that this assumption might not always be true. This rule is resistant to errors in the estimation of a posteriori probabilities [69].

It can be defined in accordance with Eq. (4.15):

$$assign\ X \rightarrow \omega_i\ if \\ \sum_{i=1}^{R} P(\omega_r|x_i) \geq \sum_{i=1}^{R} P(\omega_k|x_i)\,, k = 1, \dots, M \tag{4.15}$$

The *max rule* estimates the mean of the a posteriori probabilities by their maximum value as follows by Eq. (4.16):

$$assign\ X \rightarrow \omega_i\ if \\ max_{i=1}^{R} P(\omega_r|x_i) \geq max_{i=1}^{R} P(\omega_k|x_i), k = 1, \dots, M \tag{4.16}$$

The *min rule* is the exact opposite of the max rule and can be defined accordingly to Eq. (4.17):

$$assign\ X \rightarrow \omega_i\ if \\ min_{i=1}^{R} P(\omega_r|x_i) \geq min_{i=1}^{R} P(\omega_k|x_i), k = 1, \dots, M \tag{4.17}$$

If *a priori* probabilities are assumed to be equal, the sum rule can be regarded as the average of the a posteriori probabilities. However, if one of the classifiers produces an outlying value, the average will be affected and this may result in an incorrect decision. This can be remedied by using the median, leading to the *median rule* – Eq. (4.18):

$$assign\ X \rightarrow \omega_i\ if \\ median P_{i=1}^{R} P(\omega_r|x_i) \geq median P_{i=1}^{R} P(\omega_k|x_i), k = 1, \dots, M \tag{4.18}$$

4.3.1.2 Density-based fusion

The next technique is density-based fusion. In this case, it is necessary to define S_{gen} which denotes genuine comparison scores and S_{imp} which denotes impostor comparison scores. Also, let $F_{gen}(s)$ be the distribution function of S_{gen} and $f_{gen}(s)$ be the corresponding density – see Eq. (4.19) [58]:

$$P(S_{gen} \leq s) = F_{gen}(s) = \int_{-\infty}^{s} f_{gen}(v)\, dv \tag{4.19}$$

Accordingly, F_{imp}(s) is the distribution function of S_{imp} and $f_{imp}(s)$ is the corresponding density function – see Eq. (4.20):

$$P(S_{imp} \leq s) = F_{imp}(s) = \int_{-\infty}^{s} f_{imp}(v)\, dv \tag{4.20}$$

The densities $f_{gen}(s)$ and $f_{imp}(s)$ represent the probability density functions of the comparison score. They are usually not known in advance and need to be approximated from a training set of genuine and impostor classes. The estimation can be done either by parametric or non-parametric methods [70].

4.3.1.3 Classifier-based fusion

The last approach is the classifier-based fusion. In this technique, a pattern classifier is used to learn the relationship between the score vector and the a posteriori probabilities of the genuine and impostor classes [70].

In this method, the vectors are split into two categories based on the aforementioned classes. Given a training set, the pattern classifier derives a boundary between the two classes. Since the classifier is able to learn the decision boundary regardless of the format of the score vectors, they are not required to be homogenous [58]. With this approach, there are several models on which the classifiers can be based, including but not limited to [71]:

- k-nearest neighbor,
- decision tree,
- logistic regression,
- linear discriminant.

For example, the authors of [72] implemented a biometric system fusing data on the score level with a decision tree and linear discriminate classifiers. They combined fingerprint, face, and hand geometry modalities.

4.4 Experimental results

The previously described methods for the retina and iris images processing have been tested on several public and private databases. For testing purposes, images of the retina from multiple sources were used. Testing the program using databases from various sources was chosen, so that the ability of the created program to work with the images without the need to configure parameters after a change of the inclusion for retinal image creation would be tested. All the described algorithms were implemented in C++ language using OpenCV open source computer vision library.

Retinal databases:

- **DRIVE**[1] – retinal images were captured by Canon CR5 non-mydriatic 3CCD camera with a 45° field of view (FOV). Each image is with 8 bits per color plane at 768×584 pixels. The FOV of each image is circular with a diameter of approximately 540 pixels. For this database, the images have been cropped around the FOV. The set of 40 images has been divided into training and a test set, both containing 20 images. For the training images, a single manual segmentation of the vasculature is available and for the test cases, two manual segmentations are available.
- **STARE**[2] – contains 400 raw images acquired in 24-bits per pixel with a dimension of 576×768 pixels. It also contains a list of diagnosis for each image with expert annotations visible in each image. There are also segmented blood vessels including 40 hand-labeled images.
- **Gold Standard Database for Evaluation of the Fundus Image Segmentation Algorithms**[3] – this database consists of 48 images, with a resolution of about 8 MPix. Those images are divided into three groups. The first one contains images of healthy eyes; the second one contains eyes afflicted by glaucoma and the last one are eyes afflicted by diabetic retinopathy. The database contains manually segmented blood vessels.
- **Retina EBD STRaDe DB** – set of images supplied by the STRaDe (research group at the Faculty of Information Technology, Brno University of Technology (CZ), focused on security in IT and biometric systems) laboratory. The database contains 684 images of

[1] Available at http://www.isi.uu.nl/Research/Databases/DRIVE/
[2] Available at http://cecas.clemson.edu/~ahoover/stare/
[3] Available at https://www5.cs.fau.de/research/data/fundus-images

both retinas from 110 distinct people, totaling 220 distinct samples. Unfortunately, a significant part of this set consists of very low-quality pictures.

- **UNM** – database kindly provided by the University hospital of Martin (SK). The number of images of this database is 50 with resolution 4,288×2,848 pixels.
- **ADCIS e-optha**[4] – in total 35 healthy fundus images with various resolutions.

Iris databases:

- **CASIA-IrisV1**[5] - this database consists of 756 iris images from 108 distinct people. The database contains close-up grayscale pictures of varying quality. In this database, some irises are clearly visible, while others are partially obscured by eyelids and eyelashes. There are almost no anomalies in the images in this aspect, no dots of light that would require additional attention.
- **DIARETDB1**[6] - The database consists of 89 color fundus images of which 84 contain at least mild non-proliferative signs (Microaneurysms) of the diabetic retinopathy, and 5 are considered as normal which do not contain any signs of the diabetic retinopathy according to all experts who participated in the evaluation. Images were captured using the same 50° FOV digital fundus camera with varying imaging settings.
- **Iris EBD STRaDe DB** – set of images supplied by the STRaDe laboratory. The database 684 images of both retinas from 110 distinct people (220 distinct retina samples) with 4,288×2,848 pixel resolution.

4.4.1 Optic disc localization

4.4.1.1 Optic disc localization based on pixel intensities

The following results follow the detection procedure described in chapter 4.1.1.1. The correct application behavior is that the optic disc center is successfully recognized. The case where the application misclassifies the optic disc center and continues in running is considered as incorrect. The results are shown in Tab. 4.1. The algorithm has troubles with locating the optic disc in the images of the eyes which are highly affected by diabetic retinopathy.

Set	Correctly localized [%]	Not localized [%]	Incorrectly localized [%]
Golden	89.58	8.33	2.08
STRaDe	70.95	28.38	0.68
DRIVE	85.00	5.00	10.00
STARE	64.26	21.43	14.29

Tab. 4.1: Pixel intensities based on optic disc localization results.

4.4.1.2 Optic disc localization based on watershed segmentation

The optical disc is localized by the method of local variance in preprocessed red channel. In this case, the monitored values were true positive rate and false positive rate. The results of testing are shown in Tab. 4.2. They demonstrate that the algorithm can localize the optical disc with great success. The found region does not surround the whole optical disc's area, but only a part of it.

[4] Available at http://www.adcis.net/en/Download-Third-Party/E-Ophtha.html
[5] Available at http://biometrics.idealtest.org/dbDetailForUser.do?id=1
[6] Available at http://www.it.lut.fi/project/imageret/diaretdb1

Set	True positive rate	False positive rate	Success rate [%]
DRIVE	71.23	92.38	90
UNM	65.85	87.05	74
ADCIS	70.99	88.15	91

Tab. 4.2: Optic disc localization based on watershed segmentation.

4.4.2 Fovea localization

4.4.2.1 Fovea localization based on anatomical characteristics

The essential precondition for the fovea localization is the successful optic disc's center localization. The results in Tab. 4.3 consider only the situations where the precondition has been met. Incorrectly localized foveae were in cases where the optic disc was detected correctly but the fovea incorrectly.

Set	Correctly localized [%]	Incorrectly localized [%]
Golden	95.35	4.65
STRaDe	90.48	9.52
DRIVE	70.59	29.41
STARE	55.56	44.44

Tab. 4.3: Results of anatomical based fovea localization.

4.4.2.2 Fovea localization based on multilevel thresholding

For the macula localization in this work, a procedure based on multilevel thresholding was introduced in chapter 4.1.2.2. During its testing, monitored values were precision and success. Accuracy reflects the deviation ratio of the center localization to the retinal diameter. The results of the implementation are shown in Tab. 4.4.

Set	Accuracy [%]	Success rate [%]
UNM	98.13	68.00
DRIVE	96.40	76.00
ADCIS	96.38	81.00

Tab. 4.4: Results of multilevel thresholding based localization.

4.4.3 Blood vessels segmentation

4.4.3.1 Blood vessels segmentation using matched filter

The testing of blood vessels segmentation described in chapter 4.1.3.1 was driven in the way of comparing the corresponding pixels of manually segmented vessels and algorithm output after the closing operation. The final score was computed as the ratio of the same value pixels count to the count of all foreground pixels. The results can be seen in Tab. 4.5.

Set	Healthy [%]	Glaucoma [%]	Diabetic retinopathy [%]
Golden	95.78 ± 1.01	95.00 ± 0.98	94.12 ± 1.77
DRIVE	92.90 ± 2.27		
STARE	79.62 ± 7.03		

Tab. 4.5: Results of blood vessels segmentation.

4.4.4 Bifurcation points localization

The testing related to the procedure described in chapter 4.1.4 was performed by visual check only, due to the high number of points in each picture impossible to be marked. The average number of bifurcation points detected by the algorithm is 256 per one image. This number was the lowest one in the case of healthy images. On the other hand, it was the highest in the case of retinal images with a disease. It is caused by the affected retinal image with bright and dark stains. These are wrongly selected as veins, and a lot of fake bifurcation points is detected.

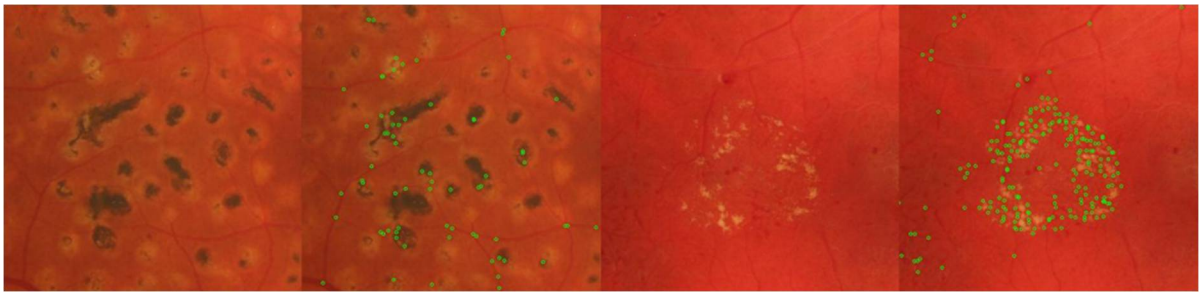

Fig. 4.17: Examples of an algorithm with diseased retinal images.

The both cases are depicted in Fig. 4.17. It can be assumed that the algorithm will have problems with a higher accuracy in diseased retinal images. The statistics of the detected bifurcation points is shown in Tab. 4.6.

	Healthy	Glaucoma	DR	Total
Average value	242	249	277	256
Deviation	50	87	59	67

Tab. 4.6: The number of bifurcation points discovered in the set of images.

4.4.5 Iris recognition using LBP

The experiment was performed on STRaDe EBD Iris database. The first results were not too satisfying – FAR = 17.8 % and FRR = 21.1 %. Based on experiments, Gaussian smooth was applied for noise reduction in the iris images before LBP. In this case, better results were achieved with FAR = 3.3 % and FRR = 3.5 % using Gaussian kernel with a size of 19×19 (see Fig. 4.18 and Fig. 4.19). In both cases, the threshold was set at the value near to ERR.

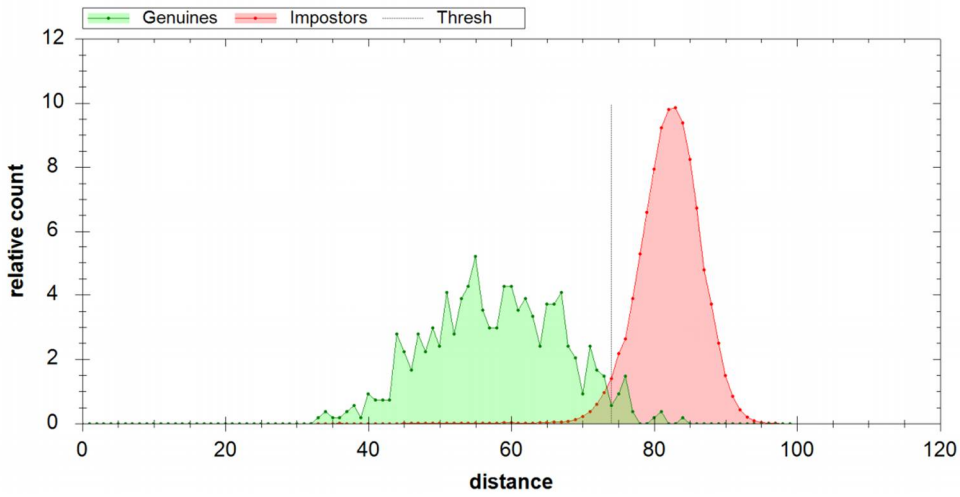

Fig. 4.18: Genuine impostor distribution for FAR = 3.3 % and FRR = 3.5 %.

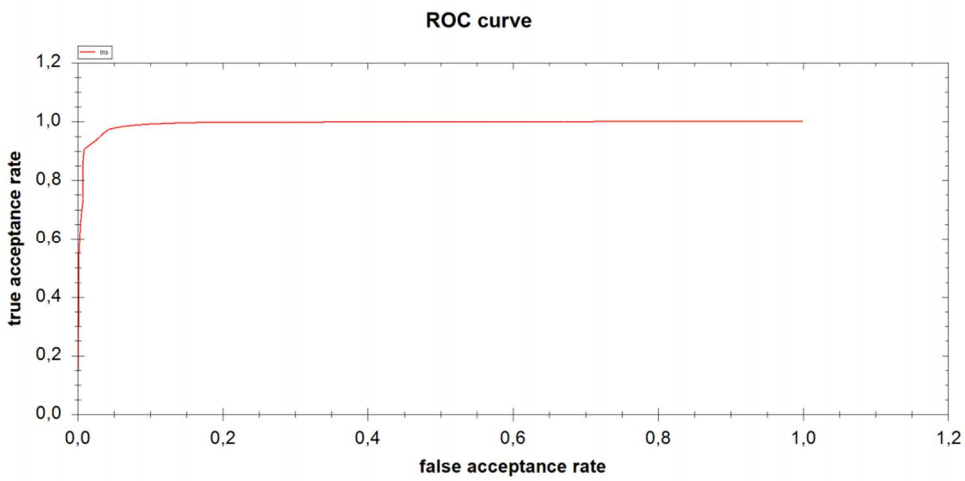

Fig. 4.19: ROC curve for FAR = 3.3 % and FRR = 3.5 %.

4.4.6 Iris and retina fusion

The fusion in such a biometric system is performed at the score level, using transformation-based methods discussed in section 4.3. Since iris and retina are statistically independent biometrics (there is no correlation between them), it would be justifiable to use different databases for the iris and for the retina.

However, given the fact that the two original databases differ in the number of images and people, they have been merged, and the people and images have been paired.

The methods used for transformation are:

- product rule,
- sum rule,
- max rule,
- min rule.

The median rule is excluded because it would not make sense to calculate the median value of two biometrics. Because of the ease of implementation, AND/OR fusion at the decision level is also incorporated, though merely for informative purposes.

Although the scores from the previous blocks of the system were normalized to fit within the interval of 0 and 1, the distribution of scores can be uneven (e.g. the threshold value of 0.5 could be too strict for the iris but too lenient for the retina), what means that further normalization is required. This is achieved by determining the minimum and maximum values of each biometric separately. After acquiring these values, the scores are adjusted accordingly and then the fusion is performed.

The developed biometric system was evaluated using two databases: the CASIA-IrisV1 database for the iris and the STRaDe group database for the retina. The former one contains 756 iris images of 108 distinct people and the latter contains 684 images of both retinas from 110 distinct people (220 distinct retina samples). After pairing of these databases, the resulting set contains in total 324 images of 108 different samples.

In order to evaluate the fusion results, the individual biometrics must first be evaluated separately. During the development of the iris recognition algorithm, parameters for the Gabor filter needed to be selected in order to achieve the best performance possible.

In Tab. 4.7 and Tab. 4.8, the performance of the system is shown using various values of wavelength and orientation of the filter, and different algorithms, respectively. The performance analysis was

tested on the full iris database. It is clear that the best results are achieved by using the wavelength $\lambda = 2$ and orientation $\theta = 0°$.

ERR				
Length of wave of Gabor filter	**Orientation**			
	-45° [%]	**0° [%]**	**45° [%]**	**90° [%]**
2	4.7	1.8	4.0	22.6
4	4.5	2.8	3.8	23.1
8	4.1	2.8	3.7	23.9
16	4.3	2.9	3.8	23.8

Tab. 4.7: ERR scores of the biometric system with various wavelengths and orientations used in Gabor filter.

During the development of the retina recognition algorithm, four score obtaining methods were considered, based on the following parameters:

1. average Euclidean distance of all bifurcation pairs (Algorithm 1),
2. average Euclidean distance of bifurcation pairs with Euclidean distance lower than a given threshold (Algorithm 2),
3. doubled number of matched bifurcation pairs / total count of bifurcations (Algorithm 3),
4. previous two methods combined (Algorithm 4).

Surprisingly, the first algorithm, which was originally intended to be used, but didn't perform as well as expected. Although the fourth algorithm is comparable to the third, it is slightly more computationally demanding. Therefore, the third algorithm was selected as the final evaluation algorithm.

The analysis was done based on the paired-off database.

	Algorithm 1 [%]	**Algorithm 2 [%]**	**Algorithm 3 [%]**	**Algorithm 4 [%]**
EER	9.8	21.0	2.4	3.8

Tab. 4.8: EER scores of four retina evaluation algorithms.

Before fusion, the performance of both algorithms is summarized in Tab. 4.9, tested on the paired-off database. The iris recognition algorithm performs slightly better than the retina algorithm. At the same time, it is clearly faster due to its small template.

	Iris	**Retina**
True Acceptance	213	210
False Acceptance	184	244
True Rejection	22,928	22,868
False Rejection	3	6
FMR	0.80%	1.06%
FNMR	1.39%	2.78%
EER	1.20%	2.40%

Tab. 4.9: Results of separate biometric evaluation performance. The values of FMR and FNMR are corresponding to the best performance of respective algorithms.

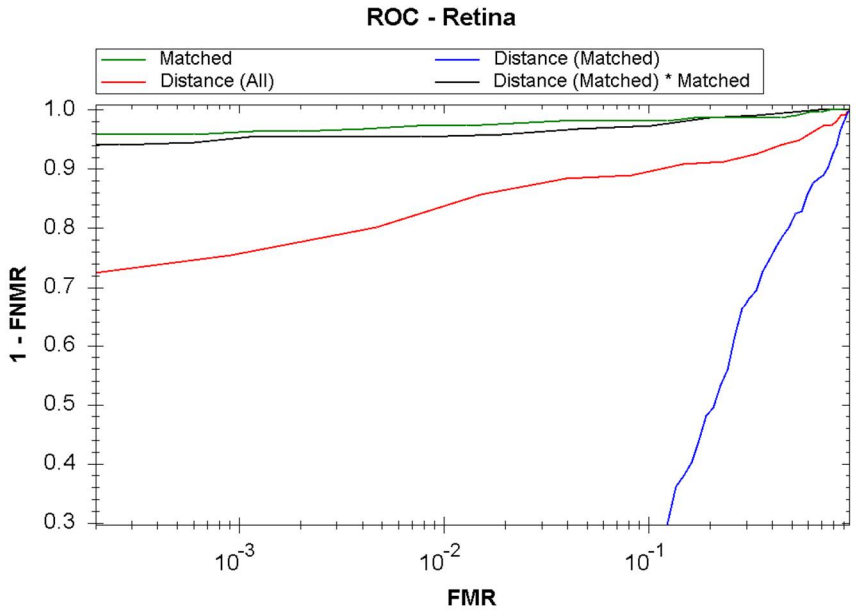

Fig. 4.20: ROC curve of the algorithms. Algorithm 1 is depicted by red, Algorithm 2 by blue, Algorithm 3 by green and Algorithm 4 by black.

Surprisingly, the performance of the minimum rule was generally worse than that of the iris algorithm. However, the other rules enhanced the performance of the biometric system, with all three having almost identical scores (they overlap significantly in Fig. 4.21). However, the best results were achieved by using the sum rule, albeit by a narrow margin (see Tab. 4.10).

	Iris [%]	Retina [%]	Min [%]	Max [%]	Sum [%]	Product [%]
FMR	0.80	1.06	0.13	0.03	0.01	0.06
FNMR	1.39	2.78	2.31	0.00	0.00	0.00
EER	1.20	2.40	1.85	0.02	0.01	0.03

Tab. 4.10: Results of particular biometric evaluation performance. The values of FMR and FNMR are corresponding to the best performance of the respective algorithms.

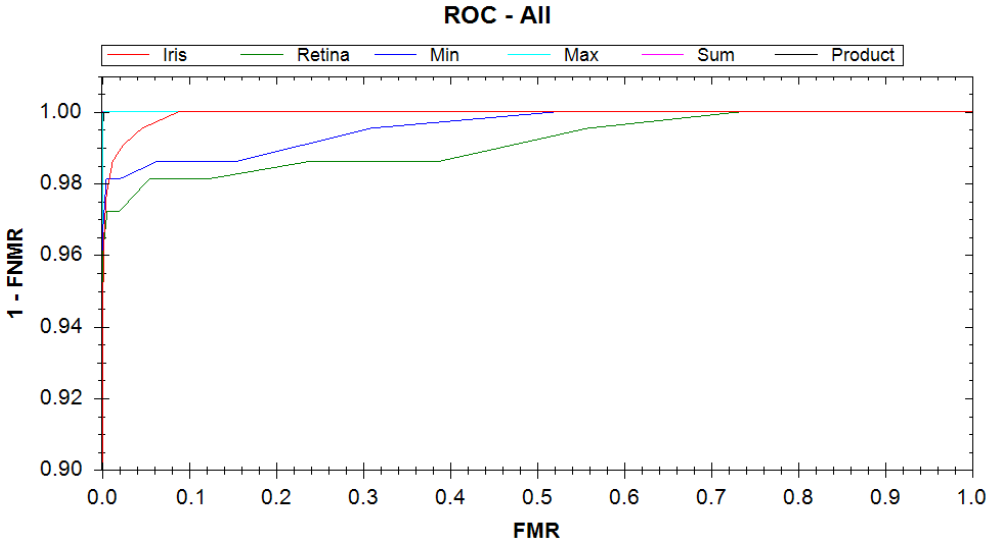

Fig. 4.21: Linear curve of four fusion methods for the iris and retina algorithms.

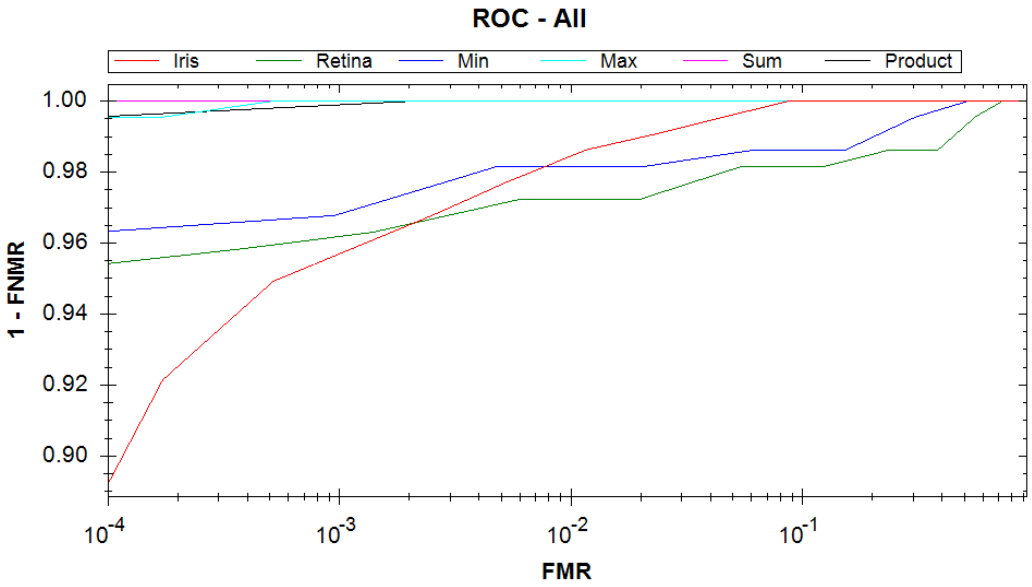

Fig. 4.22: Logarithmic ROC curve of four fusion methods for the iris and retina algorithms.

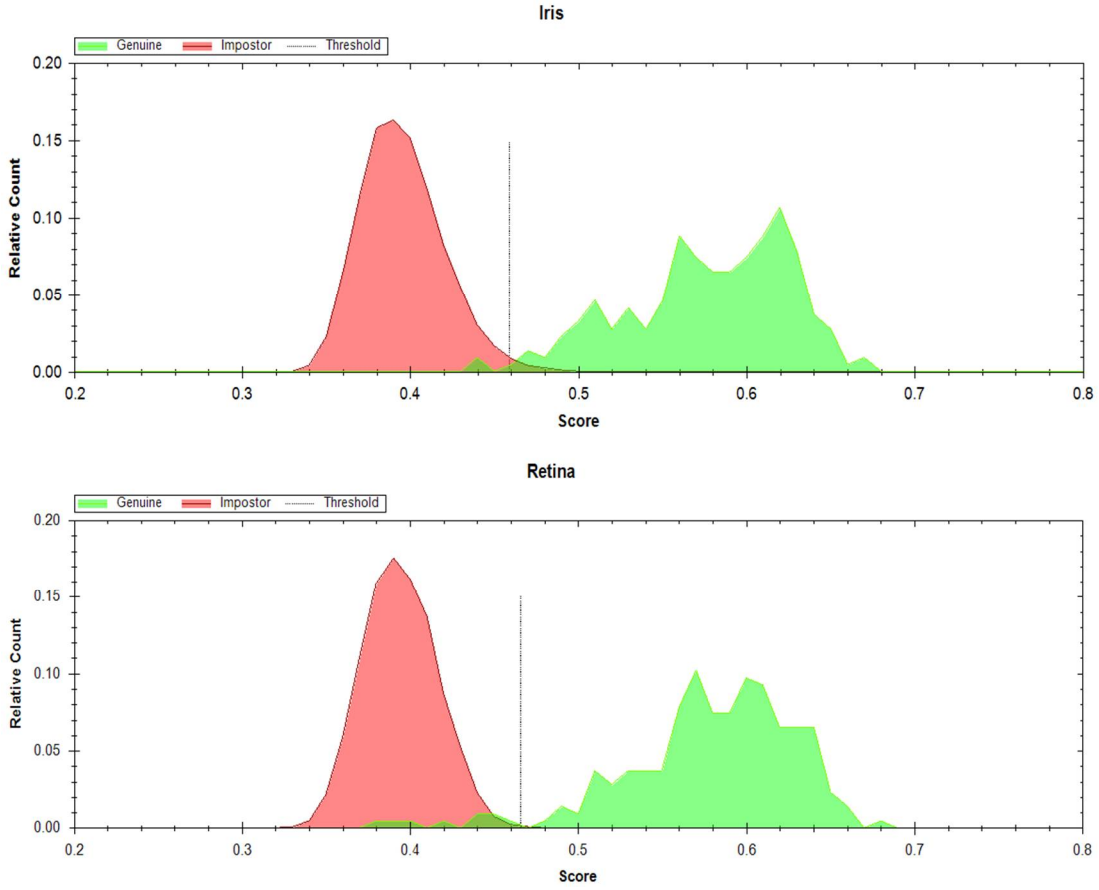

Fig. 4.23:. Iris and retina recognition performance.

The purpose of the fusion was to develop a multimodal biometric system combining the iris and retina images. For this reason, the algorithms for iris and retina recognition were designed. A database containing 324 pairs of images of 108 people was used.

The developed iris algorithm is based on Daugman's iris code, which involves unrolling the iris annulus to a stripe and demodulating it using a 2D Gabor filter. The resulting code is compact and there-

fore the iris recognition algorithm is fast. Within the specified database, the Equal Error Rate of the system is 1.2 %. The developed retina algorithm is based on matching bifurcations. This entails segmentation of the retinal vascular structure, thinning it to the width of 1 pixel and locating the bifurcation points. Out of four possible evaluation algorithms, the ratio of the number of matched bifurcations to the total count of bifurcations proved to be the best, with EER of 2.4 %.

The fusion was performed at the score level using transformation-based rules, namely min rule, max rule, sum rule, and product rule. Before the fusion, the results of the separate biometrics evaluation were normalized using minimum and maximum values.

The performance results of this system have shown that this fusion mostly achieves substantial improvement when compared with the separate biometric evaluation. Min rule achieved the worst results (EER = 1.85 %). The remaining three rules achieved much better results: max rule has an EER of 0.02 %, sum rule has an EER of 0.01 %, and product rule has an EER of 0.03 %. Out of the four tested rules, sum rule has provided the best results.

The developed program displays both fused and non-fused results for comparison. The program also displays statistics and graphs depicting the performance of the system. In the program, databases can be selected for evaluation. The program itself could be developed further in the future and expanded with more fusion methods for comparison. To make other levels of fusion more interesting for study, new modalities could be introduced into the program.

The conclusion, which can be drawn from the results, is that the score-level biometric fusion is a viable option in the development of biometric systems based on combining the iris and retina images.

5 Recognition of eye diseases

Eye diseases and their potential detection in images play a very important role in biometrics. Unless recognition algorithms are optimized and adjusted, the users suffering from any disease impacting the biometric characteristic cannot fully use an acquisition device or cannot use the technology at all.

Any graphical operation in the retinal images affected by disease may have completely different impact on the result in comparison with a healthy retina. The number of features correctly detected in image depends on the size of area affected by the disease and on the algorithm ability to recognize features in inhomogeneous environments. This chapter deals with several ways of algorithms improvements for features extraction, illness detection, and subsequent classification.

Medical visualization of retinal images is very important for ophthalmologists and can discover diseases related to (hence not only) to eye. Automatic detection and classification of diseases can save time and simplifies doctor's work with database of patients. Automatic recognition can be very useful part of an ophthalmologic device where the semi-automatic expert system is able to recognize, classify and track development of disease of a patient. This is also mentioned in patent [P01]. Some ways of detection and classification were described in the article [R02].

5.1 Retinal diseases detection and classification

Diseases can significantly impact the process of recognition. If a disease disrupts the retinal structure, it may result in a wrong evaluation or a possibility of complete rejection of biometric template creation.

In [50], authors used semi-linear feed forward neural network as an effective system for learning discriminant patterns. An input pattern is applied to the network and further propagated through the network using the initial node connection weights. This method can be very accurate but however requires well normalized retinal pictures and large training retinal database.

Work [51] describes a combined method for classifying the type of retinal diseases and automatic diagnosis using a neural network classification technique. However, the paper does not deal with experiments on a larger retinal database –only the framework is introduced.

More sophisticated single purpose method for diabetic retinopathy described in [52] also uses preprocessing segmentation and feature extraction steps but for detection density analysis, the bounding box techniques are used. The classification of the miscellaneous stages of eye disease is done using Random Forests technique [137] based on the area and perimeter of the blood vessels. An accurate assessment of the classified output revealed that normal cases were classified with 90% accuracy.

The mentioned methods require image preprocessing in phases of segmentation and feature extraction. On the other hand, [53] presents a way for the detection without any preprocessing. It is based on Amplitude-Modulation and Frequency-Modulation method [138] for extraction of potentially relevant features. The main mentioned advantage of this approach is the lack of any preprocessing step with high accuracy.

Hemorrhages and microaneurysms detection was described more in detail in [98] using multilevel correlation with different coefficients. For precise detection of pathologies, dynamic thresholding is used. In [99], morphologic operations are used for detection of the candidate areas. Then, for determination of correctly identified areas from candidate regions, a classifier based on density is used. Automated system for detection of microaneurysms was also introduced in [100]. In the first step, a vascular bed is extracted from the retinal image. That is because vessels have similar characteristics and intensity

as searched pathologies. By this step, the number of incorrectly classified areas was lowered while the precision of the localization process was improved. Then a method based on Gabor filtering, by which the candidate areas are obtained, was introduced. Then, from the areas, microaneurysms and hemorrhage areas are obtained using a classifier.

The most obvious findings, through which it is possible to classify diseases such as age-related macular degeneration, are druses. These could be divided into soft and hard groups. Another finding in the retina with diagnosed advanced stage of ARMD is geographic atrophy.

Symptoms of the diabetic retinopathy (DR), which could be detected in fundus images, include hard and soft exudates, hemorrhages and microaneurysms. As hemorrhage and microaneurysms have very similar attributes, it is not easy to distinguish between them.

Druses and exudates in fundus images have a very similar characteristic – we will consider those localized lesions as if they were two similar groups of pathologies. For their distinction, we will consider the fact that if exudates are present on the retina, hemorrhages and microaneurysms can also often be seen on the retina.

Except for objects that need to be detected, objects that are typical for the retina and that can affect the whole classification process, are also present. Because of that, it is necessary to localize them and take them into account while evaluating the findings. It can also be necessary to create preprocessed images so that the specific features of objects would be highlighted and by that, their identification would be simplified.

5.1.1 Segmentation and features extraction

The system for features extraction is based on the fact that both retinal databases have a set of binary black and white images which have been segmented by human experts to pixels containing areas of the image with (black) and without vessels (white).

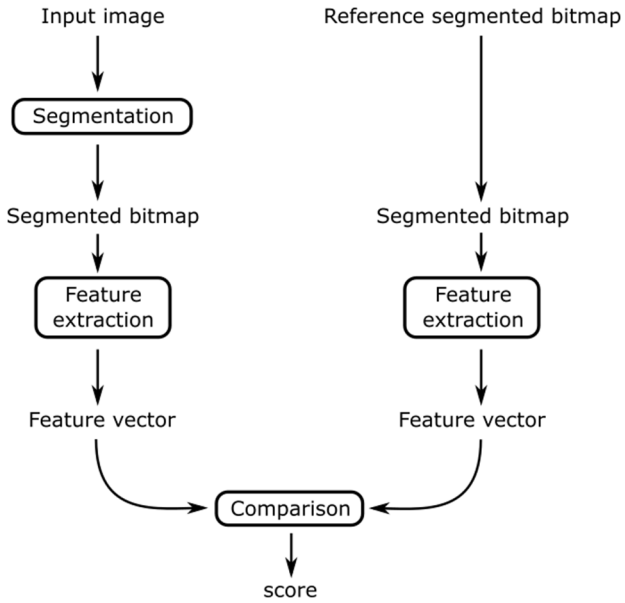

Fig. 5.1: Block diagram of algorithms evaluation.

So it is possible to perform own segmentation from the initial image and get two versions of bitmap – own segmented and already segmented by an expert. A block diagram of evaluation is depicted in Fig. 5.1; it is based on the comparison of extracted features from both bitmaps.

5.1.1.1 Segmentation, features extraction and comparison

The aim of segmentation is to discover all the pixels related to the vessels and get a bitmap comparable with reference to already segmented bitmaps from the retinal databases. Segmentation is divided into these steps:

1. Mask creation using thresholding with a threshold value calculated from the average brightness of pixels on the edge of image. The purpose is to get a circular border of an retinal image.
2. Conversion to one channel image – from the source RGB image the green channel is extracted, which has the best contrast of blood vessels against the background of the retina.
3. Masking against mask obtained in the first step.
4. Histogram expansion.
5. Difference of Gaussians (DoG) [139] for vessels detection.
6. Again – histogram expansion for vessels highlighting.
7. Thresholding with a high threshold value. The brightest pixels in the image are considered as vessels.

The thinning algorithm described in chapter 4.1.3.4 is applied to the image. In the resulting thinned bitmap, there are searched all the points with 8-surrounding which contain at least three color transitions white-black. These points are considered as vessels crossings or bifurcations, and their location is stored into the feature vector.

Feature comparison is based on two features vectors – one acquired by the processing of the input image, and the second acquired by processing of the referential bitmap. Comparison gives the quality value of the input image extraction.

Each feature vector is a set of points where bifurcation or crossing was detected. The coordinates of the points are normalized into interval <0, 1> where the left-top corner has coordinates (0,0) and right-bottom corner has (1,1). To get a matching score *s*, the following equations are used (5.1) (5.2):

$$s = \frac{match(V_1, V_2) + match(V_2, V_1)}{2} \tag{5.1}$$

$$match(A, B) = \frac{|\{a \in A | \exists b \in B : ||b - a||^2 < 0.00002\}|}{|A|} \tag{5.2}$$

where V_1 is the extracted feature vector from the initial image, V_2 is the referential feature vector, $||x||$ is the Euclidean norm, and s is the resulting matching score.

The constant 0.00002 is a maximal distance between two features which are still considered as equal. It is a second power of normalized coordinates, so it is corresponding to a distance of 0.32 % diagonal of the image.

Value $match(V_1, V_2)$ or "correctness" is a value of how many found features are located near to any found feature in the reference vector.

Value $match(V_2, V_1)$ or "completeness" is a value of how many features in the reference vector are located near to any other feature in the original image.

The total matching score s is in interval <0, 1>. Value 1 means a complete concordance, on the other side, value 0 is a complete disconcordance and two random vectors get score near to zero.

5.1.2 Detection of diseases

A different way for blood vessels segmentation can be used for disease detection if an image contains any disease which has already affected its significant part. In this case, complete blood vessels cannot be segmented. On the rest of the image where correctly detected vessels do not occur, there is a high probability of illness occurrence.

For the purpose of disease detection, a proper segmentation algorithm has to be used. The first step is the extraction of blood vessels from the image using morphological operations. The method was inspired by paper [52]. The green channel only (high contrast) is used from RGB image, and the following operations are used in this order:

1. Contrast limited adaptive histogram equalization.
2. Gaussian filtering.
3. Black-hat transformations [55].
4. Adaptive thresholding.
5. Opening (morphological operation).
6. Closing (morphological operation).
7. Connected component labeling.

The results are the labeled regions in the image. For each region, the circularity is calculated, and an assumption is made that a noise in the image has a circular character differing from veins which are linear. Thus all regions with circularity higher than 0.2 are removed. Circularity is calculated according to equation (5.3):

$$circularity = 4 \times \pi \times (\frac{surface}{perimeter})^2 \tag{5.3}$$

A disease can be detected by the continuous free space area on the segmented surface with a given size of threshold. The rest of image is segmented as a proper blood vessel surface with a limited number of features.

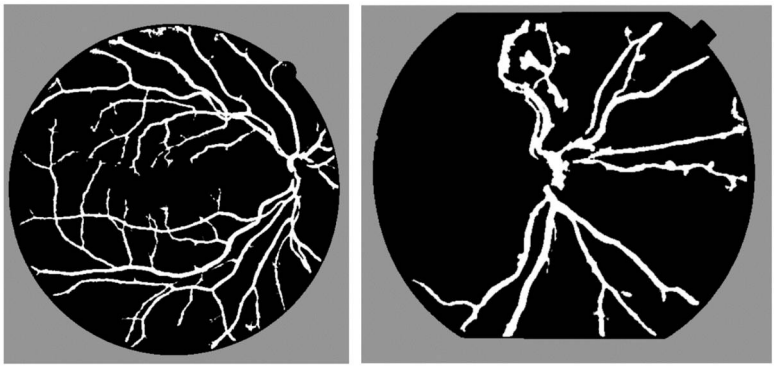

Fig. 5.2: Segmented blood vessels in a healthy (left) and diseased (right) retina.

As can be seen in Fig. 5.2, in the picture from healthy users (on the left side), blood vessels are uniform on almost the whole surface of retina while on the picture from diseased users (on the right side) there are many places where vessels are hidden behind disease artefacts. Thus the vessel cannot be extracted, and a large free space in the image can mean a retinal image with disease.

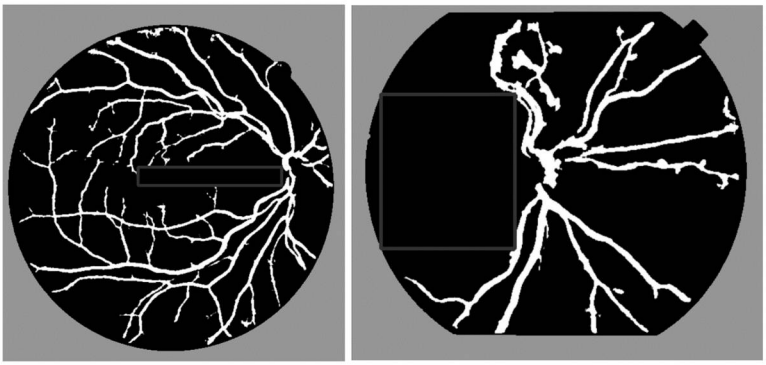

Fig. 5.3: Disease detection – area denotation.

For its detection, a maximal possible rectangle is inserted into this free space (Fig. 5.3). If the rectangular surface is higher than the preset threshold, the image is labeled as a retina with disease.

5.1.3 Classification of diseases

Two unconventional approaches have been tested for retinal diseases classification. The first one is inspired by content based image recognition. Second approach uses LBP features and SVM classifier.

5.1.3.1 Surf, dictionary and SVM

This approach was inspired by CBIR [57] and is able to detect specific disease – diabetic retinopathy. Before the algorithm is used, it is necessary to create SVM classifier set by labeling polygons and bordering diseases artefacts (Fig. 5.4).

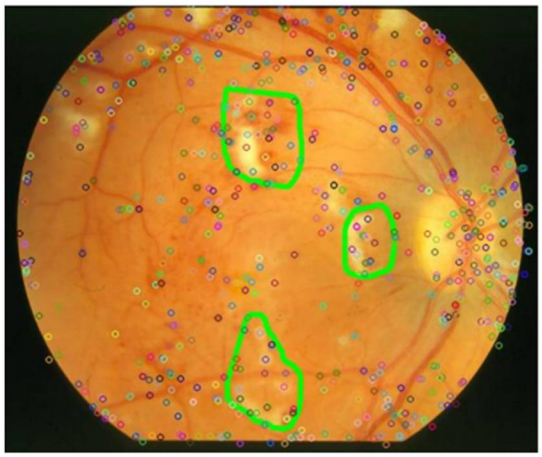

Fig. 5.4: Labeled disease artefacts.

It is necessary to have as many pictures as possible with the same disease as a training set. Small circles in the image show the local SURF features. All the local features, which are inside the green polygons, are selected as a training set. Afterward, a set from healthy retinas is created. In this case, two sets were created (healthy / diseased retinas). Both were divided into 500 clusters and 500 visual words were created, and are called dictionaries. Both dictionaries were joined into one with 1,000 visual words.

Now the SVM classifier with linear kernel can be trained. Training sets of diseased and healthy retinas are taken, and each image is described by the visual words created by the previous procedure. Features vectors used for SVM training are created.

In a similar way, the feature vector for each classified retinal image is also acquired and processed by the SVM and results in a decision whether diabetic retinopathy disease is in the image or not. The whole algorithm is clearly described by pseudocode in [57].

As expected, this method is not very accurate because the local SIFT or SURF features are not very suitable for this kind of tasks because the geometric shape of the disease varies across each set of the retinal images. These approaches are more suitable for tasks where the geometric shape is immutable.

5.1.3.2 LBP and SVM

This approach is able to recognize not only a disease but also its location. The basis of this method is the creation of training set – database of retinas with diabetic retinopathy diagnosis taken, the places of disease are labeled in the image and then LBP can be calculated. The acquired feature vectors are used for SVM classifier training. Disease detection is performed by a sliding window moving over the whole image and requesting SVM classifier if there is a disease location. Results are depicted in Fig. 5.5.

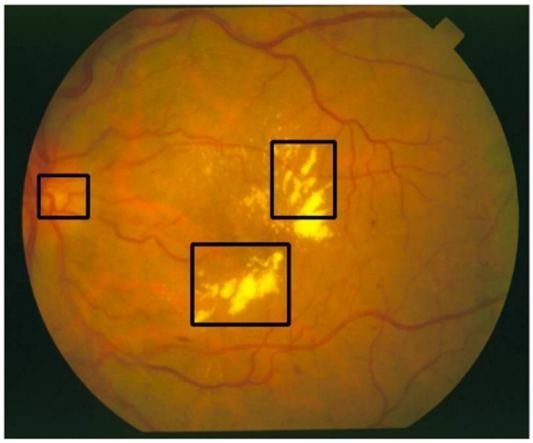

Fig. 5.5: Results of LBP algorithm.

5.1.3.3 Hemorrhages and microaneurysms detection using Gabor filter and classifier

Hemorrhages and microaneurysms detection is inspired by the approach described in [100]. The process of detection is divided into more phases. In the first phase, extraction of the candidate areas is done, containing detection of all the red regions and extraction regions which belong to the vascular bed. Subsequently, an attribute vector is created for each candidate area. In the last phase, a classifier which evaluates the candidate areas by their parameters is used. Some of the results presented in this chapter were achieved in a close cooperation with a MSc. student working on his diploma thesis [12].

Obtaining of candidate areas

Microaneurysms are dark red spots or stains on the retina. They are most contrasting in the green channel of RGB color model. The identification of these pathologies by an ophthalmologist is not difficult. The problem of the algorithm comes with factors such as various brightness level of the images, substitution of candidate areas and vessels or presence of various lesions types in the eye retina. To find the optical disc and other small lesions, an operation of morphological closure is used.

$$[\delta^{sB}(f)](x) = max_{b \in sB}[f(x+b)] \tag{5.4}$$

$$[\varepsilon^{sB}(f)](x) = min_{b \in sB}[f(x+b)] \tag{5.5}$$

$$[\emptyset^{sB}(f)](x) = \varepsilon^{b \in sB}[\delta^{b \in sB}(f)] \tag{5.6}$$

Let us define B set as a subset of set $\mathbb{Z}$ and moving window sB of size $s \in \mathbb{N}$. Then the morphological closure (5.6) is defined by dilatation (5.4) and erosion (5.5) [55]. After this operation, a smoothened image, where dark lesions and vessels only are present, is obtained. To simplify the detection of these objects, the operation for contrast improvement is used. This process is contrast limited adaptive histogram equalization (CLAHE) [128]. It differentiates from the classic method of histogram equalization, because while in the classic method, one histogram for all image pixels is calculated, in this method more histograms are used. Each particular area has its own histogram and in them, classic histogram equalization is done. Thanks to this, it can improve local image contrast and highlight edges in each subsequent region. To prevent the increase of the background noise, the contrast in individual areas is limited based on calculated local statistics. The result of the preceding step is inverted. In the inverted picture, a local variance is calculated for each pixel by equation (5.7), where e_1 is the inverted picture.

$$e_2(x) = \frac{1}{N-1} \sum_{\varepsilon \in W(x)} (e_1(\varepsilon) - \mu_{e1}(x))^2 \tag{5.7}$$

By thresholding the local variances, the candidate areas are obtained.

$$e_C = e_{CA} - e_{BV} \tag{5.8}$$

From these areas e_{CA}, it is further necessary to remove regions that belong to blood vessels e_{BV} (5.8).

Creating attribute vector and area classification

Microaneurysms are specific by relatively easily recognizable characteristics from the other findings. These parameters can be divided into four groups:

- Attributes based on finding's shape, for example the size and constancy of finding's outlines.
- Attributes based on finding's intensity. These are calculated from the green channel with adjusted contrast.
- Color attributes of the image, e.g. brightness and color saturation.
- Statistic attributes as entropy or energy of the candidate area.

The areas obtained by the previous procedure must further be divided so that it is possible to calculate their attribute vectors. For this, watershed segmentation [92] is used. Two mask markers for this transformation are applied. First one is created using erosion and the second one using dilatation. Both of these morphological operations are applied to the mask of the candidate areas. For each candidate area that was separated in this way, an attribute vector is created, and it possesses the following characteristics:

1. *Area*, i.e. sum of all pixels in the candidate area.
2. *Eccentricity*, i.e. the ratio of the distances between the ellipse's focal point and its major axis. This value equals zero for an object with a circular shape.
3. *Perimeter*, i.e. circumference of the candidate area.
4. *Compactness*, i.e. $C = P^2/4A\pi$, where A and P are area and perimeter of the candidate area respectively.
5. *Aspect ratio*, i.e. ratio of the candidate area lengths through its major and minor axes.
6. *Middle and standard deviation of the inner area* of the candidate area marked in the green channel of the RGB spectrum.

7. *Middle and standard deviation of the inner area* of the candidate area marked in the green channel of the RGB spectrum, in which the contrast was improved by CLAHE [128] method.
8. *Middle value of threshold pixels* of candidate area.
9. *Middle value of all pixels* in squared area which are located outside the candidate area.
10. *Middle value of all channels* of colored HSV model. These are hue, saturation, and brightness.
11. *Standard variance for all channels* of colored HSV model.
12. *Entropy*, i.e. randomness rate. It is used when characterizing an area's texture.
13. *Energy*, i.e. ratio of the sum of all pixels in the candidate area to the overall number of pixels in the picture.

Thanks to those attribute vectors, a classifier is created. Probability Bayes classifier which works on the principle of Bayes' decision rules was chosen. This can classify a candidate area into two groups, i.e. as correctly/incorrectly found area.

5.1.4 Experimental results

Retinal databases used for evaluation has been already described more in detail in chapter 4.4.

5.1.4.1 Evaluation of segmentation and features extraction in diseased retinal images

For experiments related to the procedures described in the previous chapter, the following set of input data was used:

- 20 images from DRIVE database with appropriate reference images,
- 11 images from STARE database with appropriate reference images,
- 20 randomly chosen pairs of not mutually related images and their reference images.

The aim is to get a score near to 1 from the first two sets of images, while the third set is used as a check and the aim is to get a score near to zero. Tab. 5.1 shows the minimal, maximal and average score for each set of data processed by the original implementation.

Set	Min.	Avg.	Max.
Healthy retinas (DRIVE)	0.309003	0.469132	0.563636
Diseased retinas (STARE)	0.025320	0.350384	0.535088
Not mutually related retinas	0.000000	0.019855	0.127890

Tab. 5.1: Evaluation of comparison.

Following images from STARE DB got a score less than 0.3:

- Image No. 0040 (score 0.025320, diagnosis: "Retinitis, Disease"),
- Image No. 0324 (score 0.138596, diagnosis: "Hollenhorst Plaque").

Algorithm improvement

Algorithm has failed on the image No. 0044 because of wrong generated mask. Mask generation is used as a sample of the background, two points from the middle of the left and right edge of the image. In Fig. 5.6, there can be seen that the image 0044 has retinal area partially depicted on the point where

the background was expected. By changing the point of location to the quarters of the edge, we have got the score for this image 0.604478 which is even the best score from all the images.

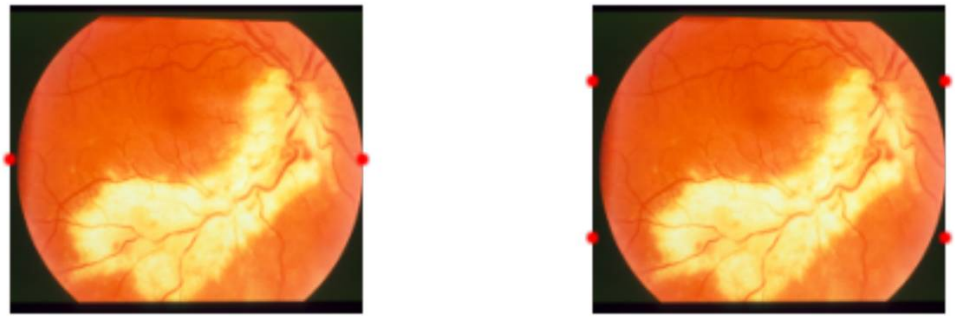

Fig. 5.6 Points of background samples before and after adjustment.

After the adjustment of the mask, we got the following images with score less than 0.3:

- Image No. 0291 (score 0.219436, diagnosis "Vasculitis").
- Image No. 0324 (score 0.255556, diagnosis "Hollenhorst Plaque").

Image No. 0291 has at the first look unusual coloration but does not affect its green channel very much. The small score is probably caused by a number of fake features found near to the top edge of the image. If we increase the value of the threshold for mask generation or if we calculate the threshold by Otsu's method [56], we get much better score 0.402299. Image No. 0324 has also low contrast, and it causes the algorithm not to detect less visible vessels.

After algorithm adjustment, the following results were obtained – see Tab. 5.2.

Set	Min.	Avg.	Max.
Healthy retinas (DRIVE)	0.309003	0.469281	0.563636
Diseased retinas (STARE)	0.219436	0.400721	0.604478
Not mutually related retinas	0.000000	0.015804	0.074319

Tab. 5.2: Results from the improved algorithm.

5.1.4.2 Evaluation of diseases classification using LBP

Experiments were performed on three datasets STARE, DRIVE, and DIARETDB1. DRIVE contains a database of healthy retinas and DIARETDB1 retinas with diabetic retinopathy disease. These two databases were used for SVM training as a negative and positive set.

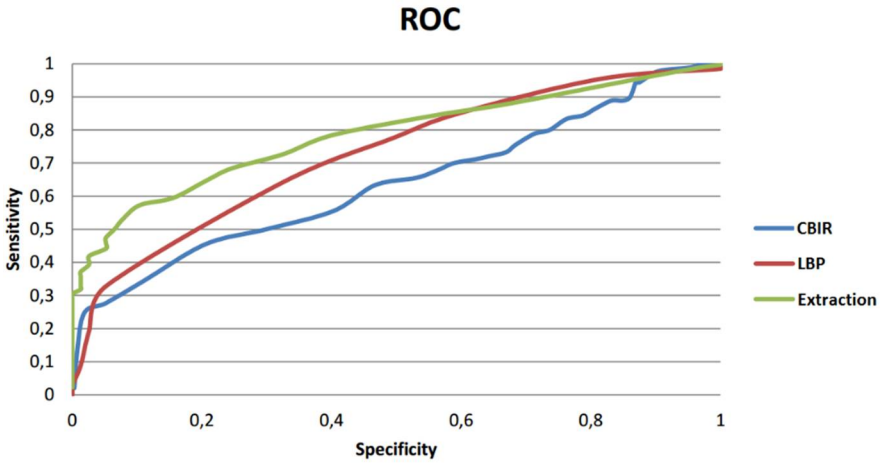

Fig. 5.7: Resulting ROC curves of used methods.

The result was tested on STARE database and contained various sorts of diseases including several healthy retinas. Experimental results are plotted in Fig. 5.7. It can be seen that the LBP has better results than the CBIR approach. This is expected because of the sliding window which gives a more specific area of disease and because CBIR is not very suitable for this type of tasks as mentioned before.

5.1.4.3 Hemorrhages and microaneurysms detection using Gabor filter and classifier

Values, which were recorded during the tests, were true positive rate and false positive rate. The results are shown in Tab. 5.3. In this case, a possibility to see reversed results arises, as it does during hemorrhages and microaneurysms detection. Even though there is a minimum of incorrectly marked regions, the ratio of correctly marked regions is also low. This can be attributed to the fact that the vascular bed areas are removed from the candidate areas. If too many areas incorrectly classified as those that contain vessels do exist, it is likely that also some microaneurysms and hemorrhages were classified as vessels.

Set	True positive rate [%]	False positive rate [%]
DRIVE	58.00	99.86
UNM	59.43	85.36

Tab. 5.3: Results of bright regions detection in the image.

The most important factor for the detection of any object in the retinal image is if the background mask was successfully localized. If it hasn't been achieved with enough precision, boundary retinal pixels can be incorrectly classified as lesions.

Also, if the vascular bed area is misclassified, it is very probable that it will influence the lesions detections. If the vascular bed's mask contains huge number of incorrectly classified areas, it is possible that in these areas, microaneurysms and hemorrhages are present. If some of the vessels are not contained in the vascular bed's mask, it would mean that these unclassified vessels will be marked as hemorrhages. In this case, however, there is no possibility to adjust the method's parameters, and thus a possibility to further improvement this method arises in a way which would lower the probability of incorrect area classification.

5.1.5 Summary

As can be seen in Tab. 5.1, the score reached by the original algorithm shows that features extraction from healthy retinas worked with medium quality in range of 35 %. In the case of some diseases, the extraction worked with similar scores but depending on the disease, sometimes it failed with a minimal score of 3 % and fell into an interval 0 % – 13 %, similarly like random feature vector.

By algorithm adjustment, the average score has been improved to 40% for all pictures even for diseases (see Tab. 5.2). The method used for feature extraction based on Difference of Gaussians (DoG) in the green channel of the image seems to be the most robust against various picture quality and various kinds of retinal diseases.

The medium quality of this method can be better improved, of course. However, the resulting data is meaningful and useful for non-critical applications. The process of feature extraction is not perfect because the used segmentation algorithm cannot process small holes in the image and creates ribs structure in these places thus a lot of fake bifurcations are detected. This is the main problem of the segmentation algorithm and when fixed, it can significantly improve the success of segmentation.

Fig. 5.7 shows the evaluation of diseases classification by algorithms designed rather for static objects. Quality detection and recognition of pathological findings is difficult mainly due to the miscellaneous shapes and colors of diseases in the retina. Another problem was that public retinal databases do not have enough images for proper SVM training. If we have a larger retinal database, the results

could be much better. Experiments were tested on 30 images for training (retinopathy diagnosed images). The rest (37 images) was used for testing.

The LBP method can be improved by feature vector expansion with color histograms. Another way is to use convolutional networks which could significantly increase the success rate.
Although a lot of work has been done, automatic diagnosis of retinal diseases at an earlier stage still remains an open problem. The described approaches use unusual algorithms in this field for the detection and classification but still with interesting results.

6 Conclusion

This thesis dealt with a proposal and realization of the optical system for iris and retinal scanning as a basis of the system for medical and biometric use. Usually, employed unimodal systems fail in cases of lack of appropriate biometric data of the given trait. That is the reason why the use of more biometric characteristics and their mutual fusion is very suitable for significant improvement of the robustness of the whole system.

New features of the approach presented are indicated by numbers. The presented core of the dissertation comprises (1) the proposal and realization of the optical system in order to obtain images for biometric and or medical use, that a retinal and iris image is obtained in a one step of scanning; in the case of biometric utilization, the mutual fusion (2) of the both biometric traits is described which significantly improves uniqueness, universality and a safety of the whole system. In the case of medical utilization, it also describes an utilization of the detection and classification of the diseases in the retinal images (3) as a basis for an expert system for ophthalmological purposes which can help medical doctors to make a reliable and quick eye disease diagnosis of pathological finding in the retinal (or iris) image. All the three parts of the dissertation core are covered by publications listed in Appendix A.

Unimodal biometric systems have to contend with issues like non-universality, unacceptable error rates, intra-class variations, etc. Some of these limitations can be solved by the deployment of multimodal biometric systems that integrate the evidence presented by a multiple sources of information. In general, one of the most important issues of a biometric system is the uniqueness of its biometric information included in the specific biometric characteristic, which influences the strength of such system. The variability in biometric characteristics in the population can be described by biometric entropy. It is also related to a biometric fusion and is interesting to see an evaluation of the biometric information for each biometric characteristic separately and the possible gain from their fusion. Multimodal biometric systems elegantly solve several of the problems present in current unimodal systems. By the combination of multiple sources of information, multimodal systems increase population coverage, improve matching performance and are more resistant against sensor counterfeit. Various fusion levels are possible in multimodal systems. The most popular is the biometric fusion at the match score level thanks to the ease of accessing. Improving matching scores and performance gain is more distinct when uncorrelated traits are used in a multimodal system. In the case of the retina and iris and in such a system according to current standards, it becomes very difficult to counterfeit (if at all). It is very safe and at the same time both biometrics evince sufficient amount of information (large entropy) to cover a larger amount of people than are living currently on the whole Earth.

In conclusion, we can say that a biometric technology has a big chance of success and is currently displacing conventional non-biometric solutions in many areas. Thanks to combining with cryptographic methods, biometric also penetrates the field of data protection. The field of biometric systems is very alive, still expanding and innovative solutions that are perfectly usable in industrial applications are coming to the market every year. It can be assumed that even if the eye retina recognition is not currently very popular (there is no retina recognition device currently available in the market), it has undeniable advantages and will evolve and expand. Room for utilization improvement is primarily in high-secured areas such as nuclear plants, military purposes or secret research laboratories.

6.1 Future work

Currently, we are concluding the work on the third version of the optical system for retinal imaging. When finished, the system will be supplemented by a mechanism for iris imaging and an adjustable platform; thus the whole process of scanning will be automated.

The use for medical doctors will be enhanced by the implementation of an expert system, where the extracted features for the known eye retina and iris diseases will be stored. The semi-automatic recognition system will offer a list of possible eye diseases which could be found on the base of the acquired image analysis. This will surely help the medical doctors to make a reliable and quick eye disease diagnosis. Furthermore, the medical software will allow storing the patient's images, i.e. the medical doctor can check the progress of treatment or changes of the eye disease, whereas the software can provide an automatic comparison of all the stored images of one concrete patient.

Bibliography

[1] Stan Z. L. (editor): *Encyclopedia of biometrics*. Springer, 2009, ISBN 978-0-387-73003-5.

[2] Roberts D.: *Anatomy of the eye. MD Support*, 2013, [Online; accessed 5-July-2016]. URL: http://www.mdsupport.org/information/99-2.

[3] Holmes J. P., Wright, L. J., Maxwell, R. L.: *A Performance evaluation of biometric identification devices*. Sandia National Laboratories, 1991, Technical Report SAND91-0276.

[4] Simon C., Goldstein I.: *A new scientific method of identification*. New York State Journal of Medicine, Vol. 35, No. 18, pp. 901-906.

[5] Tower P.: *The fundus oculi in monozygotic twins: Report of Six Pairs of Identical Twins*. AMA Archives of Ophthalmology, 1955, 54, pp. 225-239.

[6] Tistarelli M., Li S. Z., Chellappa R.: *Handbook of remote Biometrics: For Surveillance and Security*. Springer Publishing Company, 2009, ISBN 978-1-447-12670-6.

[7] National Science and Technology Council: *Iris recognition*. Committee on Technology, 2006, [Online; accessed 5-July-2016]. URL: http://www.biometrics.gov/Documents/irisrec.pdf.

[8] PR Newswire: *Retica Systems Inc. announces the world's first iris-retina biometric system*. News 2006, [Online; accessed 5-July-2016]. URL: http://www.prnewswire.com/news-releases/retica-systems-inc-announces-the-worlds-first-iris-retina-biometric-system-55935287.html.

[9] Daugman J. G.: *Biometric personal identification system based on iris analysis*. US Patent 5291560, 1994.

[10] Wildes R. P., Asmuth J. C., Hanna K. J, Hsu S. C., Kolczynski R. J., Matey J. R., McBride S. E.: A*utomated, non-invasive iris recognition system and method*. US Patents 5572596 and 5751836, 1996.

[11] Wikimedi Commons: *File:Retina.svg.* [Online; accessed 5-July-2016] https://commons.wikimedia.org/wiki/File:Retina.svg

[12] Macek J.: *Klasifikace a rozpoznávání patologických nálezů v obrazech sítnice oka (Classification and Recognition of Pathologic Foundings in Eye Retina Images)*. Mater's thesis, Faculty of Information Technology, Brno University of Technology, 2015.

[13] Tisse C., Martin L., Torres L., Robert M.: *Person identification technique using human iris recognition*. In: Proceedings of ICVI 2002, pp. 294–299, 2002.

[14] Dubey R B., Abhimanyu M.: *Iris localization using daugman's intero-differential operator*. International Journal of Computer Applications, pp. 6-12, May 2014.

[15] Rai, H., Yadav, A.: *Iris recognition using combined support vector machine and hamming distance approach*. Expert systems applications, Vol. 41, No. 2, pp. 588–593, Feb. 2014.

[16] Barbosa M., James A. C.: *Joint iris boundary detection and fit: a real-time method for accurate pupil tracking*. Biomedical Optics Express, Jul. 2014, DOI: 10.1364/BOE.5.002458.

[17] Saad I. A., George L. E.: *Robust and fast iris localization using contrast stretching and leading edge detection*. International Journal of Emerging Trends & Technology in Computer Science, Vol. 3, pp. 61-67, 2014, ISSN 2278-6856.

[18] Daugman, J.: *Results from 200 billion iris cross-comparisons*. University of Cambridge, Technical report, Jun. 2005, ISSN 1476-2986. URL: https://www.cl.cam.ac.uk/techreports/UCAM-CL-TR-635.pdf.

[19] Holme J. P., Wright L. J., Maswell R. L.: *A performance evaluation of biometric identification devices*. Sandia report, SAND91 – 0276, 1991, [Online; accessed 5-July-2016]. URL: http://prod.sandia.gov/techlib/access-control.cgi/1991/910276.pdf.

[20] Hill, R. B.: *Biometrics: Retina identification: personal identification in networked society*. Springer, 2006, ISBN 978-0-387-28539-9.

[21] Bouma H., Baghuis L.: *Hippus of the pupil: Periods of slow oscillations of unknown origin*. Vision Research, pp. 1345–1351, 1971.

[22] Orellana J., Friedman A. H.: *Clinico-pathological atlas of congenital fundus disorders: best's disease*. Springer, pp. 147-150, ISBN 978-1-4613-9322-1, 1993.

[23] Poretsky L. (editor): *Principles of diabetes mellitus*. Springer, 2nd edition, 2010, ISBN 978-0-387-09840-1.

[24] Camet J. D., Talabani H., Delair E., Leslé F., Yera H. and Brézin A. P.: *Toxoplasmosis – recent advances: risk factors, pathogenesis and diagnosis of ocular toxoplasmosis*. Intech, Sep. 2012, ISBN 978-953-51-0746-0.

[25] Sherman S. E.: *History of ophthalmology: The history of the ophthalmoscope*. Springer, pp. 221–228, Vol. 2, 1989, ISBN 978-0-7923-0273-5.

[26] Franklin K., Muir P., Scott T., Wilcocks L., Yates P.: *Introduction to biological physics for the health and life sciences*. Wiley Blackwell, 2010, ISBN 978-0470665930.

[27] Farmer, J: *Stop all federal abuses now! S.A.F.A.N*. Internet Newsletter, No. 264, 1997, [Online; accessed 5-July-2016]. URL: http://www.iahushua.com/WOI/illinois.htm.

[28] EyeDentify Inc.: *The ultimate in positive identification, EyeDentification system 7.5*. Leaflet, Aug. 1985, [Online; accessed 5-July-2016]. URL: http://simson.net/ref/biometrics/Biometrics/1985.Eyedentify.System7.5.pdf.

[29] Rayco Security Loss Prevention Systems, Inc.: *Retina verification, ICAM 2001, EyeDentify retina biometric reader*. [Online; accessed 5-July-2016]. URL: http://www.raycosecurity.com/biometrics/EyeDentify.html.

[30] Trans Pacific (GNF) International, Inc.: *EyeKey system*. [Online; accessed 5-July-2016]. URL: http://www.tpi-gnf.com/eky1.htm.

[31] Vision Systems Design, Inc.: *Retinal Technologies offers hand-held retinal-scanning system*. Newsletter, Aug. 2001, [Online; accessed 5-July-2016]. URL: http://www.vision-systems.com/articles/2001/08/retinal-technologies-offers-hand-held-retinal-scanning-system.html.

[32] Holmes Ch., Walmsley S.: *Biometric security in today's market: An introduction to fingerprint, retinal, and iris scanning technologies*. COP4910 – Frontiers in Information Technology, 2005, [Online; accessed 5-July-2016]. URL: http:// pegasus.cc.ucf.edu/~cholmes/homepage/Biometrics.doc.

[33] Khav P.: *Iris recognition technology for improved authentication*. SANS Institute, SANS Security Essentials (GSEC) Practical Assignment, 2002, [Online; accessed 5-July-2016]. URL:

https://www.sans.org/reading-room/whitepapers/authentication/iris-recognition-technology-improved-authentication-132.

[34] Panasonic Corporation: *Iris reader access control, BM-ET200*. [Online; accessed 5-July-2016]. URL: ftp://ftp.panasonic.com/pub/panasonic/cctv/BidSpecs/BM-ET200.rtf.

[35] ID Travel AG: *Biometric systems for secure and rapid access: IrisAccess 4000*. [Online; accessed 5-July-2016]. http://www.id-travel.ch/Downloads/FS_IrisAccess_en.pdf.

[36] Berggren L.: Iridology: A critical review. Acta Ophthalmol, Vol. 63, No. 1, pp. 1–8, Feb. 1985.

[37] Wang X., Cao H., Zhang J.: *Analysis of retinal images associated with hypertension and diabetes*. Engineering in Medicine and Biology Society, 27th Annual International Conference of the IEEE Engineering in Medicine and Biology Society, 2005, ISBN 0-7803-8741-4.

[38] Medeiros F. A., Zangwill L. M., Bowd C., Vessani R. M., Susanna R. Jr., Weinreb R. N.: Eval*uation of retinal nerve fiber layer, optic nerve head, and macular thickness measurements for glaucoma detection using optical coherence tomography*. American Journal of Ophthalmology, Jan. 2005, DOI: 10.1016/j.ajo.2004.08.069, ISSN: 0002-9394.

[39] Gao X., Bharath A.: *Measurement of vessel diameters on retinal images for cardiovascular studies*. Medical Image Understanding and Analysis conference, 2001.

[40] Hart W. E., Goldbaum M., Cote B., Kube P., Nelson M. R.: *Automated measurement of retinal vascular tortuosity*. In: International Journal of Medical Informatics, pp. 239–252, Vol. 53, 1999, ISBN 0-7803-7622-6.

[41] Daugman J.: *How iris recognition works*. Proceedings of 2002 International Conference on Image Processing, Vol. 1, 2002.

[42] Usher D., Tosa Y., Friedman M.: *Ocular biometrics: simultaneous capture and analysis of the retina and iris*. Advances in Biometrics: Sensors, Algorithms and Systems, Springer, pp. 133-155, 2008, ISBN: 1846289203.

[43] Schwiegerling, J.: *Field guide to visual and ophthalmic optics*. Society of Photo Optical, 2010, ISBN: 0819456284.

[44] Rabbetts, R.: *Bennett and Rabbett's clinical visual optics*. Elsevier Health Science, 4th ed., 2007, ISBN: 978-0-7506-8874-1.

[45] Navarro, R., Santamaria J., Bescos J: *Accommodation-dependent model of the human eye with aspherics*. Journal of the Optical Society of America, pp. 1273–1281, 1985, DOI: 10.1364/JOSAA.2.001273.

[46] WelchAllyn: *PanOptic™ Ophthalmoscope 118 series*. [Online; accessed 5-July-2016]. URL: https://www.welchallyn.com/content/dam/welchallyn/documents/sap-documents/LIT/80017/80017986LITPDF.pdf.

[47] Parker J.: *Algorithms for image processing and computer vision*. John Wiley & Sons, 1996, ISBN 0471140562.

[48] Schwiegerling, J.: *Field guide to visual and ophthalmic optics*. Society of Photo Optical, 2010, ISBN: 0819456284.

[49] Thorlabs, Inc.: *Your source for fiber optics, laser diodes, optical instrumentation and polarization measurement & control*. [Online; accessed 5-July-2016]. URL: http://www.thorlabs.de.

[50] Sivakumar R., Tamilselvi R., Archana N., Deepthi N., Priyadharisini N.: *Classification and detection of retinal diseases*. International Conference on Signal, Image Processing and Applications, Vol. 2, Singapore, pp.85-89, 2011.

[51] Jayanthi D, Devi N, SwarnaParvathi S.: *Automatic diagnosis of retinal diseases from color retinal images*. International Journal of Computer Science and Information Security, Vol. 7, No. 1, pp. 234-238, 2010, ISSN 1947 5500.

[52] Verma K., Deep P., Ramakrishnan, A. G.: *Detection and classification of diabetic retinopathy using retinal images*. Conference: India Conference (INDICON), Annual IEEE, At Hyderabad, India, 2011, DOI: 10.1109/INDCON.2011.6139346.

[53] Agurto C., Murillo S., Murray V., Pattichis M., Russell S., Abram M., Soliz P.: *Detection and phenotyping of retinal disease using AM-FM processing for feature extraction*. Signals, Systems and Computers, 42nd Asilomar Conference on, pp. 659-663, 2008.

[54] Zhang, T. Y., Suen C. Y.: *A fast parallel algorithm for thinning digital patterns*.Communications of the ACM 27(3): 236-239, March 1986, DOI: 10.1145/357994.358023, ISSN 0001-0782.

[55] Benediktsson J. A., Chanussot J., Najman L., Talbot H.: *Mathematical Morphology and Its Applications to Signal and Image Processing*. In: Proceedings of International Symposium ISMM 2015, May 2015, ISBN 3319187201.

[56] Otsu N.: *A threshold selection method from gray-level histograms*. IEEE Transaction on systems, Man, and Cybernetics, 1979, DOI:10.1109/TSMC1979.4310076.

[57] Carvalho T., Jelinek H. F., Goldenstein S., Wainer J.: *Points of interest and visual dictionaries for automatic retinal lesion detection*. Biomedical Engineering, pp. 2244 – 2253, Aug. 2012.

[58] Jain A. K., Ross A. A., Nandakumar K.: *Handbook of multibiometrics*. New York: Springer, 2006, ISBN 978-038-7331-232.

[59] Hong L., Wan Y., Jain A. K.: *Fingerprint image enhancement: algorithms and performance evaluation*. IEEE Transactions on Pattern Analysis and Machine Intelligence, pp. 777-789, 1998.

[60] Matsumoto T., Matsumoto H., Yamada K., Hoshino S., Renesse R. L.: I*mpact of artificial "gummy" fingers on fingerprint systems*. Optical Security and Counterfeit Deterrence Techniques. pp. 275-289, 2002, DOI: 10.1117/12.462719.

[61] Techbiometric: *Advantages of multi-biometric systems over unibiometric systems*. [Online; accessed 5-July-2016]. URL: http://techbiometric.com/articles/advantages-of-multi-biometric-systems-over-unibiometric-systems.

[62] Faundez-Zanuy M., O'Gorman L., Jain A. K., Ratha N. K.: *Data fusion in biometrics*. IEEE Aerospace and Electronic Systems Magazine, p. 34-38, 2005, DOI: 10.1109/MAES.2005.1396793.

[63] Nandakumar K.: *Multibiometric systems: Fusion strategies and template security*. ProQuest, 2008, ISBN: 978-0-549-61747-1.

[64] Jain A. K., Chandrasekaran B., Ratha N. K.: D*imensionality and sample size considerations in pattern recognition practice*. In: Handbook of Statistics, p. 835, 1982, DOI: 10.1016/S0169-7161(82)02042-2.

[65] Radha N., Kavitha A.: *Rank level fusion using fingerprint and iris biometrics*. In: Indian Journal of Computer Science and Engineering, pp. 917–923, 2012.

[66] Paunovic S., Jerinić I., Starčević D.: *Methods for biometric data connection in multimodal systems*. In: Proceedings of the XIV International Symposium SYMORG 2014: New business models and sustainable competitiveness, pp. 900-906, 2014, ISBN 978-8-676-80295-1.

[67] Jain A. K., Nandakumar A. R.: *Score normalization in multimodal biometric systems*. Elsevier, Pattern recognition, Vol. 38, pp. 2270-2285, 2005, ISSN: 0031-3203.

[68] Duda R. O., Hampel F. R.: *Robust statistics: the approach based on influence functions*. New York: Wiley, ISBN 2007, 978-047-1735-779.

[69] Kittler J., Hatef M., Duin R. P. W., Matas J.: *On combining classifiers*. In: IEEE Transactions on Pattern Analysis and Machine Intelligence, p. 226-239, 1998, DOI: 10.1109/34.667881.

[70] Duda, R. O.: Pattern classification. 2nd Ed. New York: J. Wiley, ISBN 04-710-5669-3, 2001.

[71] Verlinde P., Chollet G.: *Comparing decision fusion paradigms using k-NN based classifiers, decision trees and logistic regression in a multi-modal identity verification application*. In: Second International Conference on Audio and Video-based Biometric Person Authentication, 2003, DOI: 10.1.1.47.8153.

[72] Davide M., Jain A. K.: *Biometric authentication*. Springer, 2005, ISBN 978-354-0259-763.

[73] Saradhi G.V., Balasubramanian S., Chandrasekaran V.: *Performance enhancement of optic disc boundary detection using active contours via improved homogenization of optic disc region*. International Conference on Information and Automation, pp. 264-269, ICIA, 2006, ISSN 2151-1802.

[74] Siddalingaswamy P. C., Prabhu G. K.: *Automated detection of anatomical structures in retinal images.* International Conference on Computational Intelligence and Multimedia Applications, Vol. 3, No. 10, pp. 164-168, 2007, ISBN 0-7695-3050-8.

[75] Aquino A., Gegúndez M. E., Marín, D.: *Automated optic disc detection in retinal images of patients with diabetic retinopathy and risk of macular edema*. World Academy of Science, Engineering and Technology, No. 60, pp. 87-92, 2009.

[76] Parker J.: *Algorithms for image processing and computer vision*. New York: Wiley Computer Publishing, 1997, ISBN 04-711-4056-2.

[77] Chen Z., Abidi B.R., Page D. L., Abidi M. A.: *Gray-level grouping (GLG): an automatic method for optimized image contrast Enhancement-part I: the basic method*. IEEE Trans. on Image Processing, Vol. 15, No. 8, pp. 2290-2302, Aug. 2006.

[78] Basha M. S., Ramakrishnan M.: *Color image enhancement based on modified contrast limited adaptive histogram equalization*. International Journal of Engineering Research & Technology, Vol. 2, No. 2, Dec. 2013, ISSN 2278-0181.

[79] Chaudhuri S., Chatterjee S., Katz N., Nelson M., Goldbaum M.: *Detection of blood vessels in retinal images using two-dimensional matched filters.* IEEE transactions on medical imaging, No. 3, pp. 263-269, 1989, ISSN 0278-0062.

[80] N. Dede.: *Implementation of thinning algorithm in OpenCV*. OpenCV Code, [Online; accessed 5-July-2016]. URL: http://opencv-code.com/quick-tips/implementation-of-thinning-algorithm-in-opencv.

[81] Heckbert P.S.: *Graphics gems IV*. Graphic Gems Series, AP Professional, 1994, ISBN 0-12-336155-9.

[82] Ojala T., Pietikäinen T., Harwood D.: *Performance evaluation of texture measures with classification based on Kullback discrimination of distributions*. Proceedings of the 12th IAPR International Conference on Pattern Recognition, Vol. 1, pp. 582 – 585, 1994, ISBN 0-8186-6265-4.

[83] Shams M. Y., Rashad M. Z., Nomir O., El-Awady M. Z.: *Iris recognition based on LBP and combined LVQ classifier*. International Journal of Computer Science & Information Technology, Vol. 3, No. 5, Oct. 2011, DOI 10.5121/ijcsit.2011.3506.

[84] Yanoff M.: *Ophthalmology*. Mosby Elsevier, 3rd Ed., 2009, ISBN 978-0-323-04332-8.

[85] Wiggins R. L., Vaughan K. D., Friedmann G. B.: *Holography using a fundus camera*. Applied Optics, No. 1, pp. 179–181, Jan 1972, DOI:10.1364/AO.11.000179.

[86] Schachat A.P., Wilkinson Ch. P., Hinton D. R., Wilkinson P.: *Retina*. Mosby Elsevier, 4th Ed., 2005, ISBN 978-0-323-04323-6.

[87] American Optometric Association: *Diabetic eye disease*. In: Diabetic Eye Disease, 2009, [Online; accessed 5-July-2016], URL: http://www.slideshare.net/MedicineAndHealth14/diabetic-eye-disease.

[88] Tamura S., Okamoto Y.; Yanashima K.: *Zero-crossing interval correction in tracing eye-fundus blood vessels*. Pattern Recognition, Vol. 3, pp. 227–233, Jan. 1988, DOI: 10.1016/0031-3203(88)90057-x.

[89] Pinz A., Bernogge, S., Datlinger P. et al.: *Mapping the human retina*. IEEE Transactions on Medical Imaging, No. 4, pp. 606–619, 1998, DOI:10.1109/42.730405.

[90] Akita, K., Kuga H.: *A computer method of understanding ocular fundus images*. Pattern Recognition, No. 6, pp. 431–443, Jan. 1982, DOI:10.1016/0031-3203(82)90022-x.

[91] Wong D. W. K., Liu J., Tan N. M., et al.: *Automatic detection of the macula in retinal fundus images using seeded mode tracking approach*. In: IEEE Engineering in Medicine and Biology Society, Institute of Electrical & Electronics Engineers (IEEE), Aug. 2012, DOI: 10.1109/embc.2012.6347103.

[92] Sinthanayothin C., Boyce J. F., Cook H. L., et al.: *Automated localization of the optic disc, fovea, and retinal blood vessels from digital color fundus images*. British Journal of Ophthalmology, Vol. 83, No. 8, pp. 902–910, Aug. 1999, DOI :10.1136/bjo.83.8.902.

[93] Umbaugh S.: *Digital image processing and analysis: human and computer vision applications with CVIPtools*. Boca Raton, FL: CRC Press, ISBN 978-1-4398-0205-2, 2011.

[94] Kavitha, G., Ramakrishnan, S.: Identi*fication and analysis of macula in retinal images using Ant Colony Optimization based hybrid method*. In: 2009 World Congress on Nature & Biologically Inspired Computing (NaBIC), Institute of Electrical & Electronics Engineers (IEEE), 2009, DOI: 10.1109/nabic.2009.5393783.

[95] Mubbashar M., Usman A., Akram M. U.: *Automated system for macula detection in digital retinal images*. IEEE International Conference on Information and Communication Technologies, Jul. 2011, DOI: 10.1109/icict.2011.5983555.

[96] Simon A., Worthen D. M., Mitas J. A.: *An evaluation of iridology*. In: Journal of the American Medical Association, Vol. 242, pp. 1385–1387, 1979.

[97] Janecka P.: *Multimodální biometrický systém kombinující duhovku a sítnici (Multibiometric System Combining Iris and Retina)*. Mater's thesis, Faculty of Information Technology, Brno University of Technology, 2015.

[98] Zhang B., Wu X., You J., et al.: *Detection of microaneurysms using multi-scale correlation coefficients*. Pattern Recognition, Vol. 43, No. 6, pp. 2237–2248, Jun. 2010, DOI: 10.1016/j.patcog.2009.12.017.

[99] Walter T., Massin P., Erginay A., et al.: *Automatic detection of microaneurysms in color fundus images*. Medical Image Analysis, Vol. 11, No. 6, pp. 555–566, Dec. 2007, DOI: 10.1016/j.media.2007.05.001.

[100] Akram M. U., Khalid S., Khan S. A.: *Identification and classification of microaneurysms for early detection of diabetic retinopathy*. Pattern Recognition, Vol. 46, No. 1, pp. 107–116, Jan. 2013, DOI: 10.1016/j.patcog.2012.07.002.s.

[101] Moreno R. P., Gonzaga A.: *Features Vector for Personal Identification Based On Iris Texture*. Proceedings of the Irish Machine Vision and Image Processing Conference, Dublin, 2004.

[102] Latha L., Thangasamy S.: *A robust person authentication system based on score level fusion of left and right irises and retinal features*. In: Proceedings of the International Conference and Exhibition on Biometrics Technology, Vol. 2, pp. 111-120, Dec. 2010, DOI:10.1016/j.procs.2010.11.014.

[103] Muller D. F., Heacock G. L., Usher D. B.: *Method and system for generating a combined retina/iris pattern biometric*, US Patent 7248720, 2007.

[104] Find Biometrics: *Retica Systems Inc. announces the world's first iris-retina biometric system*. 2006, [Online; accessed 5-July-2016]. URL: http://findbiometrics.com/retica-systems-inc-announces-the-worlds-first-iris-retina-biometric-system.

[105] Daugman J.: *Recognizing persons by their iris patterns*. Springer US, 1999, DOI: 10.1007/0-306-47044-6_5, [Online; accessed 5-July-2016]. URL: http://www.cse.msu.edu/~stockman/CV/F09Docs/Readings/daugemanRecognizingPersons.pdf.

[106] Vishay: *Eye safety risk assessment of infrared emitting diodes according IEC 62471 (based on CIE S009)*. [Online; accessed 5-July-2016]. URL: http://www.vishay.com/docs/81935/eyesafe.pdf.

[107] Oinonen H., Forsvik H., Ruusuvuori P., Yli-Harja O., Voipio, V., Huttunen, H.: *Identity verification based on vessel matching from fundus images*. In: Proceedings of IEEE International Conference on Image Processing, pp. 4089–92, ISBN 978-1-4244-7993-1, 2010, ISSN 1522-4880.

[108] Qamber S., Waheed Z., Akram M. U.: *Personal identification system based on vascular pattern of human retina*. In: Cairo International Biomedical Engineering Conference, 2012; pp. 64–677, 2012, ISBN 978-1-4673-2800-5.

[109] Mariño C., Penedo M. G., Penas M., Carreira M. J., Gonzalez F.: P*ersonal authentication using digital retinal images*. Springer, Pattern Analysis and Applications, 2006, Vol. 9, No.1, pp.21–33, ISSN 1433-7541.

[110] Köse C., İkibaş C.: *A personal identification system using retinal vasculature in retinal fundus images*. Expert Systems with Applications, Vol. 38, No. 11, pp. 13670–13681, Oct. 2011.

[111] Barkhoda W., Akhlaqian F., Amiri M., Nouroozzadeh M.: *Retina identification based on the pattern of blood vessels using fuzzy logic*. In: EURASIP Journal of Advances in Signal Processing, pp. 113-121, 2011, ISSN: 1687-6180.

[112] Borgen H., Bours P., Wolthusen S. D.: *Visible-spectrum biometric retina recognition*. In: Proc. International Conference on Intelligent Information Hiding and Multimedia Signal Processing, pp. 1056–1062, 2008, ISBN 978-0-7695-3278-3.

[113] Jähne B.: *Digital image processing concepts, algorithms, and scientific applications*. Springer Berlin Heidelberg, 1997, ISBN 978-3-662-03479-8.

[114] Daugman, J.G: *High confidence visual recognition of persons by a test of statistical independence*. IEEE Transactions on Pattern Analysis and Machine Intelligence, Vol. 15, No. 11, pp. 1148–1161, 1993, ISSN 0162-8828.

[115] Ma L., Tan T., Wang Y., Zhang D.: *Efficient iris recognition by characterizing key local variations*. IEEE Transactions on Image Processing, Vol. 13, No. 6, pp. 739–50, Jun. 2004.

[116] Monro D. M., Rakshit S., Zhang D.: *DCT-based iris recognition*. IEEE Transactions on Pattern Analysis and Machine Intelligence, Vol. 29, No. 4, pp. 586–95, Apr. 2007, ISSN 0162-8828.

[117] Sun S., Yang S., Zhao L.: *Non-cooperative bovine iris recognition via SIFT*. Neurocomputing, Vol. 120, pp. 310–317, Nov. 2013, DOI: 10.1016/j.neucom.2012.08.068.

[118] Mehrotra H., Sa P. K, Majhi B.: *Fast segmentation and adaptive SURF descriptor for iris recognition*. Mathematical and Computer Modelling, Elsevier, Vol. 58, No. 1–2, pp. 132–146, Jul. 2013, ISSN: 0895-7177.

[119] IrisID: iCAM D1000, *An eye fundus scanner*. [Online; accessed 5-July-2016]. URL: http://www.irisid.com/productssolutions/hardwareproducts/icamd1000.

[120] Wu Gloria MD: *Diabetic retinopathy: The essentials*. LWW; 1 Har/Psc edition, Apr. 2010, ISBN 1605476625.

[121] Retinal Technologies: *A handheld scanner*. [Online; accessed 5-July-2016]. URL: http://biometrics.mainguet.org/types/eye_retinal.htm.

[122] Lahn H. E.: *Iridology: The diagnosis from the eye*. Kessinger Publishing, 2010, ISBN 978-1162622729.

[123] Drahanský M., Kolář R., Mňuk T.: Elektronické zařízení pro snímání obrazu sítnice a duhovky oka. Česká a slovenská oftalmologie (Electronic device for eye's retina and iris imaging). Vol. 71, No. 6, pp. 302-308, 2015, ISSN 1211-9059.

[124] Yang L.: *Iris/retina biometrics*. CPSC 4600@UTC/CSE, [Online; accessed 5-July-2016]. URL: http://web2.utc.edu/~djy471/documents/b6.1.IRIS-Retina-utc.ppt.

[125] Daugman J.: *How iris recognition works*. IEEE Transactions on circuits and systems for video technology, Vol. 14, No. 1, Jan 2004, [Online; accessed 5-July-2016]: URL: https://www.cl.cam.ac.uk/~jgd1000/csvt.pdf.

[126] Adam M., Rossant F., Amiel F., Mikovicova B., Ea T.: *Reliable eyelid localization for iris recognition*. Conference: Advanced Concepts for Intelligent Vision Systems, ACIVS 2008, Oct. 2008, DOI: 10.1007/978-3-540-88458-3_96.

[127] Vision Express: *Myopia and hypermetropia*. [Online; accessed 5-July-2016]. URL: http://www.visionexpress.com/eye-health/eye-conditions/myopia-hypermetropia.

[128] Johar T., Kaushik P.: *Iris segmentation and normalization using Daugman's rubber sheet model*. International Journal of Scientific and Technical Advancements, Vol. 1, No. 3, 2015, ISSN: 2454-1532.

[129] Zhang D. D.: *Automated biometrics: Technologies and systems*. Springer Science & Business Media, Nov. 2013, ISBN 1461545196.

[130] Kumar A.: *Biometric security: iris recognition*. [Online; accessed 10-August-2015] URL: http://www.slideshare.net/piyushmittalin/biometric-security-iris-recognition.

[131] Iritech, Inc.: *IriShield™ series*. [Online; accessed 5-July-2016]. URL: http://www.iritech.com/products/hardware/irishield%E2%84%A2-series#.

[132] Jóźwik A., Siedlecki D., Zając M.: *Analysis of purkinje images as an effective method for estimation of intraocular lens implant location in the eyeball*. Optik - International Journal for Light and Electron Optics. Vol. 125, No. 20, pp. 6021–6025, Oct. 2014, DOI: 10.1016/j.ijleo.2014.06.130.

[133] Lihteh W.: *Ophthalmologic manifestations of toxoplasmosis*. [Online; accessed 5-July-2016]. URL: http://emedicine.medscape.com/article/2044905-overview.

[134] Mayo Clinic: *Indirect ophthalmoscopy*. [Online; accessed 5-July-2016]. URL: http://www.mayoclinic.org/tests-procedures/eye-exam/multimedia/indirect-ophthalmoscopy/img-20006175.

[135] Wikimedia Commons: *Eyesection.svg*. [Online; accessed 5-July-2016]. URL: https://upload.wikimedia.org/wikipedia/commons/thumb/f/f5/Eyesection.svg/2000px-Eyesection.svg.png.

[136] Iris ID: *El salvador sugar mill uses iris recognition for time and attendance*. [Online; accessed 5-July-2016]. URL: http://www.irisid.com/el-salvador-sugar-mill-uses-iris-recognition-for-time-and-attendance.

[137] Benyamin D.: *A gentle introduction to random forests, ensembles, and performance metrics in a commercial system*. CitizenNet, Nov. 2012. [Online; accessed 5-July-2016]. URL: https://citizennet.com/blog/2012/11/10/random-forests-ensembles-and-performance-metrics.

[138] Herrera M., Manuel V.: *AM-FM methods for image and video processing*. Dissertation thesis, Dec. 2008, [Online; accessed 5-July-2016]. URL: http://repository.unm.edu/handle/1928/7633.

[139] Collins R.: *LoG and DoG Filters*. CSE/EE486 Computer Vision I, class lecture, 2007, [Online; accessed 5-July-2016]. URL: http://www.cse.psu.edu/~rtc12/CSE486/lecture11_6pp.pdf.

Appendix A

Published articles

Journal publications

[H05] Hájek J., Drahanský M., Drozd R.: *Extraction of Retina Features Based on Position of the Blood Vessel Bifurcation*. Journal of Medical Research and Development. Hong Kong: 2013, Vol. 2, No. 3, pp.55-59. ISSN 2303-9345.

Conference publications

[H01] Hájek J., Drahanský M., Kolář R., Odstrčilík J., Borovský J.: *Bimodal eye imaging system*. In: Signal-Image Technology and Internet-Based Systems. Bangkok: Institute of Electrical and Electronics Engineers, 2015, pp. 572-575. ISBN 978-1-4673-9721-6.

[H02] Kolář R., Semerád L., Drahanský M., Odstrčilík J., Hájek J., Borovský J.: *Bimodal Eye Imaging System for Biometric and Medical Applications*. In: Security and Protection of Information 2015. Brno: Brno University of Defence, 2015, pp.83-95. ISBN 978-80-7231-997-8.

[H03] Hájek J., Doležel M., Drahanský M.: *Biometric device for retina and iris recognition in intelligent houses*. In: Beiträge zum Usability Day XII Assistenztechnik für betreutes Wohnen. Dornbirn: University of Applied Sciences Vorarlberg, 2014, pp. 143-147. ISBN 978-3-89967-943-4.

[H04] Hájek J., Drahanský M., Kolář R.: *Experimental ophthalmic multimodal imaging system for iris and retina*. In: Proceedings of IIAI 3rd International Conference on Advanced Applied Informatics. Kitakyushu: IEEE Computer Society, 2014, pp. 676-679. ISBN 978-1-4799-4174-2.

[H06] Drozd R., Hájek J., Drahanský M.: *An algorithm for retina features extraction based on position of the blood vessel bifurcations*. In: Biometric Recognition. Guangzhou: Springer London, 2012, pp. 308-315. ISBN 978-3-642-35135-8. ISSN 0302-9743.

Book chapter

[H07] Drahanský M., Orság F., Hájek J. et al.: *Biometrie*. Brno: Computer Press, s.r.o., 2011. ISBN 978-80-254-8979-6.

Under review

[R01] Hájek J., Drahanský M.: *Biometrics Fusion of Iris and Retina Templates*. Computer Methods and Programs in Biomedicine, ISSN: 0169-2607.

[R02] Hájek J., Drahanský M., Kuřátko J.: *Detection and classification of diseases in retinal images.* Journal of Biomedical Informatics, ISSN: 1532-0464.

Patents

[P01] Name: Ophthalmic Diagnostic Apparatus and Method of its Operation.
Registration: 2013, approval: 2014, expiration: 2024.
Authors: Drahanský Martin, Provazník Ivo, Kolář Radim, Hájek Josef
Type: international patent

Owner: Brno University of Technology
Patent No.: WO/2015/043553
Link: https://patentscope.wipo.int/search/en/detail.jsf?docId=WO2015043553

[P02] Name: Ophthalmic diagnostic apparatus.
Registration: 2013, approval: 2014, expiration: 2024.
Authors: Drahanský Martin, Provazník Ivo, Kolář Radim, Hájek Josef
Type: national utility model
Owner: Brno University of Technology
Patent No.: 26535
Link: http://spisy.upv.cz/UtilityModels/FullDocuments/FDUM0026/uv026535.pdf

[P03] Name: Ophthalmic diagnostic apparatus and the way of its use.
Registration: 2013, approval: 2015, expiration: 2020.
Authors: Drahanský Martin, Provazník Ivo, Kolář Radim, Hájek Josef
Type: national patent
Owner: Brno University of Technology
Patent No.: 305278
Link: http://spisy.upv.cz/Patents/FullDocuments/305/305278.pdf